ABSTRACT

Title of Document: AN ANALYTICAL APPROACH FOR FATIGUE LIFE ESTIMATION OF COPPER TRACES FOR DESIGN OPTIMIZATION IN ELECTRONIC ASSEMBLIES.

Sandeep Menon, Doctor of Philosophy, 2015

Directed By: Professor Michael G. Pecht,
Department of Mechanical Engineering

This dissertation investigates the durability of the copper traces using experimental results from a fully reversed four point bend test and finite element analysis. The durability data collected from the experiment was used in conjunction with the finite element based critical trace strain, to develop a set of compatible fatigue model constants that best fit the failure behavior observed in the tests. Experimental studies were also conducted in order to determine the impact of assembly variations on the trace fatigue failures including the presence of a surface finish, solder mask as well as the presence of assembled components. In order to validate the established fatigue life model constants further testing was conducted at a different load level. The model was able to predict the test out come with an error of less than 5 %

Parametric studies using finite element analysis were also conducted in order to determine the relationship between the various geometric and loading conditions and the critical trace strain in the copper traces. Based on these relationships as well as the

experiments to determine the impact of assembly variations of failure of the traces, an analytical model was developed in order to approximate the copper trace strain which is used as the input to the trace fatigue model.

To understand the crack initiation and crack propagation process in copper traces, experiments were conducted where the crack growth was periodically monitored. Based on these experiments, the constants for the fatigue crack propagation in copper traces based on Paris's Law were also determined in this study.

Finally the analytical model for trace strain developed was also validated by comparing the copper trace strain evaluated using finite element modeling for the test vehicle used in the experiments. The strains estimated based on the analytical model match well with the strains based on the finite element modeling.

AN ANALYTICAL APPROACH FOR FATIGUE LIFE ESTIMATION OF COPPER TRACES FOR DESIGN OPTIMIZATION IN ELECTRONIC ASSEMBLIES.

By

Sandeep Menon.

Dissertation submitted to the Faculty of the Graduate School of the
University of Maryland, College Park, in partial fulfillment
of the requirements for the degree of
Doctor of Philosophy
2015

Advisory Committee:

Professor Michael G. Pecht, Chair
Professor Abhijit Dasgupta
Professor Peter Sandborn
Professor Patrick McCluskey
Professor David Barbe
Senior Research Scientist Dr. Michael Osterman

Dedication

To my family for their unconditional love and support throughout my life

Acknowledgements

I express my like to express my gratitude to my advisor Prof. Michael Pecht, for his support and guidance towards my research. The insights, both academic and real world, as well as the constructive critique he provided helped shape this dissertation.

I would also like to thank Dr. Osterman, for taking an interest in my research and providing me with constant direction and inputs during the course of my dissertation.

I would like to also express my gratitude to Prof. David Barbe, Prof. Patrick McCluskey and Prof. Peter Sandborn for being a part of my thesis committee and reviewing my research. I would like to especially express my thanks to Prof. Abhijit Dasgupta, for considering me as an "honorary" student of his. Without him playing "devil's advocate" and constantly questioning my work this dissertation would not have come to be.

I would also like to thank Dr. Das for taking a chance on a young man in India (a.k.a me) and providing him the opportunity to come to the University of Maryland. His quick wit and fabulous sense of humor have always kept things interesting.

I would like to express thanks to my friends both past and present who have shared the ups and downs of a graduate student's life with me and helped me deal with stress filled days (and nights) over the past six years. I would specially like to thank Bharath Madapusi Govindarajan for the constant support he has provided me over the past six years as well as the "*zen*" view on life that he has inspired me to embrace.

Any acknowledgement of mine would not be complete without mentioning my family away from my family, my uncle Mohan Nair, my aunt Renuka Nair and my cousin

Nikhil (oops Nik) Nair. Without them providing me the guidance and being my safety net to fall back on these past six years, I am not sure I would have made it this far.

Finally, I would like to thank the three most important people in my life: my father a.k.a the angry “young” man K. Pradeep Kumar from whom I learnt how to be always be professional, my mom, Radhika Menon, who instilled in me mental strength and determination and the drive to always be better and my sister, Deepti Menon who has been ready to be my listen to my every problem and gripe, as insignificant it might have been, at any time of the day. I love y’all.

Table of Contents

Dedication ii
Acknowledgements iii
Table of Contents v
List of Tables vii
List of Figures viii
Chapter 1: Introduction 1
Fatigue in Copper Foils 3
Board Level Characterization of Copper Trace Fatigue 6
Trace Failures: Occurrence and Design Alternatives 12
Effects of I/O position and trace routing angle 12
Effect of turning angle 12
Effect of Trace/Pad ratio 13
Effect of Pad Shape 13
Preliminary Testing 13
Test Vehicle 14
Experiment Setup 14
Results 17
Finite Element Modeling 19
Comparison with current life prediction models 20
Gaps in Existing Research 21
Approach 23
Chapter 2: Materials Characterization 24
Material Characterization of Laminate 24
Stress-Strain Response of Electrodeposited Copper Foils 28
Chapter 3: Board Level Testing 36
Test Board Design 36
Experimental Setup 42
Board Level Testing Results 46
Impact of Pad Width. 48
Impact of Trace Width. 49
Impact of Pad Shape. 50
Summary of Bare Copper Failure Data 52
Impact of Assembly Variations. 54
Impact of Surface Finish. 54
Impact of Solder Mask 57
Impact of Assembled Components 62
Chapter 4: Trace Fatigue Life Modeling 66
Finite Element Modeling 66
Total Strain based Fatigue Life Model 73
Validating Model Constants 76
Crack Initiation and Crack Growth 78
Chapter 5: Analytical Model for Critical Trace Strain 87

Trace Strain vs. Board Strain 89
Trace Strain vs. Trace Thickness 91
Trace Strain vs. Pad Width 91
Trace Strain vs. Trace Width 92
Trace Strain vs. Pad Length 93
Trace Strain vs. Radius of Curvature 95
Trace Strain vs. Trace Orientation 96
Trace Strain vs. Pad shape 97
Circular Pad 98
Tear Drop Pad 99
Analytical Model 100
Model Validation 104
Chapter 6: Dissertation Contributions 105
Chapter 7: Limitations and Future Work 106
Bibliography 108

List of Tables

Table 1: Test Matrix 15
Table 2: Consolidated results for the straight traces 18
Table 3: Specimen dimensions for material characterization of laminate 25
Table 4: Transforming load vs. displacement curve to stress vs. strain curve 26
Table 5: Average modulus measured for the laminate 27
Table 6: Grades of copper foil as per IPC-4562 28
Table 7: Trace and pad design variations on test board 38
Table 8: Test matrix 45
Table 9: Failure Statistics for board strain level: 5000 µstrain 52
Table 10: Failure Statistics for board strain level: 4000 µstrain 53
Table 11: Failure Statistics for board strain level: 2000 µstrain 53
Table 12: Failure Statistics for board strain level: 5000 µstrain for ENIG surface finished boards 57
Table 13: Failure Statistics for board strain level: 5000 µstrain for solder masked boards 61
Table 14: Failure Statistics for board strain level: 5000 µstrain for assembled boards 65
Table 15:Critical trace strain ranges evaluated from stress- strain hysteresis plots ... 72
Table 16: Total strain life model constants determine in this study. 76
Table 17: Example of regressed material constants for fatigue crack growth in traces with pad width 1.575mm and board strain level 5000µstrain. 86
Table 18: Estimated assembly level calibration factors 103

List of Figures

Figure 1: Illustration of stress-buffer-enhanced package 7
Figure 2: Damage model incorporating the high-cycle fatigue Basquin curve and the low-cycle fatigue Coffin–Manson curve. 9
Figure 3: Fatigue curve describing the low cycle fatigue 10
Figure 4: Test Specimens. 11
Figure 5: High stress location in traces 12
Figure 6: Test Vehicle for Preliminary Test 14
Figure 7: Test Fixture 15
Figure 8: Strain Gage Location 16
Figure 9: Experimental Setup 16
Figure 10: Example of Measured Strain Data 17
Figure 11: Failure sites 18
Figure 12: Global FEA model and Contour plot of displacements in the global FEA analysis 19
Figure 13: Example of local submodel 20
Figure 14: Comparison plot of predicted life vs ,observed life, with y=x line drawn for clarity 21
Figure 15: Flow chart of approach 23
Figure 16: Schematic of three point bend testing of laminate 25
Figure 17: Average load vs. displacement curve for the weave direction of the laminate material 26
Figure 18: Stress vs. strain curve for the weave direction of the laminate material 27
Figure 19: Summary of modulus values reported for copper foils [19]-[21],[23]-[25],[27],[29], [38]-[40] 29
Figure 20: Summary of yield stress values reported for copper foils[19]-[21],[23]-[25],[27],[29], [38]-[40] 30
Figure 21: Expected grain structure for electrodeposited copper foil [21] 31
Figure 22: Expected grain structure for rolled copper foil [21] 31
Figure 23: Stress vs. strain response for electrodeposited and rolled copper foils 32
Figure 24: Rolled copper foil at 1500X magnification 33
Figure 25: Electrodeposited copper foil at 1500 X magnification 34
Figure 26: Electrodeposited copper foil at approx 10000X magnification 34
Figure 27: Top side of board 37
Figure 28: Bottom side of board 37
Figure 29: Bare copper board 39
Figure 30: ENIG finished board 40
Figure 31: Solder mask covered board 40
Figure 32: Assembled board 41
Figure 33: Shorted solder pads 41
Figure 34: Schematic of four point bend test 42
Figure 35: Four-point bend test setup 43
Figure 36: Fully reversible four-point bend test fixture 44
Figure 37: Location of strain gages 46

Figure 38: Trace crack observed in bare copper boards - Pad Width 125 mil - Trace Width 80 mil - Pad Shape: Rectangle - Cycles to failure 30140 47
Figure 39: Trace crack observed in bare copper boards - Pad Width 100 mil - Trace Width 48 mil - Pad Shape: Rectangle - Cycles to failure 24041 47
Figure 40: Trace crack observed in bare copper boards - Pad Width 100 mil - Trace Width 32 mil – Pad Shape: Circle - Cycles to failure 24041 48
Figure 41: Two parameter Weibull distributions for board strain level: 5000 μstrain, Pad shape: rectangle and Trace to pad width ratio: 0.48 49
Figure 42: Two parameter Weibull distributions for board strain level: 5000 μstrain, Pad shape: rectangle and Pad Width: 125 mil 50
Figure 43: Two parameter Weibull distributions for board strain level: 5000 μstrain, Trace Width 40 mil and Pad Width: 125 mil 51
Figure 44: Two parameter Weibull distributions for board strain level: 5000 μstrain, Trace Width 32 mil and Pad Width: 100 mil 51
Figure 45: Comparison of ENIG finished and bare copper boards for board strain level: 5000 μstrain, pad shape: rectangle, pad width 125 mil and trace width 80 mil.55
Figure 46: Comparison of Cycles to N50 failure for all trace geometries for board strain level: 5000 μstrain (bare copper vs. ENIG finished boards) 56
Figure 47: Solder mask finished board 58
Figure 48: Comparison of solder masked boards and bare copper boards for board strain level: 5000 μstrain, Pad shape: rectangle, Pad width 125 mil and Trace width 80 mil. 59
Figure 49: Comparison of Cycles to N50 failure for all trace geometries for board strain level: 5000 μstrain (Bare copper vs. Solder masked boards) 60
Figure 50: Trace cracking in solder masked boards 61
Figure 51: Comparison of solder masked boards and bare copper boards for board strain level: 5000 μstrain, Pad shape: rectangle, Pad width 125 mil and Trace width 80 mil. 63
Figure 52: Comparison of Cycles to N50 failure for all trace geometries for (board strain level: 5000 μstrain Bare copper vs. assembled boards) 64
Figure 53: Trace cracking in assembled boards 65
Figure 54: Global finite element model of test 67
Figure 55: Strain profiles used for simulation 68
Figure 56: In-plane strain of the global model at maximum displacement 69
Figure 57: Local model for pad shape: rectangle, pad width 125 mil and trace width 80 mil 69
Figure 58: Fine mesh in near trace to pad interface for pad shape: rectangle, pad width 125 mil and trace width 80 mil 70
Figure 59: Mises stress contour plot indicating critical cross section of trace for pad shape: rectangle, pad width 125 mil and trace width 80 mil 71
Figure 60: Volume-weighted average cyclic stress-strain hysteresis for pad shape: rectangle, pad width 125 mil and trace width 80 mil 72
Figure 61: Schematic of the three fatigue life equations. 75
Figure 62: Copper trace fatigue life curve determined in this study. 76
Figure 63: Cycles to N50 failure for validation test (3000 μstrain load level). 77

Figure 64: Comparison of experimentally observed cycles to N50 failure and model predicted N50 cycles to failure. 78
Figure 65: Crack propagation in traces 79
Figure 66: Crack growth curves in traces 80
Figure 67: Typical crack propagation curves in materials 81
Figure 68: Impact of mean stress on crack propagation 82
Figure 69: Modes of cracking 84
Figure 70: Direction of crack propagation in traces 85
Figure 71: Determination of constant of Paris' law: 86
Figure 72: Flow chart for evaluating trace strain 89
Figure 73: Board strain ranges for analytical model 90
Figure 74: Board strain range vs. trace strain range 90
Figure 75: Trace thickness vs. trace strain range 91
Figure 76: Pad width vs. trace strain range 92
Figure 77: Trace width vs. trace strain range 93
Figure 78: Pad width and pad length in a rectangular pad. 94
Figure 79: Pad length vs. trace strain range. 94
Figure 80: Trace strain ranges for varying pad shapes in the experiment. 95
Figure 81: Trace strain ranges vs. radius of curvature at trace to pad interface. 96
Figure 82: Trace angle with respect to loading direction. 96
Figure 83: Trace strain ranges vs. trace angle. 97
Figure 84: Pad width and length of tear drop in circular and tear drop pads. 98
Figure 85: Trace strain ranges – square pad vs. circular pad. 99
Figure 86: Trace strain ranges (Tear drop pad). 100
Figure 87: Strain Concentration Factor 101
Figure 88: Determining trace strain based on fatigue life curve and experimental cycles to failure for board strain level: 5000 μstrain, Pad shape: rectangle, Pad width 125 mil and trace width 80 mil. 103
Figure 89: Estimated Trace Strain vs. FEA Strain 104

Chapter 1: Introduction

Manufacturers of electronics are continually seeking out methodologies to meet the ever increasing demands of portability and functionality. To meet these demands modern electronic systems are being built into more intricate and smaller packages. The decrease in size of electronic systems coupled with increased portability has resulted in consumer electronics being exposed to more mechanical loads (drop/shock, vibration, bend, torsion and so on), resulting in an increased concern about the mechanical robustness of these systems.

When conducting reliability and qualification studies for electronics under such type of mechanical loads; the failure of the solder interconnect is the widely considered the dominant failure mode. Improvements in interconnect design, increased exposure to flexural loads and the use of stiffer (higher density) packages have however resulted in an increasing concern regarding the fatigue failure of the copper metallization (traces and solder pads) on the board [1]-[6]. Failures of copper traces have been reported predominantly under mechanical loading, including bend testing [1][7]-[9], vibration [1][10], drop/shock [11][12] and torsion testing [13]. However, there have been trace failures that have been reported under temperature cycling conditions as well [14].

However, when analyzing the failure and characterizing the failure distributions in reliability studies there is often no distinction made between the solder interconnect failures and trace failures. Early studies discussing the fatigue of copper used in electronics were based in fatigue testing of copper foils and focused predominantly on the high cycle fatigue. More recently however, work has been conducted to

investigate fatigue of copper traces on electronics assembly. There is however still discrepancy in the literature regarding the model constants used to determine the fatigue life of the copper traces on electronic assemblies.

As the trace failures are typically reported at the interface of the trace solder pad interface or at trace turning locations on the electronics assembly, studies have suggested design changes for copper traces [2][3]. However, no attempts have been made to quantify the impact of these design changes on the fatigue behavior of the traces. Also, in most electronic assemblies the copper traces often have a surface finish (ENIG, ImAg and so on), solder mask as well as assembled components which may alter the cycles to failure of the traces. The impact these surface finishes have on the fatigue behavior of has not been investigated.

Also, unlike the analytical models developed to evaluate strain levels in the solder interconnect [14][15], there have been no attempts to build analytical models to evaluate strain levels in copper traces. An analytical model for strain levels in copper traces may help in evaluation of fatigue life of traces and determine how design changes in the assembly might affect the same. This may help in overall design optimization of the electronics assembly.

The following sections and discuss the prior work that has been carried out to in terms of material fatigue and board level reliability of copper traces as well as design solutions that have been suggested in literature to improve the fatigue durability of copper in electronics. Further, the preliminary work in this study to evaluate the existing trace fatigue life models is also discussed along with the gaps in the existing research and the proposed approach that will be used in this study.

Fatigue in Copper Foils

Preliminary work in understanding the fatigue behavior of copper used in electronics focused on experimental results from fatigue testing of copper foils. It has been well established in literature that the fatigue in thin foils is vastly different from the bulk form of the same materials. Further, the processes involved in the manufacturing of the foils influence the material response and as such can result in varying fatigue behavior. Typically, the two kinds of foils that are used in the manufacturing of electronics include a rolled and an electrodeposited copper foil. The introduction of flexible circuitry created in an increased concern regarding the fatigue durability of copper used in such circuits. Since rolled copper foils are typically the choice of foils in flexible circuitry (owing to their high ductility values), a lot of the early studies regarding fatigue in copper foils involved testing of rolled copper foils [17]-[19]. In 1987, Engelmaier presented a study conducted by IPC evaluating the ductility of copper foils from a variety of different manufacturers [20]. The primary objective of this study was to determine the minimum ductility requirements for IPC standard on copper foil for printed wiring applications. However, this study also provided insights to how the fatigue ductility test method can be used to predict high cycle fatigue behavior of the copper foils. A purely empirical relationship between the fatigue life and the strain from a flex testing setup was provided in this study.

Merchant et al [21] investigated the mechanical fatigue behavior of thin copper foils where foil specimens (electroplated and rolled) were subjected to strain controlled cyclic bending tests. The failures obtained during this test were utilized to obtain hardening exponents (n) and fatigue ductility (D_f) parameters. It is shown that for a

given foil thickness a universal relationship exists between the fatigue ductility and the strength (σ) normalized cycles to fatigue life (N_f/σ). It was also shown that the propagation of the crack through the foil thickness and across the sample width is related to the grain structure for each foil type; pancaked grains for the rolled foil and equiaxed grains for the electrodeposited foil. For both electrodeposited and rolled Cu foils (especially for heat treated foils) enhanced N_f and Df data with decreasing foil thickness are also presented in this study.

Keller et al. [22]investigated the fracture behavior of electrodeposited copper films under tensile loads. The study indicated that the finer grain structures of the electrodeposited copper foils attributed to their lower ductilities as well as the higher strengths. The study also indicated that the crack growth occurred by the formation of an intergranular micro crack ahead of the main crack tip followed by linking, which took place by the easiest available path, intergranular or transgranular.

Hong and Weil [23] conducted fatigue test comparisons on thin copper foils (electroplated and wrought) and bulk copper. It was seen that all foils obeyed the Basquin's equation. It was also found that the fatigue strength coefficients were related to the cyclic hardening exponents and were of the same magnitude as the tensile strengths. The electroplated copper displayed higher fatigue strengths compared to the wrought copper foils and the bulk copper.

Hwangbo and Song [24][25] conducted studies to evaluate the fatigue life and plastic deformation behavior of electrodeposited copper films. Fatigue tests were performed at varying mean stress levels and the cyclic plastic strains and monotonic plastic strains were measured simultaneously. It was seen that irrespective of mean stress or

fatigue life the copper film fails when it reaches a limited value of monotonic plastic strain. The monotonic strain was then used as a damage parameter to assess the fatigue life of copper films. A method to predict the monotonic plastic strain was also developed using a Weibull distribution function.

Hommel et al. studied the behavior of very thin copper films (0.5 μm to 2 μm thick layers) on 125 μm thick polyimide substrates. The results indicate a very strong strain hardening accompanied by an asymmetric deformation behavior.

Harboletz et al [27] investigated the fatigue behavior of both rolled and electrodeposited copper foils with varying thickness in an attempt to understand the 'size' effect on fatigue crack growth in foils. A size-effect was detected for fatigue crack growth data of rolled foils. Based on the monitored crack propagation in this study, the threshold stress intensity factor values were provided for both the rolled and the electrodeposited copper foils comparable threshold stress intensity factor values of the ED foils with rolled material was observed.

Weiss et al [28] conducted studies to characterize the mechanical and thermal properties of thin copper foils. These studies indicated a pronounced effect of the temperature on the elastic plastic response of the foils especially for the electrodeposited copper foils. This behavior was further corroborated by Merchant et al, where the studies indicated that the dependence of elastic modulus for electrodeposited copper foils is much greater than that of a rolled copper foil. Their study also indicated that the elastic modulus, the tangent modulus, the strain hardening exponent as well as the yield stress were all inversely proportional to the grain structure of the copper in the foils.

Simmons et al [30] conducted a study on thin rolled copper foils with varying thickness and comparable microstructure. Their results indicated that the thickness of the foils has an influence on the mechanical behavior in the size regime studied. When the thickness is reduced from 250 μm to 10 μm, the fracture strain decreases for the as-received foils from approximately 20% to 0.2% and for the samples with heat treatment from 35% to 15%.

Lee and Song [31]conducted a study to investigate the fatigue behavior of thin copper films under variable amplitude loading. Their study suggested that the interactions of the varying load levels reduce the fatigue life, resulting in non-conservative predictions of fatigue life by using a linear damage accumulation rule (Miner's rule). A modified formulation to predict fatigue life based on the mean monotonic plastic strain was proposed in this study.

Han et al [32] investigated the fatigue behavior of thin copper foils for flexible printed circuit boards and concluded that the mechanical behavior of the rolled copper foils is highly dependent on the direction of rolling. They also indicated that the fatigue life of the electrodeposited copper foils is significantly longer than the rolled copper foils.

Board Level Characterization of Copper Trace Fatigue

There has been limited research that has been carried out in order to investigate the board level copper trace fatigue and to develop a life prediction model for copper traces in electronic assemblies. A lot of the work on board level fatigue behavior of copper traces is focused on flexible printed wiring assemblies.

Chou et al [33] developed an impact life prediction model to model trace failures within a stress-buffer-enhanced packages (Figure 1). The stress-buffer-enhanced package applies a thick and soft buffer layer to protect solder joints; however, metal traces embedded inside the buffer layer are instead broken.

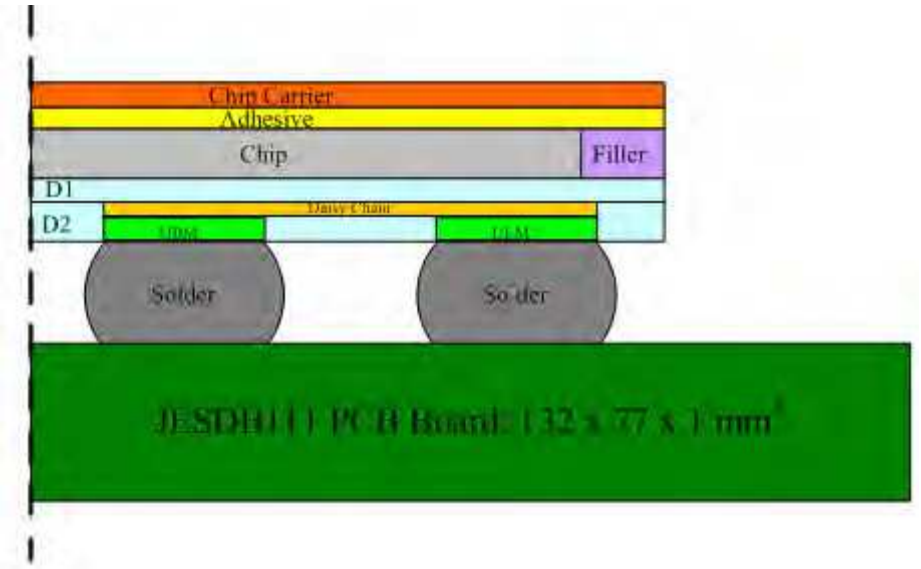

Figure 1: Illustration of stress-buffer-enhanced package

The test vehicle was developed using JEDEC standards and drop testing was performed based on JESD22-B111 drop test condition B. The peak acceleration, pulse duration and drop height were 1500 G, 0.5 ms and 112 cm respectively. The soft stress buffer layer absorbed the impact, thereby ensuring that the solder joints are protected. However, the metal lines within stress buffer layer suffered relatively larger deformation resulting in their failure. Because the failure mode of stress-buffer enhanced package focused on the broken metal lines, the configuration of trace layout becomes a significant factor affecting the impact reliability of this package. Therefore, two kinds of trace layout, the straight trace and the curved trace, were then

experimented. As the dynamic response of each of the packages on the board is different, each one was considered individually and finite element models were developed in order to evaluate the strains experienced on the traces during the drop testing. The fatigue damage was considered to be a process of damage accumulation. Since the drop test is a low cycle fatigue test the failure is dominated by the accumulation of plastic strain. Therefore the impact life prediction models proposed in this study was based on the cumulative plastic strain during the drop test. The developed model was then used to predict the number characteristic drops to failure and showed good correlation with experimental results.

Farley et al [1][34][35] investigated the fatigue durability of copper traces on printed wiring boards under quasi static cyclic mechanical flexure. A test vehicle populated with micro lead frame components was subjected to three point bend loads and a three-dimensional finite element model was used to evaluate the stresses and strains occurring at the failure sites during the cyclic loading. As the loading was not fully reversed, a mean stress correction factor was developed to force a saturation of the mean stress effect at higher stress levels for the tensile mean stress. In order to determine the copper elastic-plastic constants and the fatigue durability constants that model the observed durability behavior an iterative methodology was developed based on the average cross section strains at the failure sites (Figure 2). To further improve these fatigue constants the damage initiation and propagation of the failure was considered separately and an incremental damage approach was used iteratively to determine the refined fatigue constants for copper. The fatigue life of the traces was then modeled using a generalized strain life power law. The strains used in this

model were evaluated using a finite element analysis with the updated materials models for copper developed in this study. The developed methodology and model constants were compared with failures obtained on test boards populated with resistor packages subjected to four point bending loads. The model appears to predict the failures reasonably well.

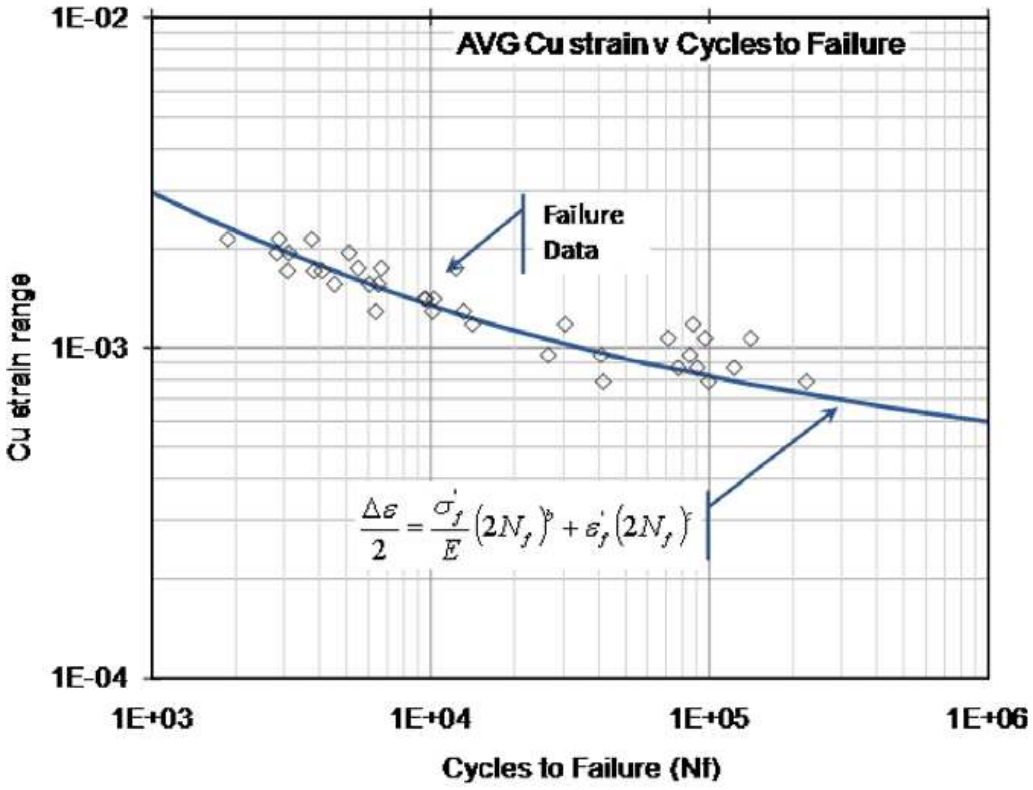

Figure 2: Damage model incorporating the high-cycle fatigue Basquin curve and the low-cycle fatigue Coffin–Manson curve.

Lall et al [2] attempted to address the need for life prediction models for copper traces on printed wiring boards subjected to high magnitudes of cyclic mechanical loads (drop/shock). The test boards used in this study were unpopulated to isolate the copper trace cracks from other failure modes that occur in interconnects and other parts of the component assembly. Each test vehicle had 9 traces running along its

length on either side. To study the effect of pad to trace dimensional ratio on the reliability of traces, the 9 traces on either side were laid as combinations of 3 different pad and trace sizes. Traces were also laid out in a zig-zag pattern to evaluate the effect of the various angles at which the traces merge with a solder pad. A three point bend test fixture was used to simulate the flexure obtained on the boards during drop loads. A finite element model was developed to evaluate the strain at the failure locations. The generalized strain life power law was then modified in order to obtain the low cycle fatigue behavior of copper traces ().

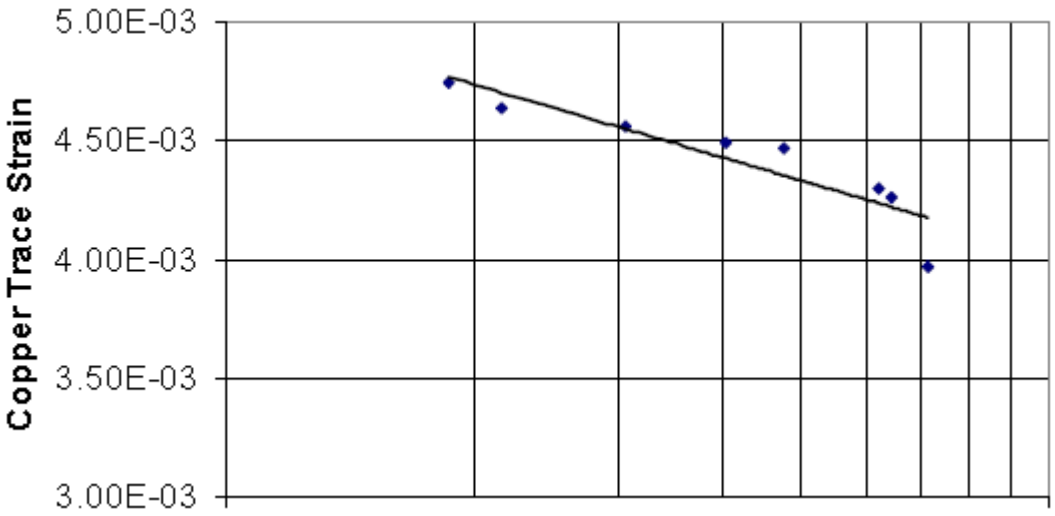

Figure 3: Fatigue curve describing the low cycle fatigue

Kim and Hsieh [36]conducted studies to predict the fatigue crack growth in copper foils embedded in a composite structure. Their studies indicated that the growth of crack in the copper and the debonding of the copper at the copper to composite interface occurred in coordination with each other. A Paris law type relationship was established between the crack growth rate and the crack tip opening angle.

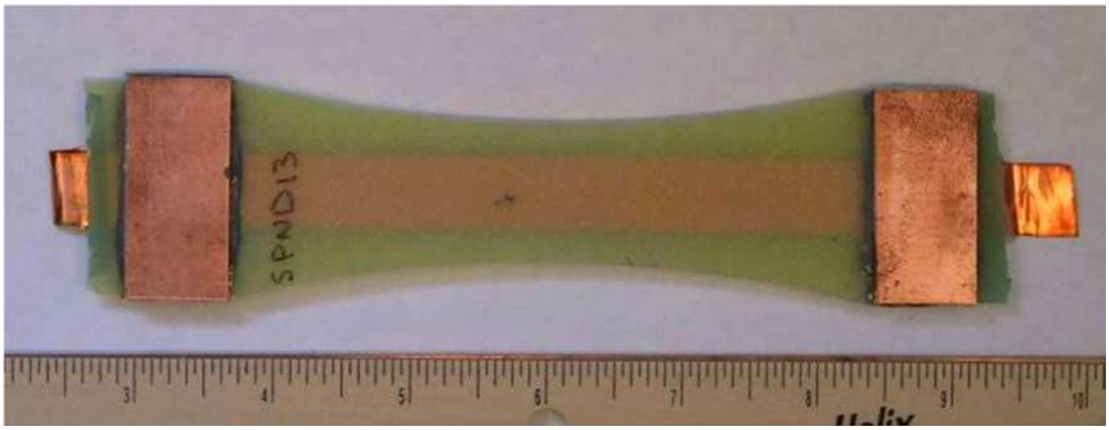

Figure 4: Test Specimens.

Kraemer et al [37] investigated the impact of copper trace routing on the drop test reliability of BGA packages. Their study revealed that copper trace failures resulted in the failure of the component. The trace failure seemed to appear only if the copper trace was routed along the direction of the highest printed circuit board deflection. As part of this study a lifetime assessment model based on a local strain map and a global energy criterion was proposed. Further a lifetime model was derived, which has the ability to predict the experimental number of cycles-to-failure for the investigated packages with an inaccuracy of less than ±25%.

Trace Failures: Occurrence and Design Alternatives

Trace failures generally occur at the junction of traces and solder pads in electronic assemblies, owing to the stress concentrations in these regions [1]-[3]. Qualitative studies have been carried out to evaluate the impact of trace/pad ratios, trace orientations, effect of turning angle, tear drop design and so on [2][3]. Design alternatives based on these qualitative results have been suggested to reduce the occurrence of trace failures in electronics assemblies.

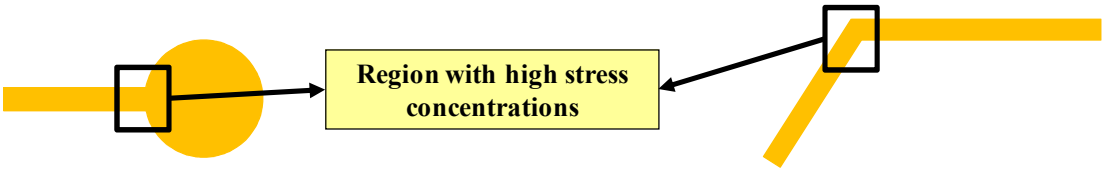

Figure 5: High stress location in traces

Effects of I/O position and trace routing angle

Multiple studies have investigated the impact of trace routing on the fatigue life of the traces [2][3][37]. Under flexural loads it has been observed the maximum stresses in the copper are observed when the traces were routed along the direction of the highest printed circuit board deflection. The maximum stresses in traces were seen to reduce as the traces were routed orthogonal to the direction of the highest printed circuit board deflection.

Effect of turning angle

It was found that irrespective of the turning angle, maximum stresses occurred at the fillet between the two traces, at the point where they met [2]. It was also observed that the sharper angles increased the maximum stresses observed and could potentially lead to earlier failure of the copper traces.

Effect of Trace/Pad ratio

It was found that Stress levels in the trace-pad junctions were seen to decrease with a decreased difference in trace width and pad diameter. [2][3]. It was also observed that for similar trace/pad ratio traces with bigger pads were seen to have lower stresses and potentially more reliable than those with smaller pads.

Effect of Pad Shape

Studies have also indicated that the shape of the pad has a significant impact on the copper trace fatigue life [3]. This is primarily attributed to the fact that the stress at the solder pad and trace interface (which drives the failure of the trace) is the dependent on the shape of the pad. It has been suggested in literature that a tear drop pad shape or a stepped change in pad width provides higher reliability than the more commonly used rectangular or circular pads.

Preliminary Testing

As seen in previous sections, there are a few fatigue life prediction models that can be used to predict the failure of copper traces under flexural loading. However the applicability of these models has not been validated. In order to carry out model validation a new test vehicle was designed and subject to four-point cyclic bend testing. To isolate failures on the traces, the test vehicle was designed without any components that may have resulted in failure of the solder interconnect.

Test Vehicle

The test vehicle was designed with 30 traces with three varying trace widths (5, 10 and 15 mil), two trace geometries (straight and bent) and two surface finishes (bare copper and ENIG). The test vehicle used is shown in Figure 6. The trace thickness was ~ 58 microns. The variation in the test vehicles allows for determining the impact of each of the design parameter on the fatigue life of the traces.

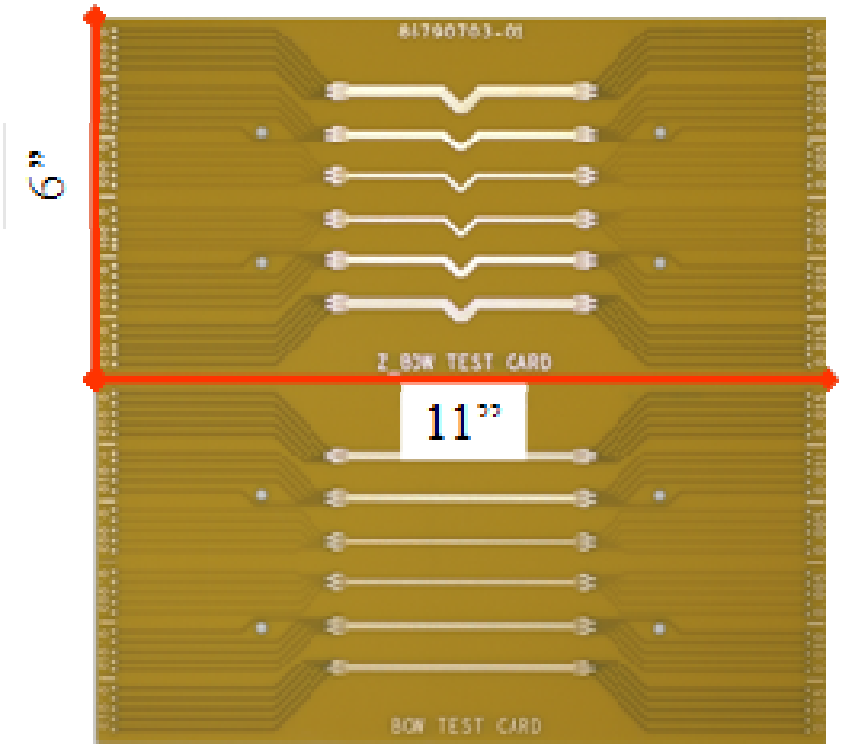

Figure 6: Test Vehicle for Preliminary Test

Experiment Setup

During this test, a commercially available servo-hydraulic machine was used in conjunction with a test fixture that is capable of applying full reversal loading (Figure 7). The full reversal capability allows for increased strain range during the test and negates the need for mean stress correction factors that were used while developing

fatigue models in literature [11]. The test matrix for the preliminary tests is shown in Table 1. Three separate strain range levels were used to test these boards in order to obtain the relationship between the strain range and cycles to failure in each of these test cases.

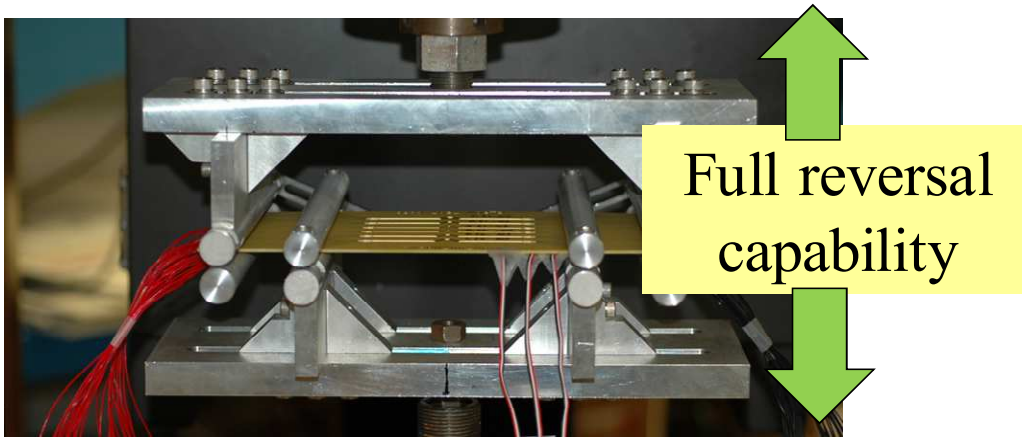

Figure 7: Test Fixture

Table 1: Test Matrix

Board Strain Range (μstrain)	Surface Finish	ENIG					
	Trace Geometry	Straight			Bent		
	Trace Width (mils)	5	10	15	5	10	15
2500	Sample size	20	20	20	20	20	20
3000		20	20	20	20	20	20
3500		20	20	20	20	20	20

The trace resistance was monitored periodically using a data logger to identify failure of copper traces. Failure was defined based on IPC-9701 standard that defines failure as a 20% increase in initial resistance value for five consecutive scans. Apart from resistance monitoring the board strain was measured periodically using uni-axial strain gages. Board strain was monitored using three strain gages attached on the PWB as shown in the Figure 8. Two strain gages (A & B) attached along the length of

the board to monitor longitudinal board strain between the load span. A third strain gage (C) was attached along the width of the board to monitor the transverse board strain between the load span. A schematic of the experimental setup is shown in Figure 9.

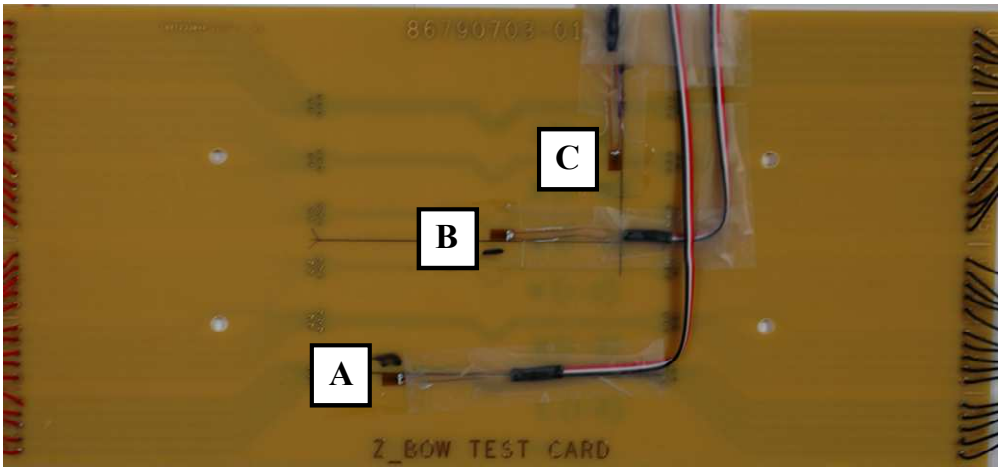

Figure 8: Strain Gage Location

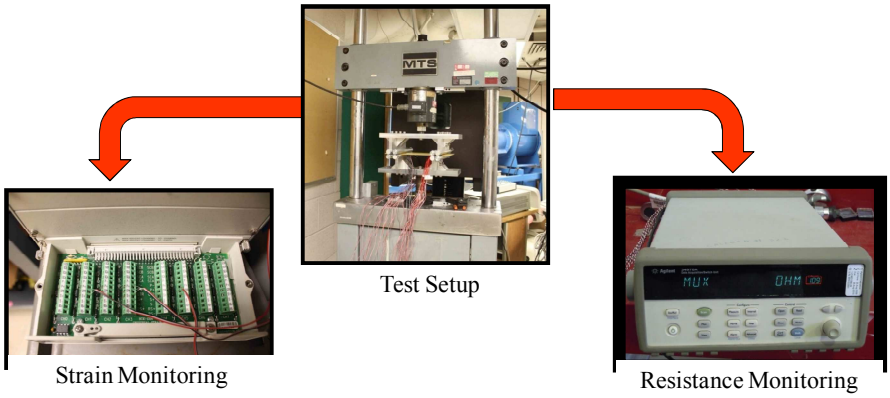

Figure 9: Experimental Setup

The monitored strain data (Figure 10) shows that the deformation of the board was predominantly in the longitudinal direction and the transverse deformation was negligible. All the testing was carried out at a cyclic frequency of 1 Hz.

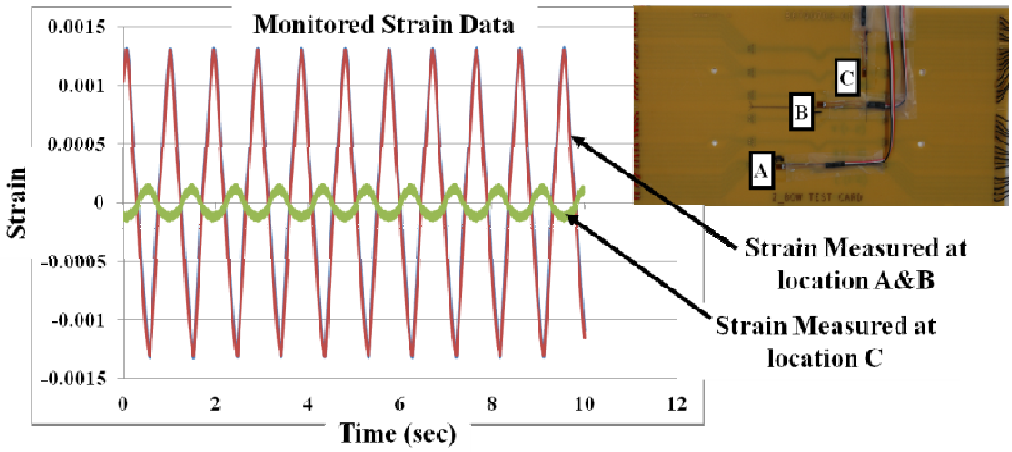

Figure 10: Example of Measured Strain Data

Results

As is seen in the literature, the failure in the copper traces were predominantly seen in the trace/pad joints and at the turning points of the traces (shown in Figure 11). The failure distribution was then modeled using a Weibull 2 parameter distribution to obtain the characteristic life of the traces. As expected the increase in loading resulted in a decrease in characteristic life of the traces. However the trace width seems to have negligible impact on the fatigue life of the traces. The consolidated results for the straight traces are shown in Table 2.

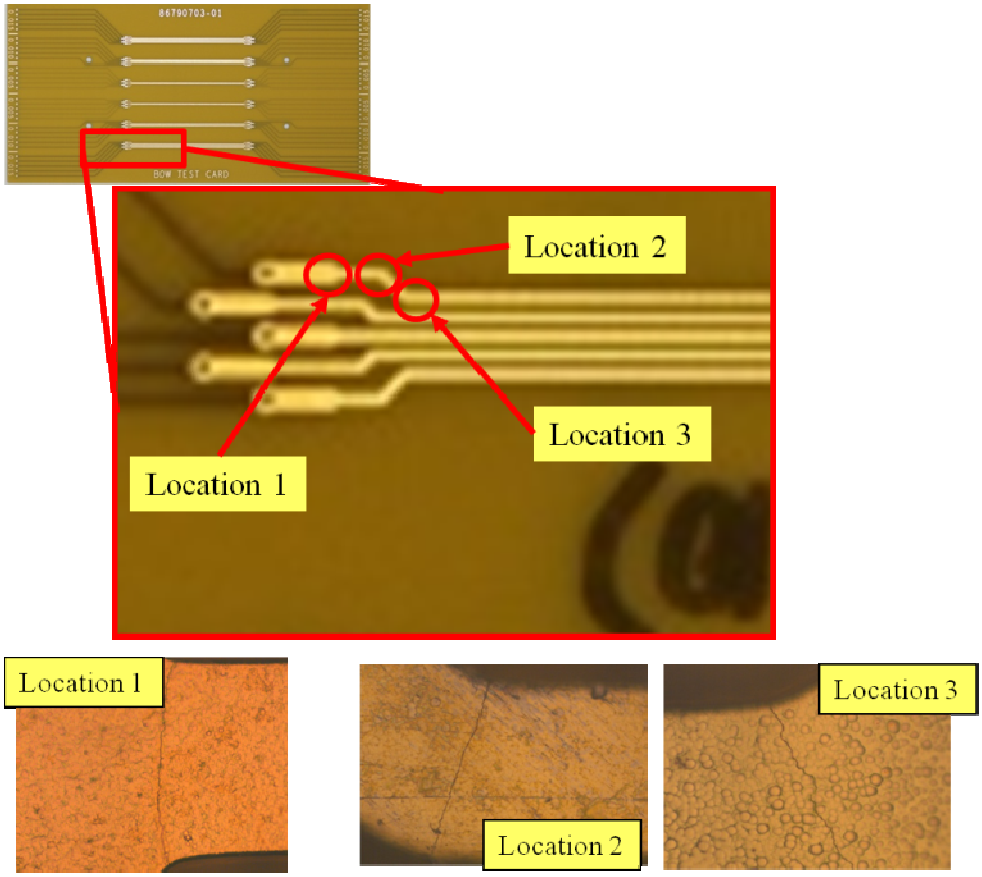

Figure 11: Failure sites

Table 2: Consolidated results for the straight traces

Board Strain (μstrain)	Tracewidth (mil)	η (sec)	β	ρ
2500	5	5.59E+05	1.587	0.9553
	10	3.46E+05	1.4655	0.9833
	15	3.75E+05	1.3772	0.9337
3000	5	9.09E+04	2.5261	0.9596
	10	6.88E+04	3.936	0.99
	15	8.89E+04	2.6935	0.9672
3500	5	2.69E+04	3.1353	0.9432
	10	2.75E+04	2.2125	0.8763
	15	4.21E+04	3.8614	0.9526

Finite Element Modeling

To evaluate the strains in the failure sites obtained during the experiment, a global-local modeling approach was utilized. A defeatured global model of the PCB was created without the copper trace architectural details and subjected to the loading conditions experienced in the experiment (Figure 12). The output displacements from the global FEA model were then used to drive the local sub models.

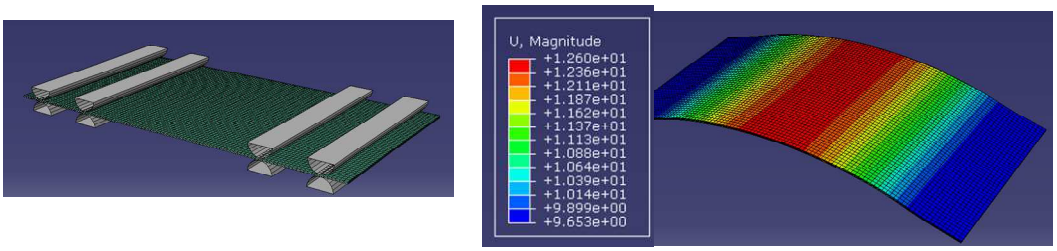

Figure 12: Global FEA model and Contour plot of displacements in the global FEA analysis

As failures obtained were localized in the trace/pad joints and at the turning points of the traces, sub models preserving acute geometric details of these regions of the PCB were developed. The material model used for the copper was obtained from the study conducted by Farley et al [1]. Each of the sub models were then analyzed by deriving their boundary conditions from the output of the global model. A good correlation was obtained between the areas of high stress as shown in the simulations and the actual failure sites Figure 13.

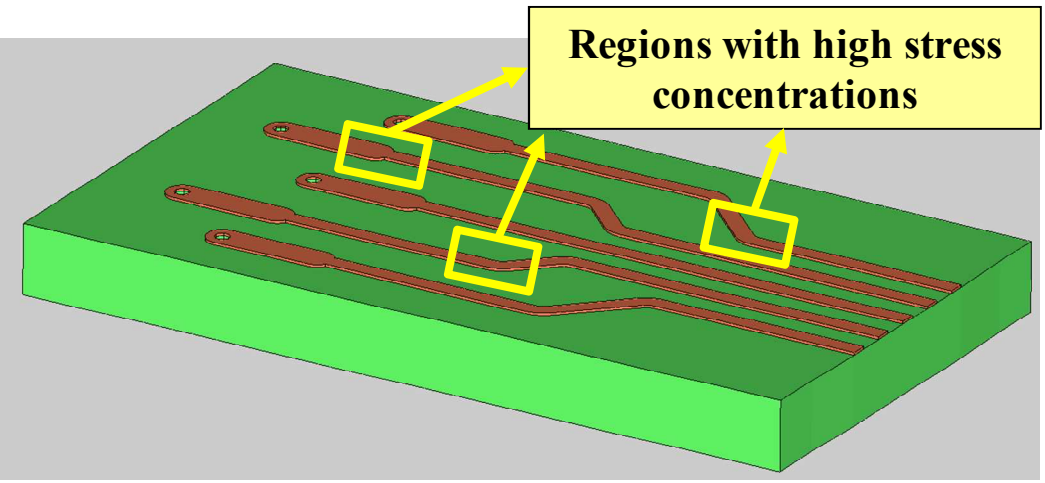

Figure 13: Example of local submodel

Comparison with current life prediction models

Similar to the previous studies [1][2] the strain range used for predictions was obtained by averaging the strain range across the cross section of the failure sites. The plots of the cycles to failure observed in the experiment were plotted against the cycles to failure predicted using the two models available in literature Figure 14.

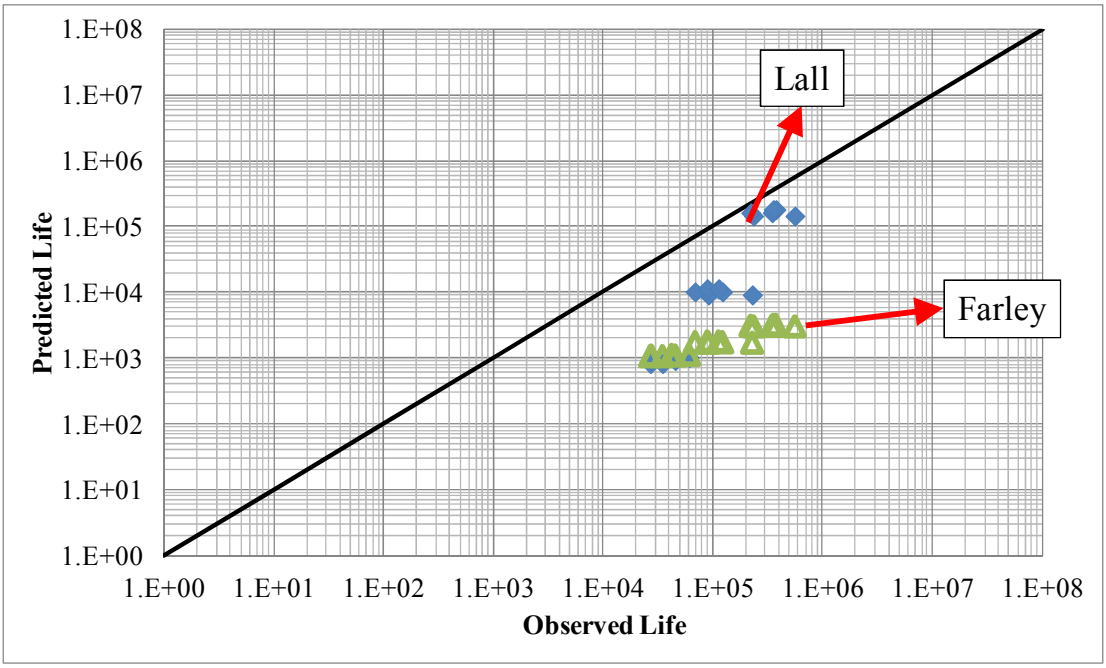

Figure 14: Comparison plot of predicted life vs ,observed life, with y=x line drawn for clarity

As seen with in the plots, the estimated life using both the available fatigue life models is lower than the observed life in the experiment. This error in predicted life could be a result of incorrect material models used in the FEA simulation which results in an error in the estimated strain in the copper traces.

Gaps in Existing Research

It is clear from the literature that the fatigue failures in copper traces are gaining importance in the electronics industry. Early work focused on material response as well as either low cycle or high cycle fatigue behavior of foils. However as seen in literature, the material properties of copper greatly depend on the fabrication process the thickness, grain structure and other such parameters. As a result the fatigue

behavior of copper foils varies based on the manufacturing technique used. Further the fatigue testing conducted was typically on free standing foils or on thin flexible substrates. However, limited studies exist that discuss the fatigue behavior of copper traces in rigid electronic assemblies. The strain based models developed by Farley et al [1] and Lall et al [2] provide insights into the fatigue life behavior of copper trace, but are dependent on the strains obtained using finite element modeling. However, neither study did any material testing to verify the constitutive models used in the finite element modeling (though Farley et al attempted to establish the constitutive model using iterative finite element modeling). As such the strains evaluated in both these studies could be erroneous and can lead to incorrect fatigue life predictions as is seen in the preliminary work. There is therefore a need to do a comprehensive study that includes material testing as well as board level fatigue testing to understand the fatigue behavior of copper traces and to establish the fatigue model constants to predict trace fatigue life in printed circuit assemblies.

Further, though qualitative assessments of design changes in the trace geometry have been made in literature, there have been no studies that quantify the impact of these design changes. There have also been limited studies that investigate the impact of surface finishes, solder mask as well as assembled components which may alter the fatigue behavior of copper traces.

Finally, we have seen in literature that strain based analytical models have been developed to address solder interconnect fatigue. However there have been no attempts to develop an analytical model to assess the fatigue life of copper traces.

Approach

In order to address these gaps in literature an approach was devised. A flowchart of the devised approach is provided in

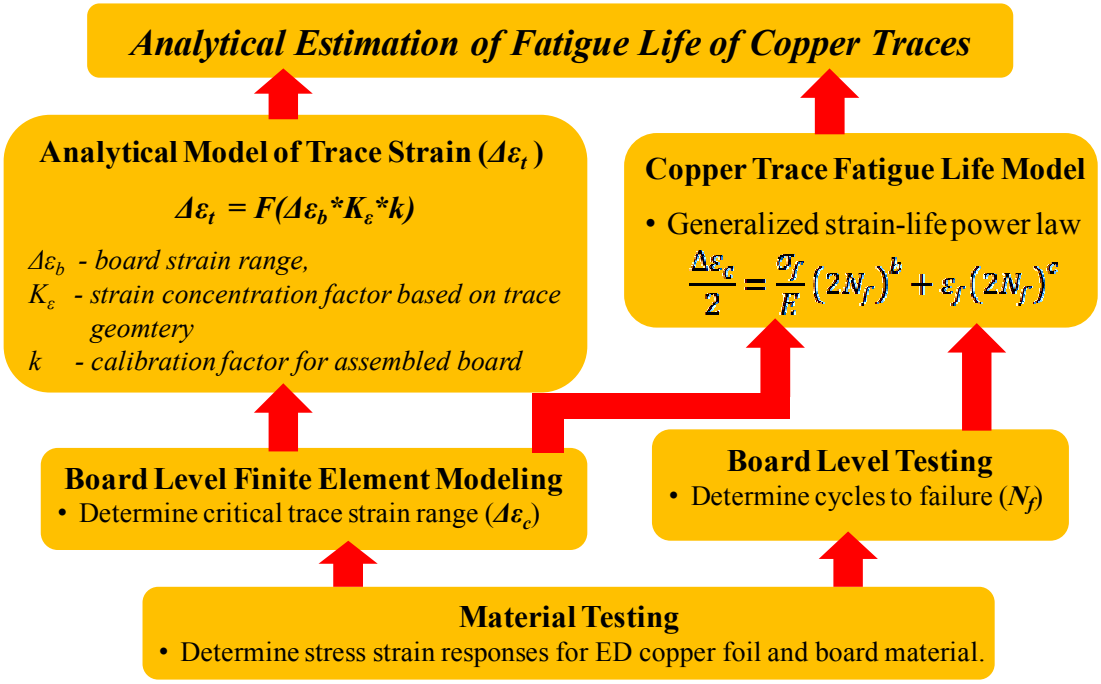

Figure 15: Flow chart of approach

Chapter 2: Materials Characterization

To define the loading limits for the board level testing (conducted in Chapter 2), material characterization was conducted on the laminate material. Further, the material characterization of the electrodeposited copper foils used to form the copper traces used in this study was also carried out in order to provide material input information for finite element analysis that is carried out later in the study. The following sections provide the details regarding the materials characterization that is carried out as a part of this study.

Material Characterization of Laminate

An FR4 laminate material was used for the designed test boards. To evaluate the stress-strain response of the material, rectangular specimens were cut out from the laminate using a high speed rotary tool. Five specimens were prepared in both the weave and warp direction of the laminate materials. The width of the specimen was reduced to approximately 10 mm using grinding and polishing. Details regarding the specimen dimension are provided in Table 3. Each of the specimens was then dried at 105^{o}C for four hours to drive any moisture present in the laminate material. The specimens were then cooled down to room temperature prior to further testing.

Table 3: Specimen dimensions for material characterization of laminate

Specimen Direction	Average Width (mm)	Average Thickness (mm)	Span Length (mm)
Weave	10.51	1.57	40 mm
Warp	10.38	1.57	40 mm

To determine the modulus of the specimens a three-point bend test was conducted in a TA Instruments' RSA Dynamic Materials Analyzer. A schematic of the testing is shown below (Figure 16). In this test, a displacement was applied to the loading anvil and the load response was monitored during the experiment.

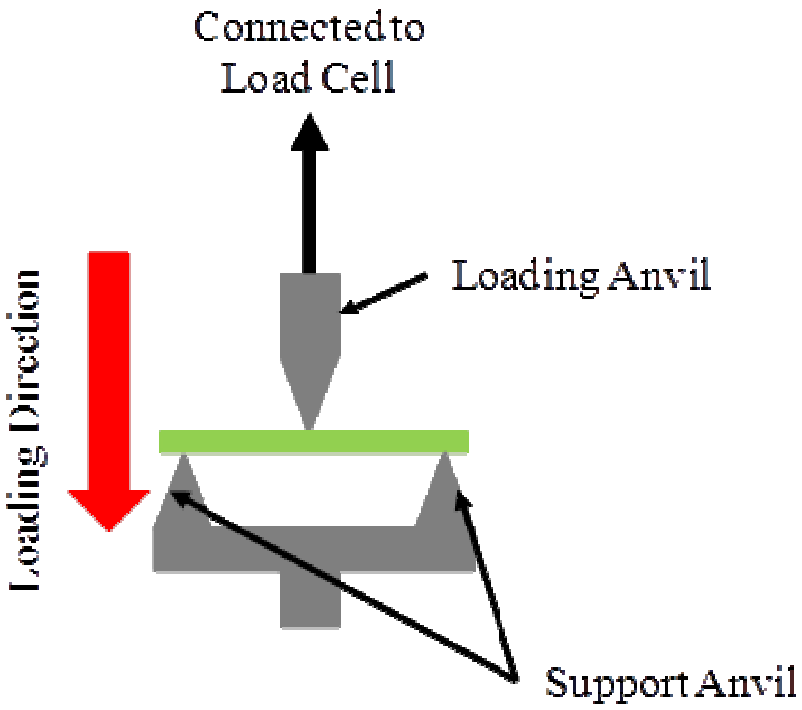

Figure 16: Schematic of three point bend testing of laminate

The load and displacement experienced on the loading anvil are continuously monitored during the experiment. Using the specimen geometry and the span length, the load vs. displacement curve (Figure 17) is transformed to a stress vs. strain curve (Figure 18) based on the equations provided in see Table 4.

Table 4: Transforming load vs. displacement curve to stress vs. strain curve

$Stress\ (\sigma) = \frac{3FL}{2bd^2}$	• F – Load on loading anvil • L – Support span length (40 mm) • b – Width of specimen • d – Thickness of specimen • D – Displacement of loading anvil
$Strain\ (\varepsilon) = \frac{6Dd}{L^2}$	

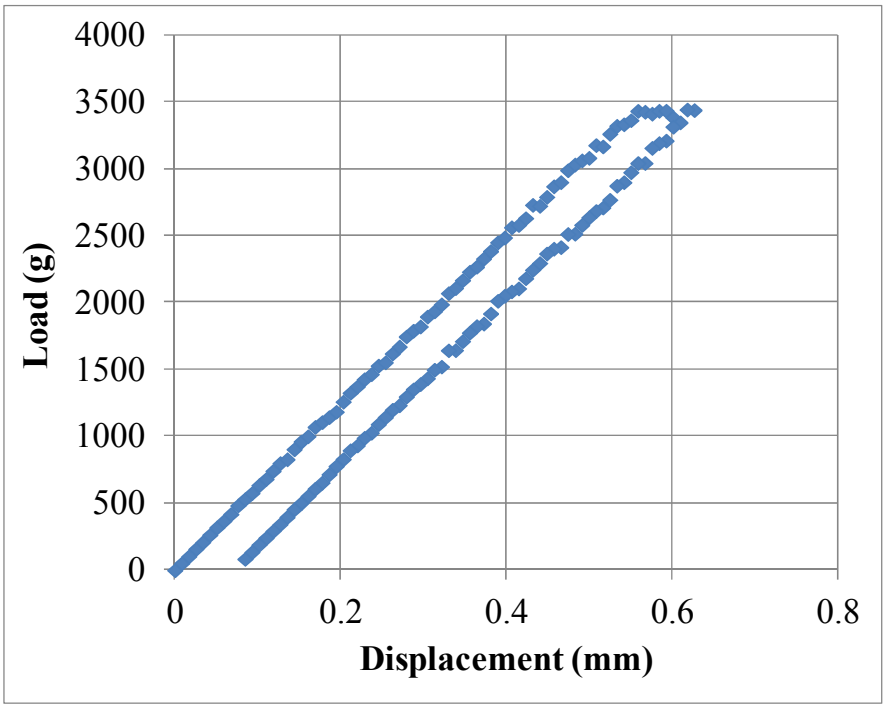

Figure 17: Average load vs. displacement curve for the weave direction of the laminate material

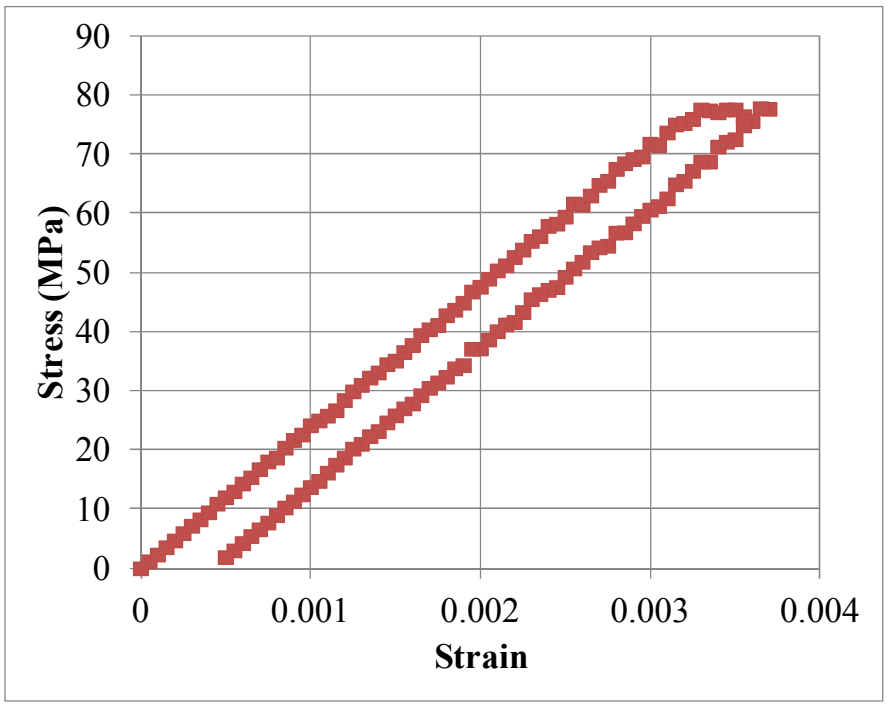

Figure 18: Stress vs. strain curve for the weave direction of the laminate material

The slope of the stress vs. strain curve describes the modulus of the sample. The measured modulus in both the weave and warp direction of the laminate are provided in Table 5. As is seen in Figure 18, the laminate material starts to yield approximately at 3000 μstrain. As such, 2500 μstrain was set as the maximum strain amplitude for further board level testing.

Table 5: Average modulus measured for the laminate

Direction	Modulus (GPa)
Weave	23.8
Warp	21.8

Stress-Strain Response of Electrodeposited Copper Foils

It has been seen in literature that the material properties of the thin copper foils used in electronics are very different from the bulk copper properties [21][22]. In order to obtain accurate strain responses in further board level finite element modeling, accurate measurement of the stress strain response of the copper foil used for forming the traces is required. IPC-4562 provides 8 grades of copper (see Table 6) that are typically used as conductive material in printed circuits.

Table 6: Grades of copper foil as per IPC-4562

Grade	Foil Description
1	Standard electrodeposited
2	High-ductility electrodeposited
3	High-temperature elongation electrodeposited
4	Annealed electrodeposited
5	As rolled-wrought
6	Light cold rolled-wrought
7	Annealed-wrought
8	As rolled-wrought, low temperature annealable

However, as is seen from the table the copper foils can be broadly classified based on their manufacturing technique as being electrodeposited or rolled. Multiple studies have been carried out in order to characterize both these kind of foils. It has been seen in literature that the rolled copper foils exhibit very different material and fatigue behavior when compared to the electrodeposited copper foils. The following figures

(Figure 19 Figure 20) illustrate the range of modulus and yield properties that have been reported in literature for both electrodeposited and rolled copper foils.

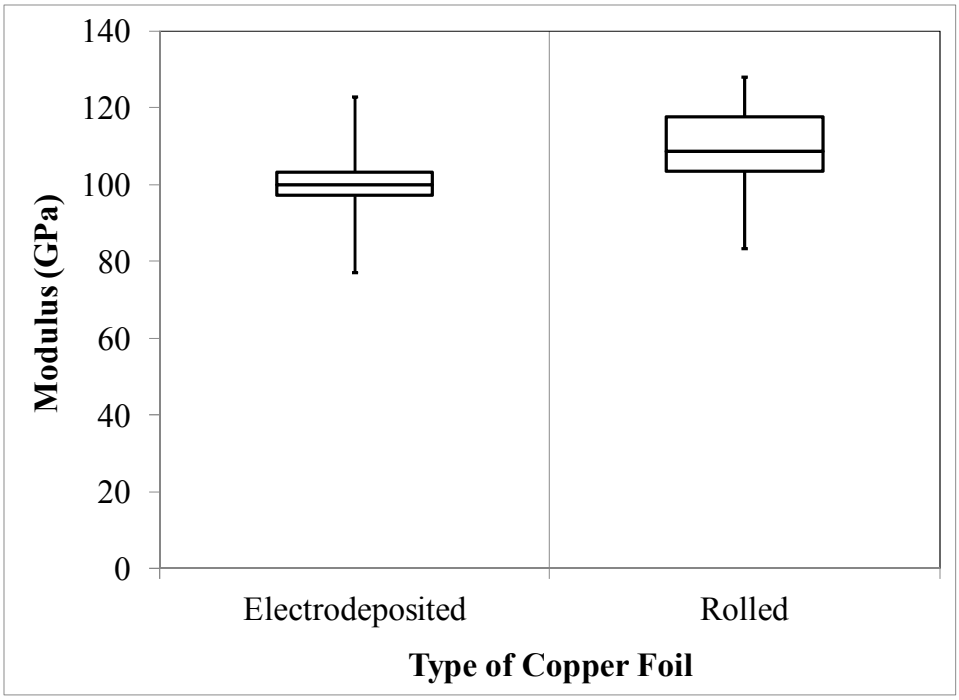

Figure 19: Summary of modulus values reported for copper foils [19]-[21],[23]-[25],[27],[29], [38]-[40]

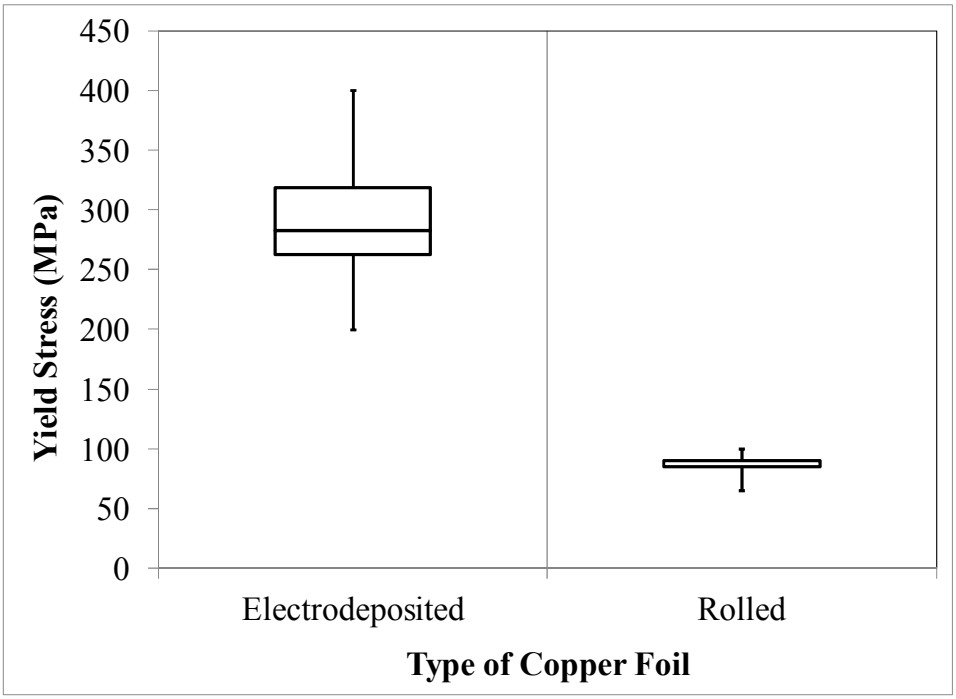

Figure 20: Summary of yield stress values reported for copper foils[19]-[21],[23]-[25],[27],[29], [38]-[40]

As is seen from the figures, the studies that have been conducted in literature indicate that though the modulus values are pretty similar for both the rolled as well as the electrodeposited copper foils, the yield stress for the electrodeposited copper foils are vastly different from that of the rolled copper foils. Merchant et al. [21] attributed this difference in yield characteristics on the potential difference in the microstructure of the two different copper foils, where the electrodeposited copper foils exhibit an equi-axed grain structure and the rolled copper foils exhibit a pancaked grain structure (Figure 21 and Figure 22)

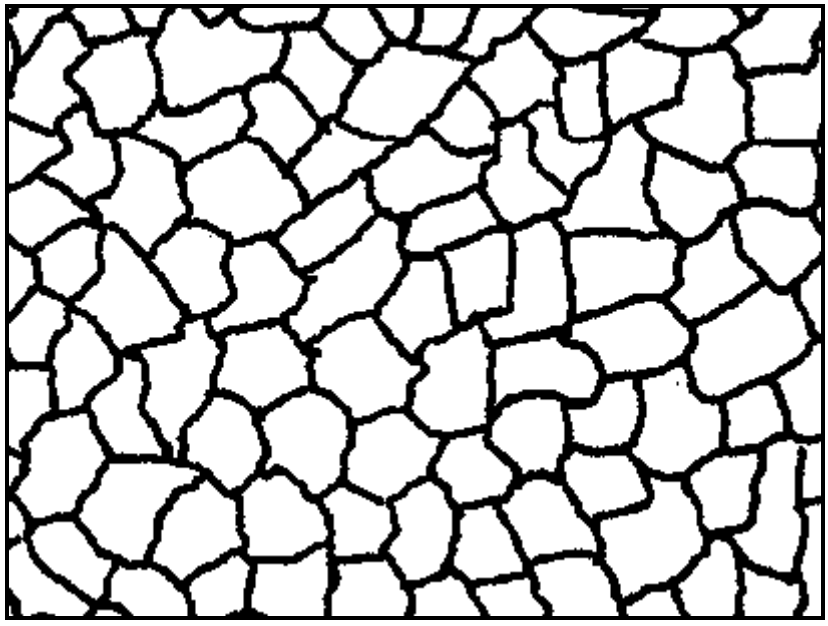

Figure 21: Expected grain structure for electrodeposited copper foil [21]

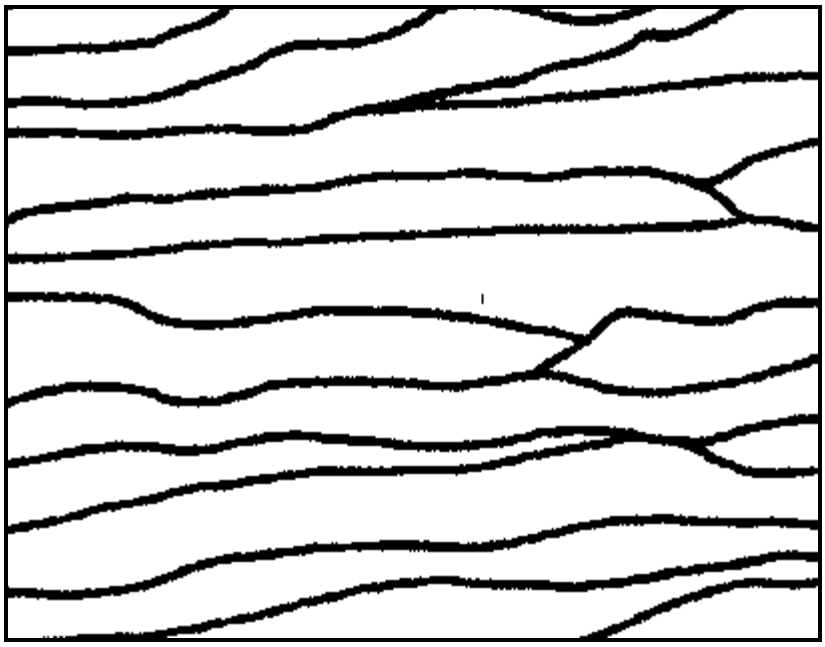

Figure 22: Expected grain structure for rolled copper foil [21]

In order to verify these claims, as well as to provide accurate stress-strain response curves for further finite element modeling, commercial grade electrodeposited copper foils and rolled copper foils were subjected to uniaxial tensile testing. The foils used in this study were 35µm thick which is the most commonly used thickness (1 oz) used for creating conductive traces in printed circuit assemblies. The samples were prepared and tested (based on the ASTM E345) for measuring stress-strain responses for thin metallic foils. The following figure (Figure 23) illustrates the mean stress-strain curves obtained from the testing of five specimens for each type of copper foil.

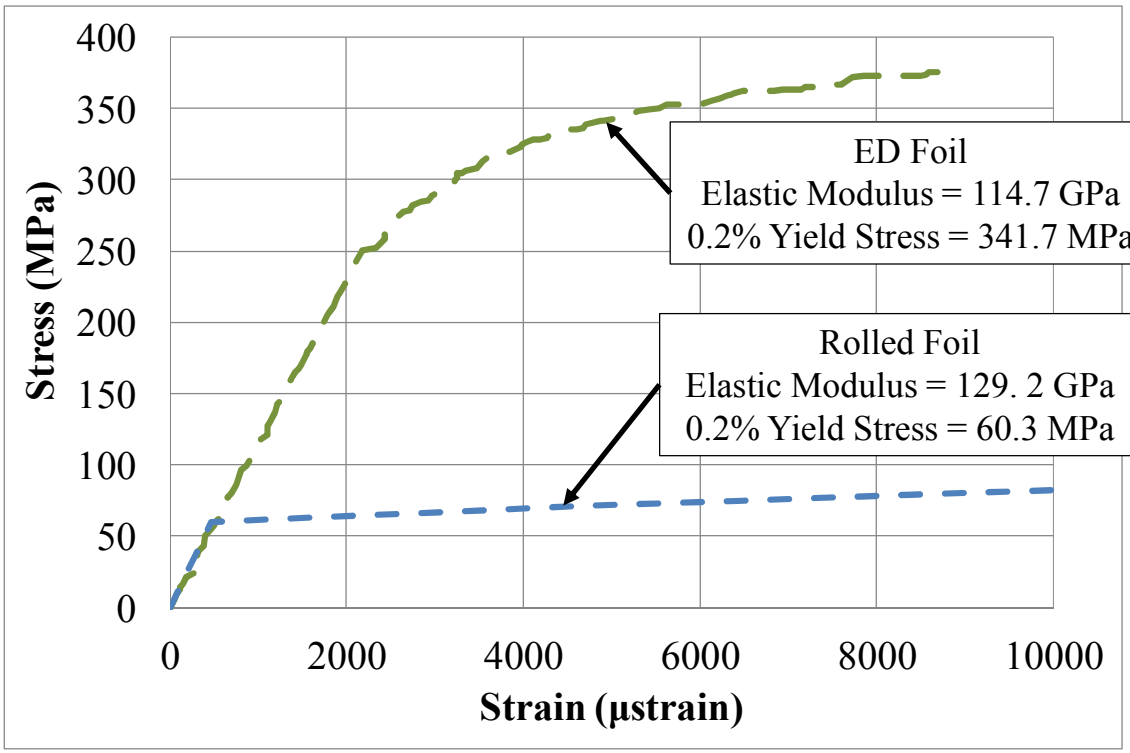

Figure 23: Stress vs. strain response for electrodeposited and rolled copper foils

As is seen in the figure, the electrodeposited copper foil exhibits a much higher yield stress as compared to the rolled copper foils. To further verify the claims made in literature regarding the differences in grain structures both the foils, samples of both the copper foils were subjected to microstructural analysis. Both the foils were potted

in a phenolic epoxy and subjected to coarse grinding (with decreasing grit sizes of SiC paper) followed by polishing (with decreasing size of diamond suspensions). The polished samples were finally etched using a 50/50 mixture of HNO3 and water to reveal the grain structures. The etched samples were then images using a scanning electron microscope. The following figures (Figure 24, Figure 25 and Figure 26) illustrate the grain structures observed in the two foils used in this study.

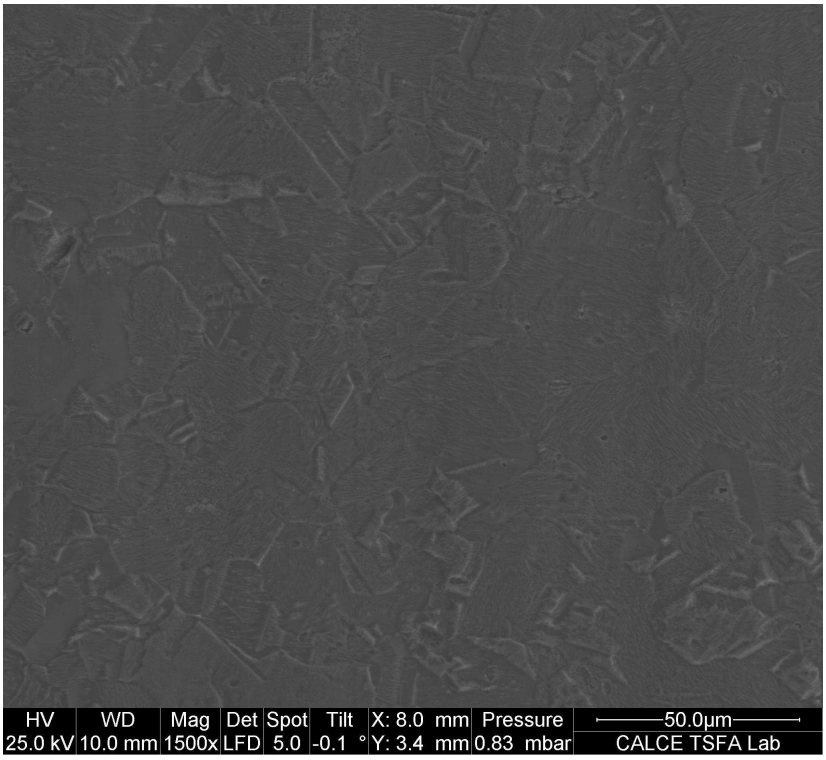

Figure 24: Rolled copper foil at 1500X magnification

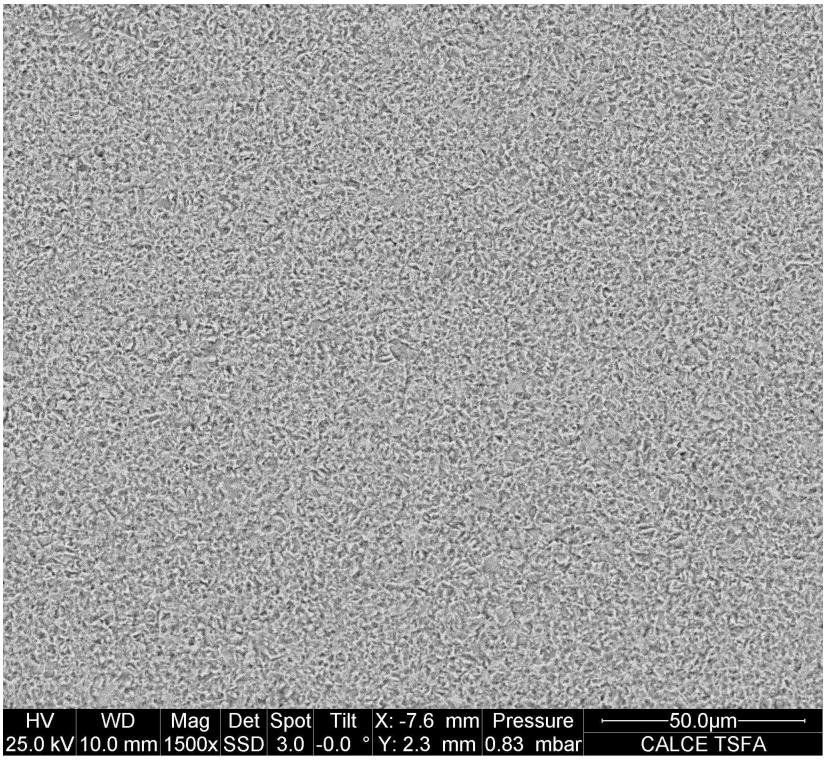

Figure 25: Electrodeposited copper foil at 1500 X magnification

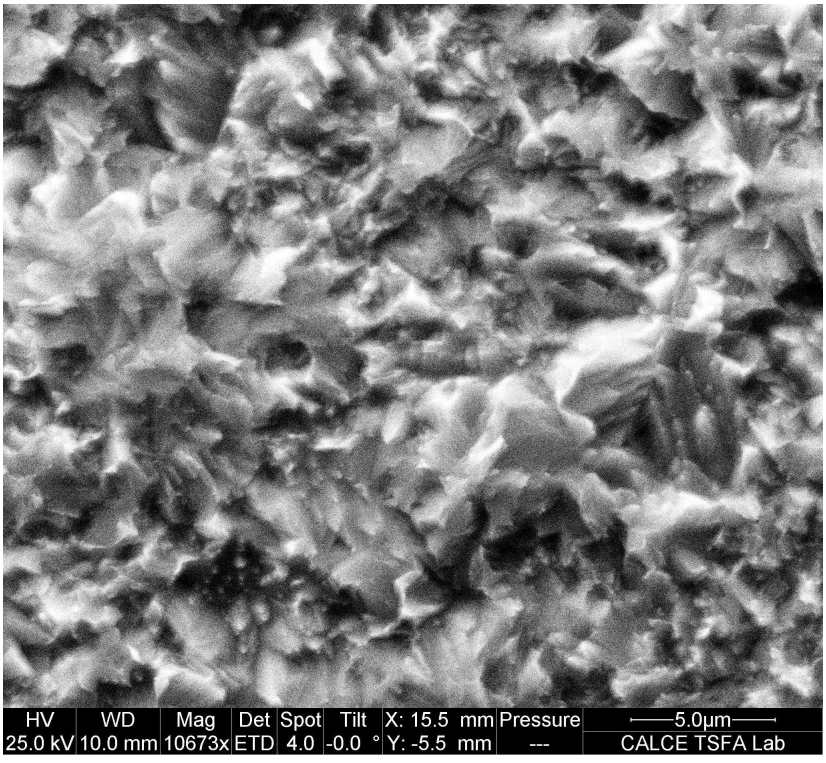

Figure 26: Electrodeposited copper foil at approx 10000X magnification

As is seen in the figure, the electrodeposited copper foils exhibit a very different surface morphology as compared to the rolled copper foils. This is in agreement with reported literature results and the impact of these differences in grain structures are evidenced by the differences in measured yield stresses seen in Figure 20. This difference in material properties has resulted in the electronics industry's use of electrodeposited copper foils in rigid printed circuit assemblies whereas the rolled copper foil materials are the choice of foils used in flexible electronics circuits (primarily as a result of the higher elongation values exhibited by the rolled copper foils). Since this study is focused on rigid electronic assemblies, the traces on the designed test vehicles were made from the same kind electrodeposited copper foils.

Chapter 3: Board Level Testing

To develop a fatigue life model for copper traces board level testing was conducted in order to generate copper trace failures on designed test boards. The boards were designed with geometric and assembly variations to quantify the impact of these variations on the fatigue durability of the copper traces. The following sections provide the details regarding the board level tests that are carried out as a part of this study.

Test Board Design

The test board was designed using the FR4 laminate and electrodeposited copper foil that was characterized in the chapter 2. The designed test board was a 12"x7"x0.063" four layer board with a 1oz (35μm) thick copper. To avoid any edge effects the traces were kept ½ inch away from the long edge of the board. As is seen in the figure (Figure 27and Figure 28) traces were designed on the both the top and bottom surfaces of the board. To monitor resistance the traces were routed using through-holes and traces routed on the inner 2 layers of the board to the pads on the short edge of the boards. The diameters of the through holes (used for routing the trace into the inner layers) were made smaller than the lowest trace width to ensure that there are no stress risers at the through-hole locations. This ensures that the copper trace failures are driven to the trace to solder pad interface.

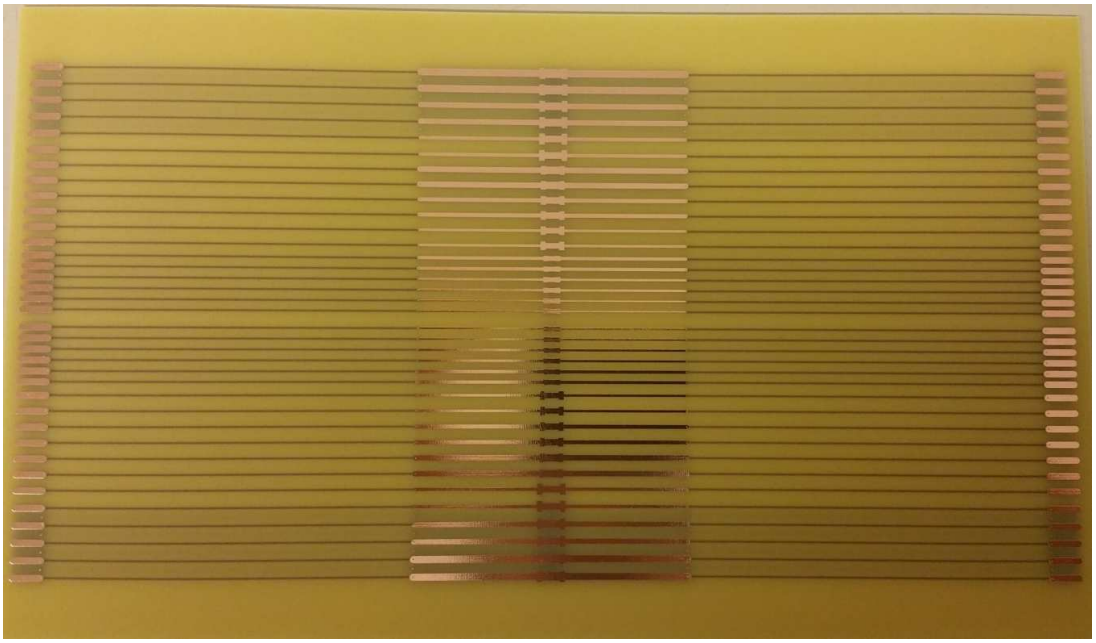

Figure 27: Top side of board

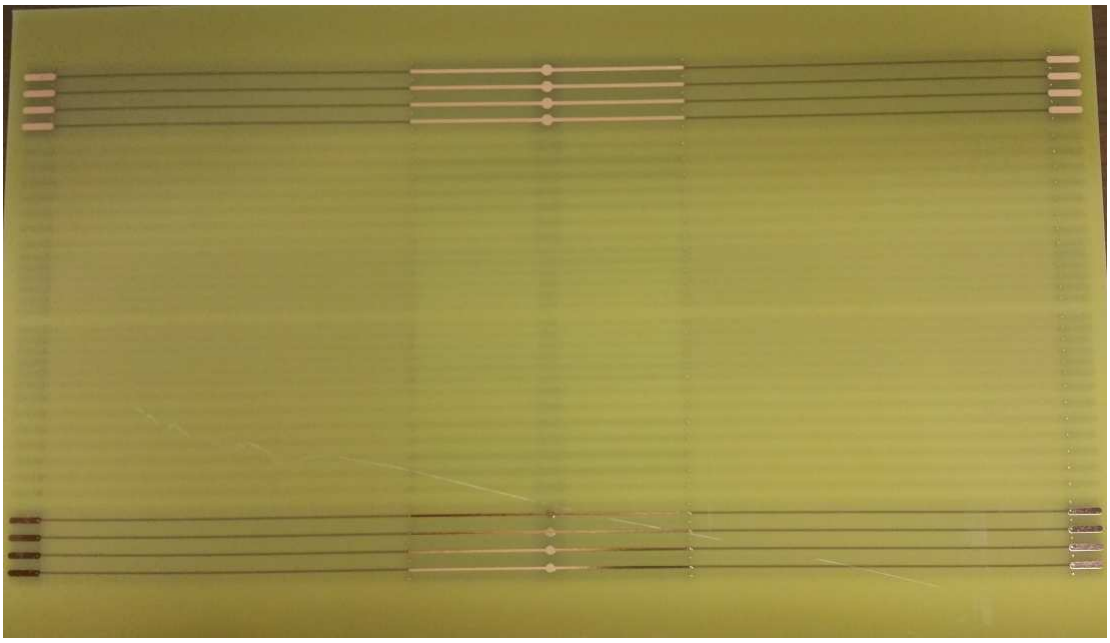

Figure 28: Bottom side of board

In order to quantify the impact of trace design variations in trace and pad geometries were designed on the test board. The design parameters that were chosen included pad and trace width as well as pad shape. The variations in trace pad design are shown in Table 7. As is seen in the table this design of test vehicle allowed for 4 samples of each geometry in a single board.

Table 7: Trace and pad design variations on test board

Pad width	Pad shape	Trace width	Number per board
125 mil	Rectangular	40 mil	4
		60 mil	4
		80 mil	4
	Circular	40 mil	4
100 mil	Rectangular	32 mil	4
		48 mil	4
		65 mil	4
	Circular	32 mil	4
62 mil	Rectangular	20 mil	4
		30 mil	4
		40 mil	4

In actual applications, the copper traces are often covered with some surface finish, the laminate is covered with a solder mask and there are assembled components on the printed circuits. In order to account for the impact of these assembly based stress risers on the fatigue life of traces, some boards were designed with an ENIG surface finish (Figure 30), some with the ENIG surface finish and a solder mask (with openings at the solder pads) (Figure 31) and some boards were assembled with chip resistors (Figure 32) along with having surface finish and solder mask.

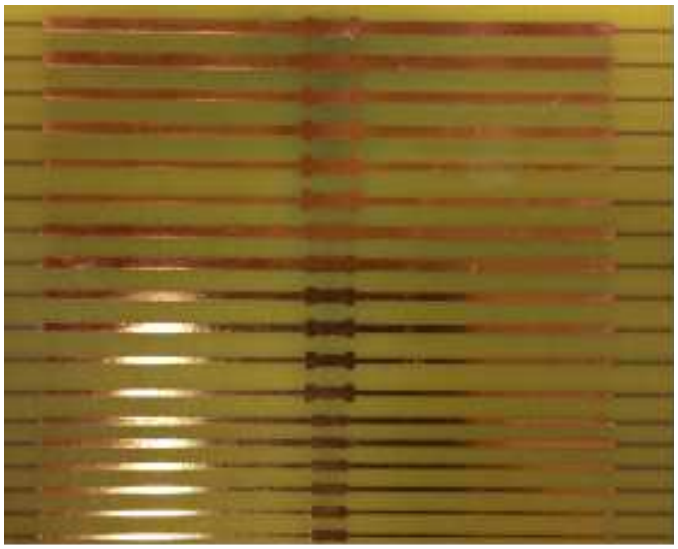

Figure 29: Bare copper board

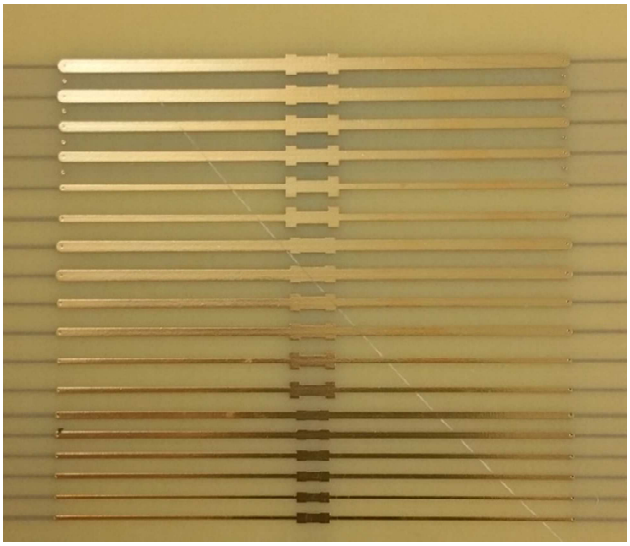

Figure 30: ENIG finished board

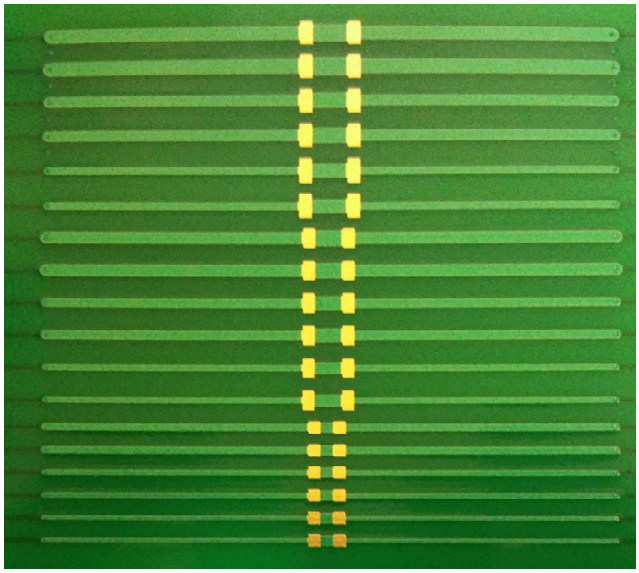

Figure 31: Solder mask covered board

Figure 32: Assembled board

The choice of the pad width was based on the sizes of resistors that were assembled on the boards which included 1206, 2010 and 2512 chip resistors. Also to ensure that the copper trace cracks were the only type of failures reported in the testing, the solder pads were shorted with a wider trace as is seen in Figure 33.

Figure 33: Shorted solder pads

Experimental Setup

A four point bend testing was conducted at a cyclic frequency of 1 Hz on the designed test boards. In a four-point bend test, the printed wiring board (PWB) is constrained between two supporting (outer) anvils and two loading (inner) anvils. The applied loading (Figure 34) results in a uniform curvature and strain on the board between the load span. This ensures that multiple samples (between the load span) can be tested at the same load level.

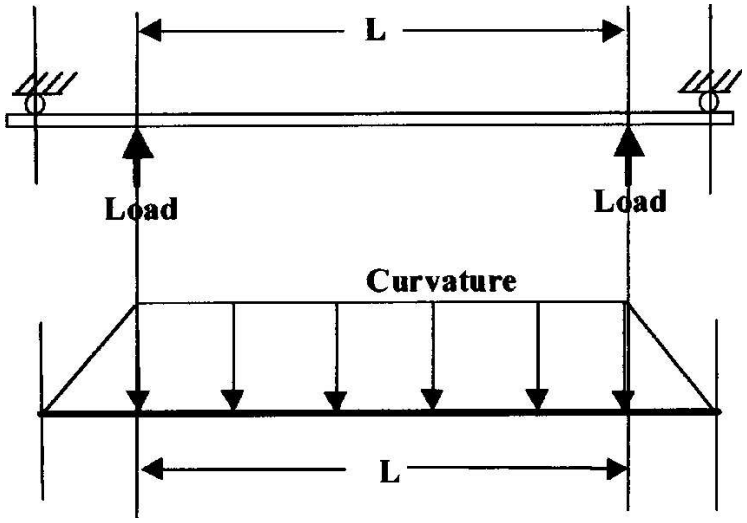

Figure 34: Schematic of four point bend test

The material characterization conducted in Chapter 2 shows that the laminate material starts yielding at 3000 μstrain amplitude. As such the maximum strain amplitude chosen for the testing was limited to 2500 μstrain to ensure that testing was conducted within the linear elastic range of the board. A general purpose hydraulic mechanical testing system was used for the purposes of this study (Figure 35).

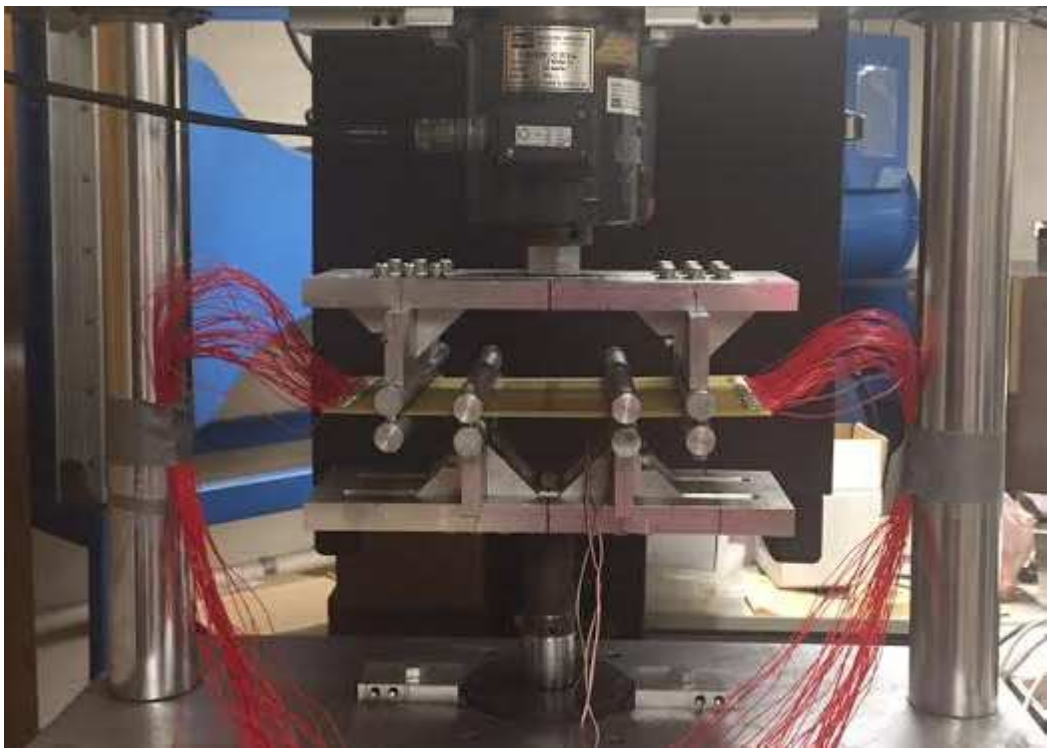

Figure 35: Four-point bend test setup

A specially designed fixture was used to enable full reversal (zero mean stress) loading of the test boards during the testing (Figure 36). This full reversal capability allows for increasing the range of loading and also negates the need for carrying out any mean stress corrections.

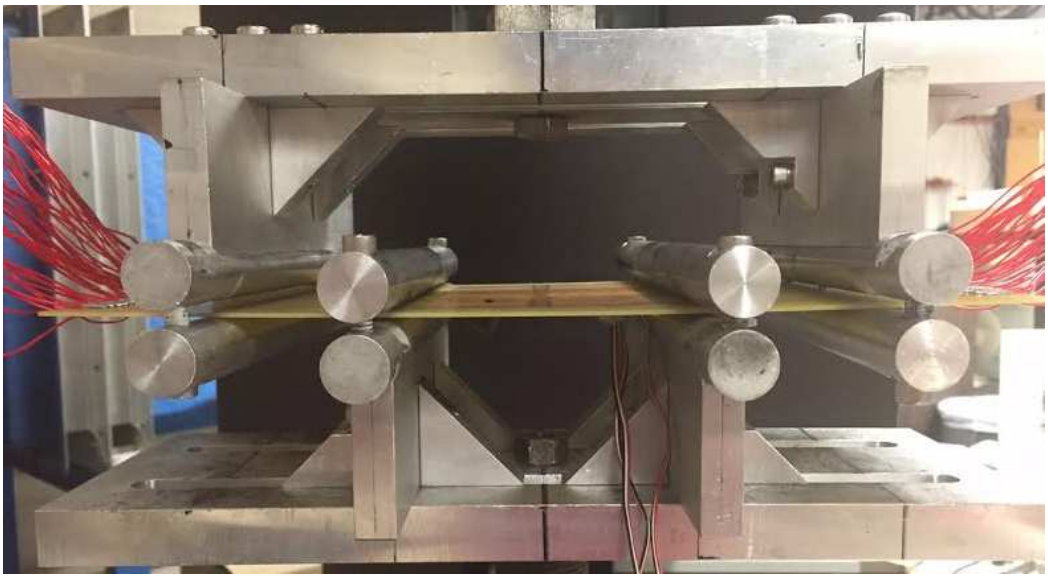

Figure 36: Fully reversible four-point bend test fixture

In order to create a spread in the durability data, tests were conducted at multiple load levels. Further to validate the fatigue life model constants determined based on the board level testing was conducted at a fourth load level. The details regarding the load levels chosen during the testing are provided in Table 8.

Table 8: Test matrix

		Updating Fatigue Life Model Constants			**Model Validation**
Board Strain Range (2 x Strain Amplitude)		**2000 (µstrain)**	**4000 (µstrain)**	**5000 (µstrain)**	**3000 (µstrain)**
Board Type	Bare Copper	2	3	3	3
	Bare Copper + ENIG Finish			3	
	Bare Copper +ENIG Finish + Solder Mask			3	
	Assembled Boards			3	

A Keysight data logger was used in conjunction with a Benchlink software to continuously monitor the resistance. Resistance was monitored continuously for individual traces throughout the test in order to detect failure. Failure was defined based on the IPC-9701 standard, which defines failure as a 20% increase in initial resistance value for at least five consecutive scans. To ensure constant testing conditions, board strain was continually measured using three strain gages attached on the board (Figure 37). Two strain gages measured the in-plane strain along the length of the board (A&B), and a third strain gage was used to measure the out of plane strain along the width of the board (C).

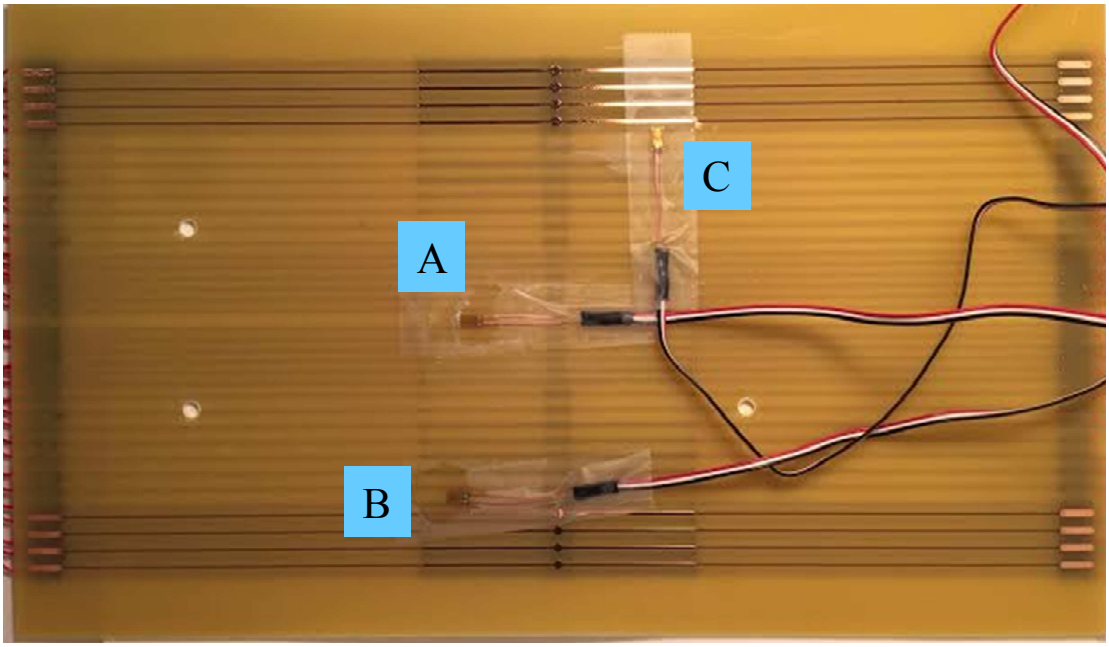

Figure 37: Location of strain gages

Board Level Testing Results

The testing was conducted until the failure criterion was satisfied for all the traces on the boards. The tested boards were the inspected under the optical microscope to detect failure sites. The failure was observed as cracks at the interface of the solder pad and trace (see figures below).

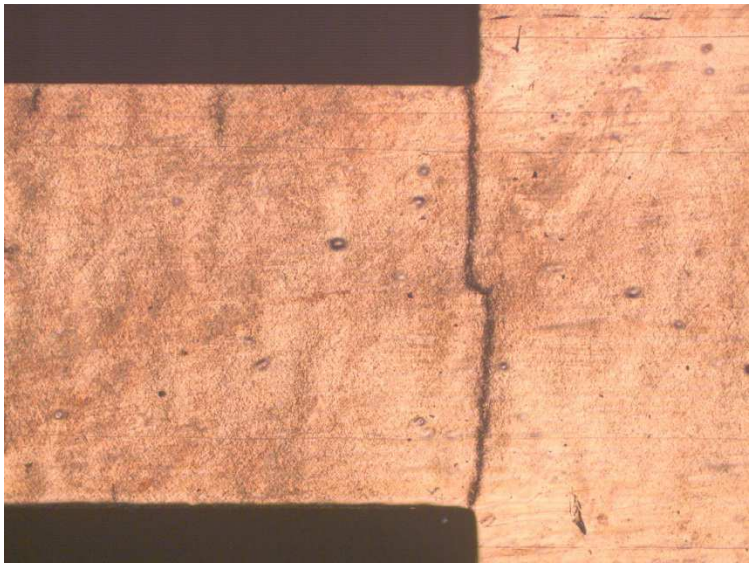

Figure 38: Trace crack observed in bare copper boards - Pad Width 125 mil - Trace Width 80 mil - Pad Shape: Rectangle - Cycles to failure 30140

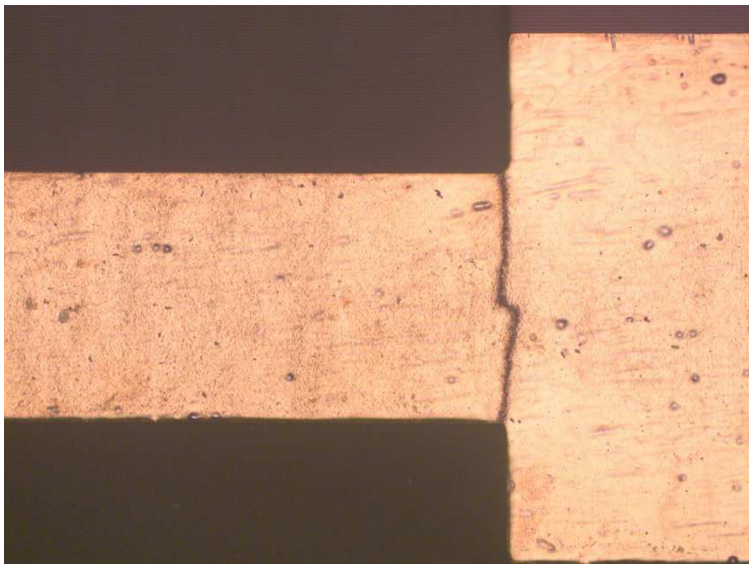

Figure 39: Trace crack observed in bare copper boards - Pad Width 100 mil - Trace Width 48 mil - Pad Shape: Rectangle - Cycles to failure 24041

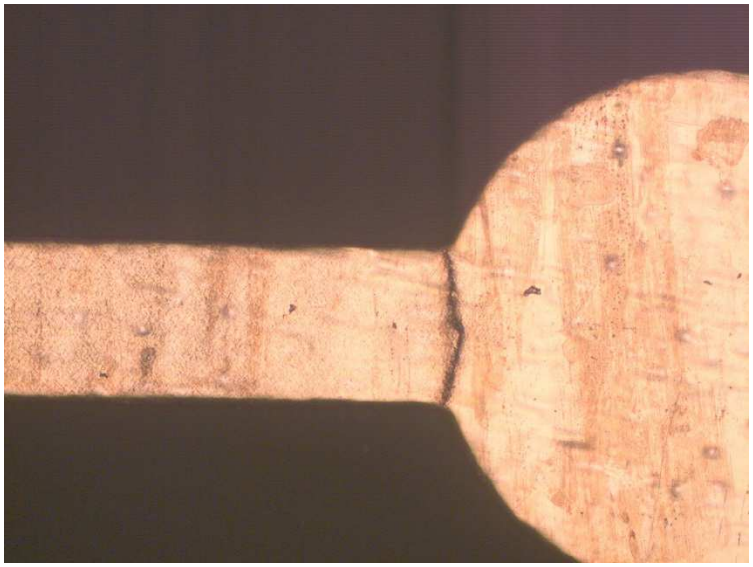

Figure 40: Trace crack observed in bare copper boards - Pad Width 100 mil - Trace Width 32 mil – Pad Shape: Circle - Cycles to failure 24041

In order to compare the impact of the different geometries and assembly variations in the test board the cycles to failure data were then fit into 2-Parameter Weibull distributions to obtain the characteristic life (η) slope (β) as well as the N50 (mean cycles to failure) life for the traces. The following sections discuss the various results obtained during the test.

Impact of Pad Width.

Three different pad widths were chosen in the test board in order to understand the impact of the pad width on the trace fatigue life. It was observed that for the same trace to pad width ratios an increase in the pad width resulted in an increase in characteristic life for the traces. Figure 41 shows an example for one pad widths are on the designed test board. The increase in characteristic life with increasing pad widths (for the same trace to pad width ratios) was observed for all three pad width ratios chosen in this study as is seen in Figure 46.

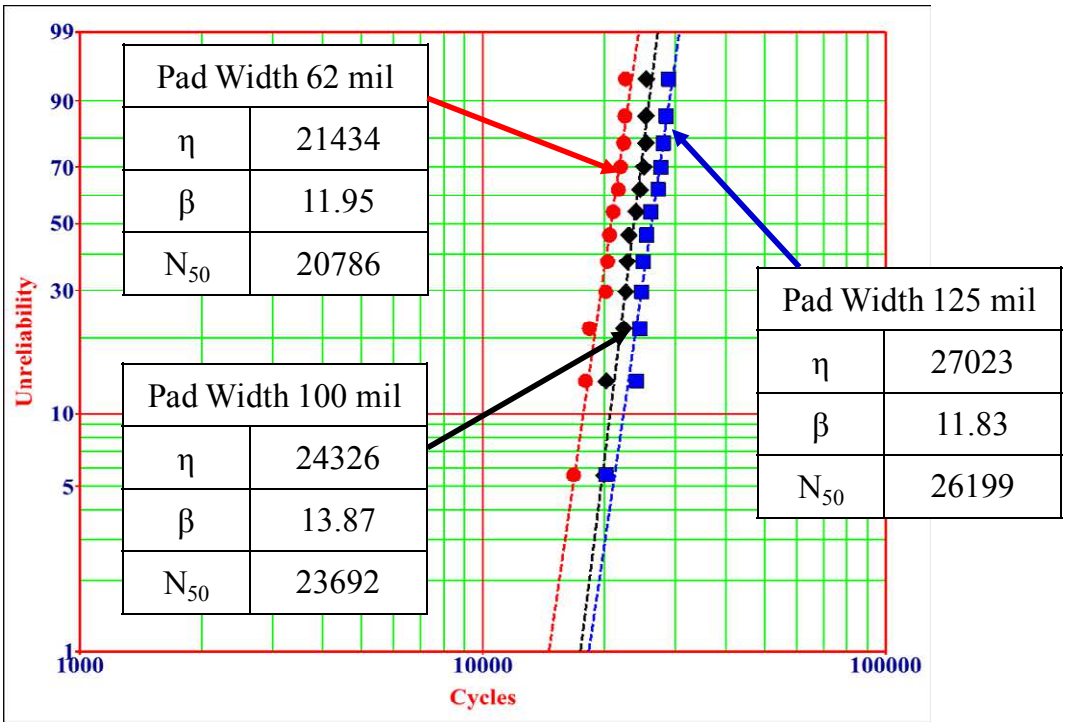

Figure 41: Two parameter Weibull distributions for board strain level: 5000 µstrain, Pad shape: rectangle and Trace to pad width ratio: 0.48

Impact of Trace Width.

For each pad width on the test board, three different trace widths were chosen. It was observed that for the same pad width an increase in the trace width resulted in an increase in characteristic life for the traces. Figure 42 shows the failure distribution of for one of the trace designs on the test board at the 5000 µstrain load level. This behavior was observed for all three pad width chosen in this study across all three load levels chosen in this study

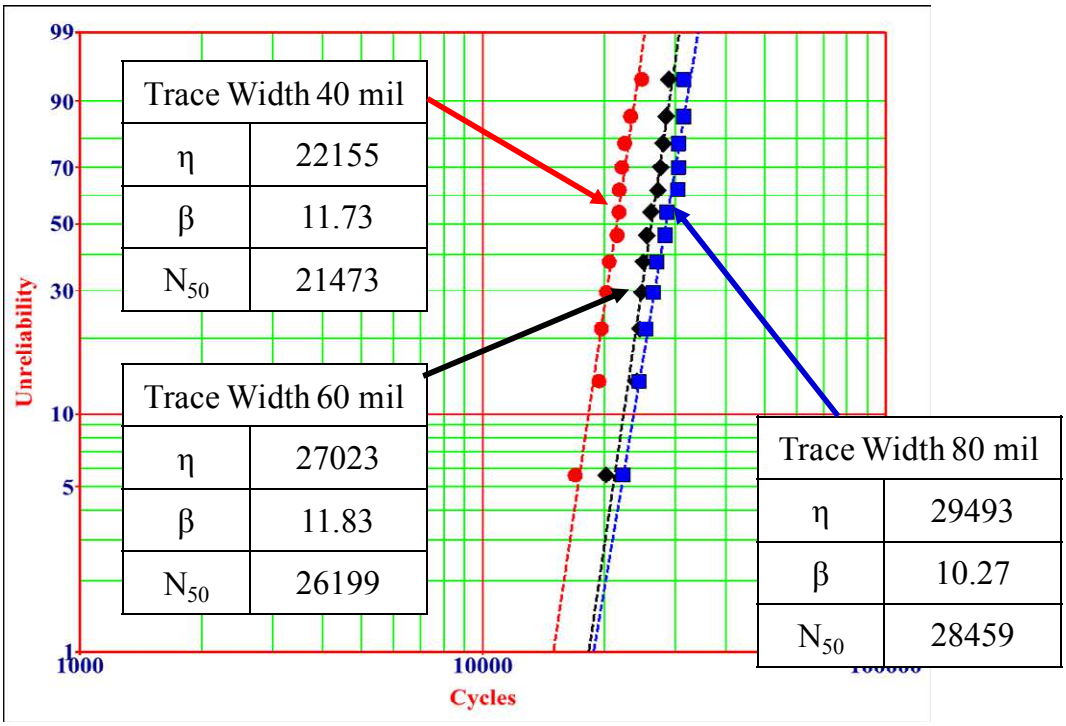

Figure 42: Two parameter Weibull distributions for board strain level: 5000 μstrain, Pad shape: rectangle and Pad Width: 125 mil

Impact of Pad Shape.

In order to understand the impact of the pad shape of the fatigue life of traces, the board design included circular pads for two pad widths (125 mil and 100 mil). It was observed that for the same trace to pad width ratio as well as the same pad width, the circular pads seems to have a lower characteristic life than the rectangular pads (for both the geometries) chosen in this study (Figure 43Figure 44). This behavior is counterintuitive to engineering knowledge and required further investigation which will be discussed in CHAPTER 4.

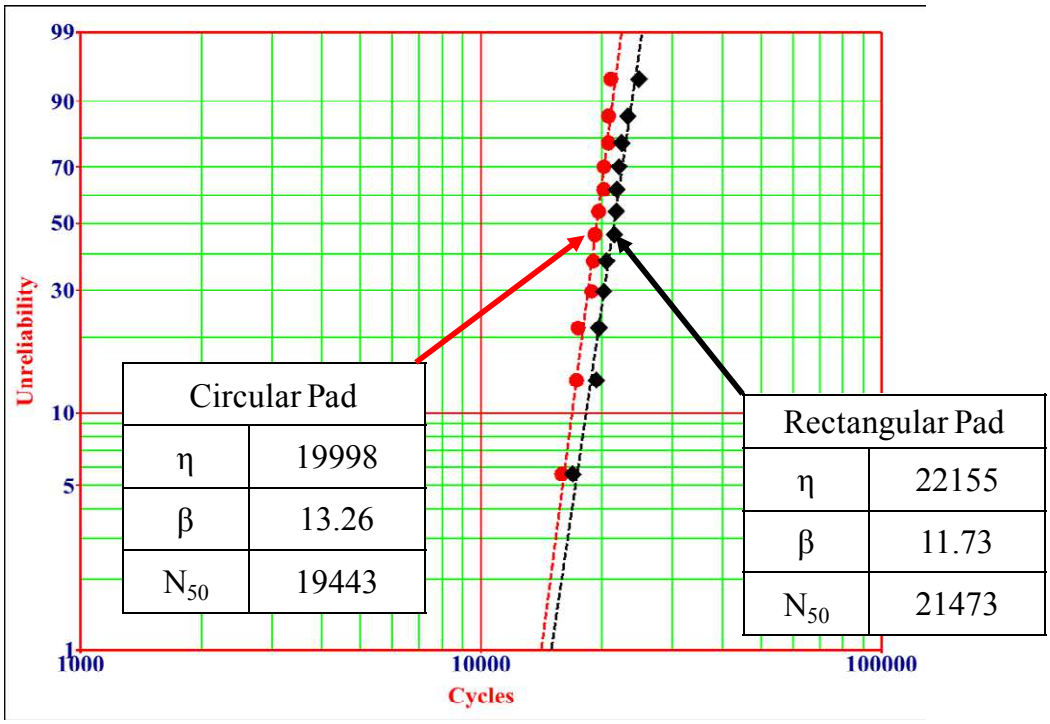

Figure 43: Two parameter Weibull distributions for board strain level: 5000 µstrain, Trace Width 40 mil and Pad Width: 125 mil

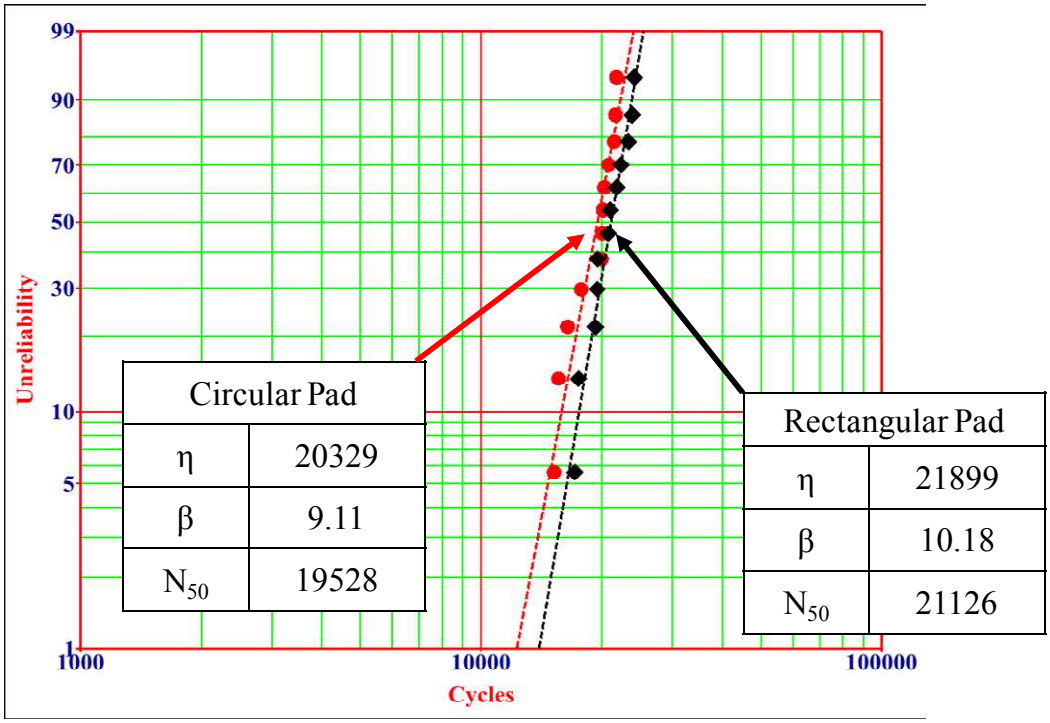

Figure 44: Two parameter Weibull distributions for board strain level: 5000 µstrain, Trace Width 32 mil and Pad Width: 100 mil

Summary of Bare Copper Failure Data

As discussed earlier there were three different loads that were used for generating failure data for determining the fatigue life model constants. The following tables (Table 9,Table 10 and Table 11)exhibit the failure statistics obtained from the experiments conducted in this study.

Table 9: Failure Statistics for board strain level: 5000 µstrain

Pad Width (mil)	Pad Shape	Trace Width (mil)	Failure Statistics		
			β	Characteristic Life (η) (cycles)	N50 (cycles)
125	Rectangular	40	11.73	22155	21473
		60	11.83	27023	26199
		80	10.27	29493	28459
	Circular	40	13.26	19998	19443
100	Rectangular	32	10.18	21899	21126
		48	13.87	24326	23692
		65	10.69	27822	26884
	Circular	32	9.11	20329	19528
62	Rectangular	20	12.38	16835	16150
		30	11.95	21434	20786
		40	9.34	25342	24367

Table 10: Failure Statistics for board strain level: 4000 µstrain

Pad Width (mil)	Pad Shape	Trace Width (mil)	Failure Statistics		
			β	Characteristic Life (η) (cycles)	N50 (cycles)
125	Rectangular	40	10.56	49597	47905
		60	9.87	61154	58925
		80	10.58	68049	65733
	Circular	40	10.28	44339	42786
100	Rectangular	32	9.95	49862	48059
		48	12.33	53994	52412
		65	8.09	60837	58141
	Circular	32	11.89	42687	41391
62	Rectangular	20	8.73	36580	35641
		30	9.49	48511	46676
		40	8.47	57377	54946

Table 11: Failure Statistics for board strain level: 2000 µstrain

Pad Width (mil)	Pad Shape	Trace Width (mil)	Failure Statistics		
			β	Characteristic Life (η) (cycles)	N50 (cycles)
125	Rectangular	40	6.78	1034651	980229
		60	5.19	1217986	1134924
		80	5.29	1491723	1391848
	Circular	40	5.82	838149	786983
100	Rectangular	32	6.17	972553	916430
		48	5.19	1165563	1086079
		65	6.16	1381745	1301975
	Circular	32	5.16	821945	765119
62	Rectangular	20	5.14	673317	627023
		30	5.84	926403	870058
		40	6.63	1097138	1038151

Impact of Assembly Variations.

In actual applications the copper traces are often covered with some surface finish, the laminate is covered with a solder mask and there are assembled components on the printed circuits. When these variations were introduced into the designed boards, there were changes introduced into the failure distribution observed for the traces.

Impact of Surface Finish.

As discussed in, some of the test boards were manufactured with a surface finish of electroless nickel immersion gold (ENIG). The surface finish thickness is approximately 5μm ($1/7^{th}$ the thickness of the copper foil used for making the traces). These boards were tested at the 5000 μm board strain range level. Figure 45 shows the impact of surface finish on one of the chosen trace geometries in the test. As is seen in the Figure 46 the surface finish seems decrease the cycles to failures observed during the test by a small amount across all the . Table 12 also provides the complete failure statistics for all the trace geometries chosen in this study.

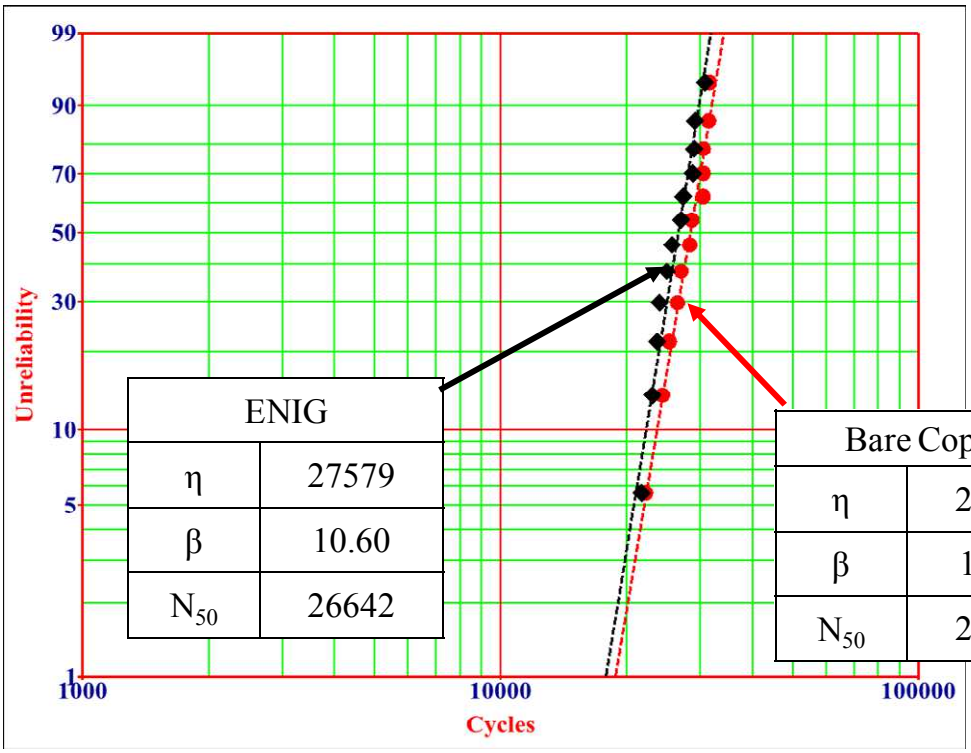

Figure 45: Comparison of ENIG finished and bare copper boards for board strain level: 5000 μstrain, pad shape: rectangle, pad width 125 mil and trace width 80 mil.

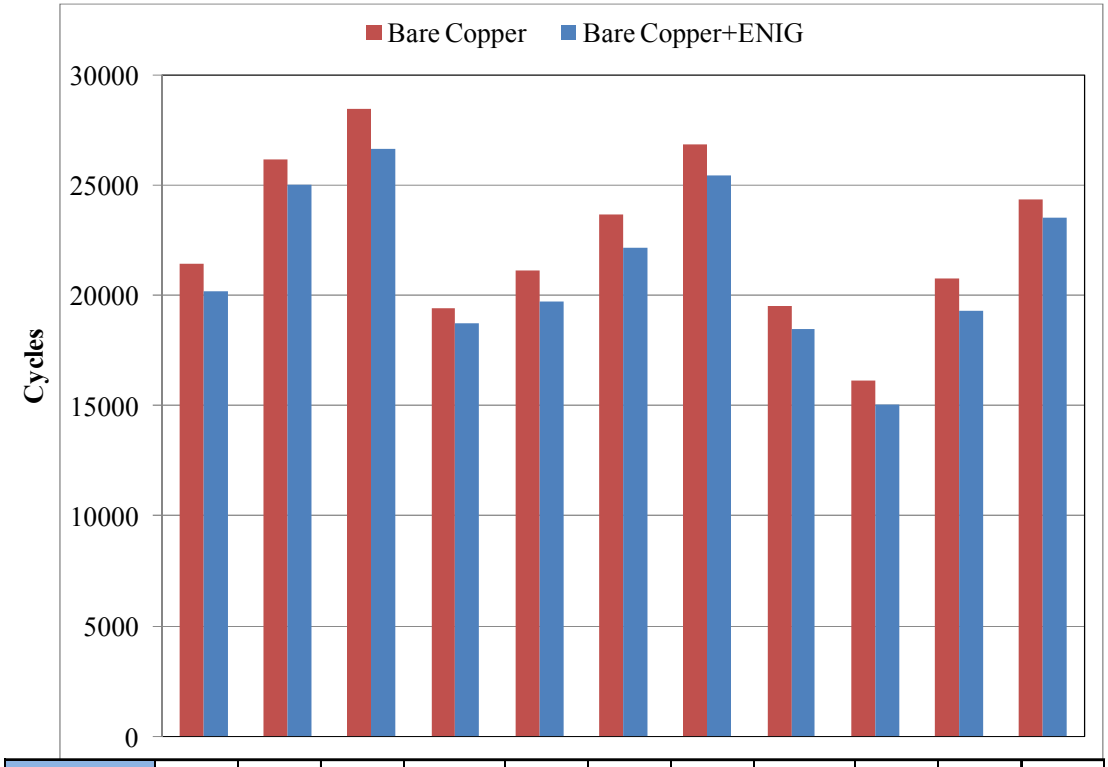

Trace Width (mil)	40	60	80	40	32	48	65	32	20	30	40
Pad Shape	Rectangular			Circular	Rectangular			Circular	Rectangular		
Pad Width (mil)	125				100				62		

Figure 46: Comparison of Cycles to N50 failure for all trace geometries for board strain level: 5000 µstrain (bare copper vs. ENIG finished boards)

Table 12: Failure Statistics for board strain level: 5000 μstrain for ENIG surface finished boards

Pad Width (mil)	Pad Shape	Trace Width (mil)	Failure Statistics		
			β	Characteristic Life (η) (cycles)	N50 (cycles)
125	Rectangular	40	9.86	20960	20195
		60	11.67	25839	25041
		80	10.60	27579	26642
	Circular	40	12.68	19292	18742
100	Rectangular	32	10.70	20397	19710
		48	11.02	22942	22192
		65	10.12	26418	25479
	Circular	32	9.29	19204	18461
62	Rectangular	20	10.37	15599	15057
		30	11.53	19930	19307
		40	9.89	24431	23543

Impact of Solder Mask

In order to understand the impact of the solder mask, some boards were also manufactured with a solder mask coated over surface finished copper traces. As is seen in (Figure 47) the solder mask is applied on the traces but leaves an opening at the solder pad. This results in a stress riser (resulting from a geometric discontinuity) at the interface of the trace and solder pad.

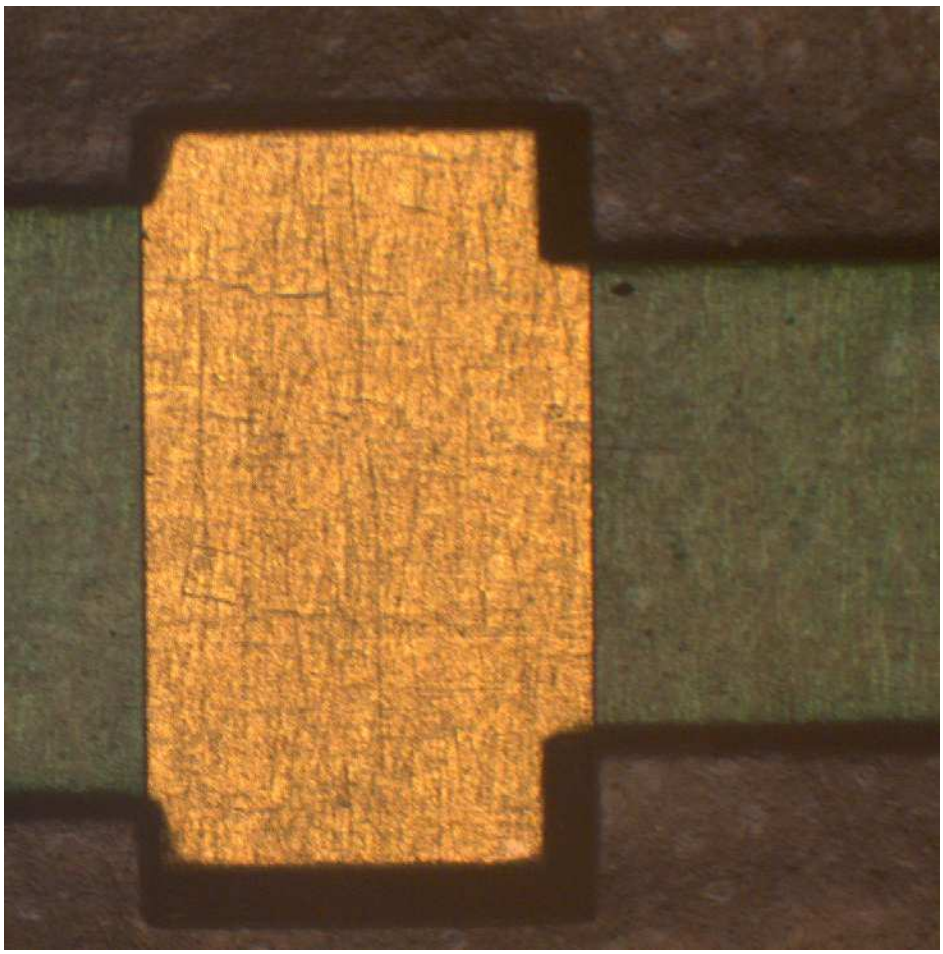

Figure 47: Solder mask finished board

The additional stress at the interface of the solder pad and trace interface results in the decreased cycles to failure observed during the test. Figure 48 shows the impact of the solder mask (over surface finish) on the failure distributions of one of the chosen trace geometries in the test. A similar behavior is observed for all trace and pad geometries on the designed test boards (Figure 49). The complete failure statistics for the solder mask (over ENIG surface finish) boards are provided in Table 13. Despite the decrease in cycles to failure seen, the cracking observed is similar to the cracks observed in the bare copper boards (Figure 50).

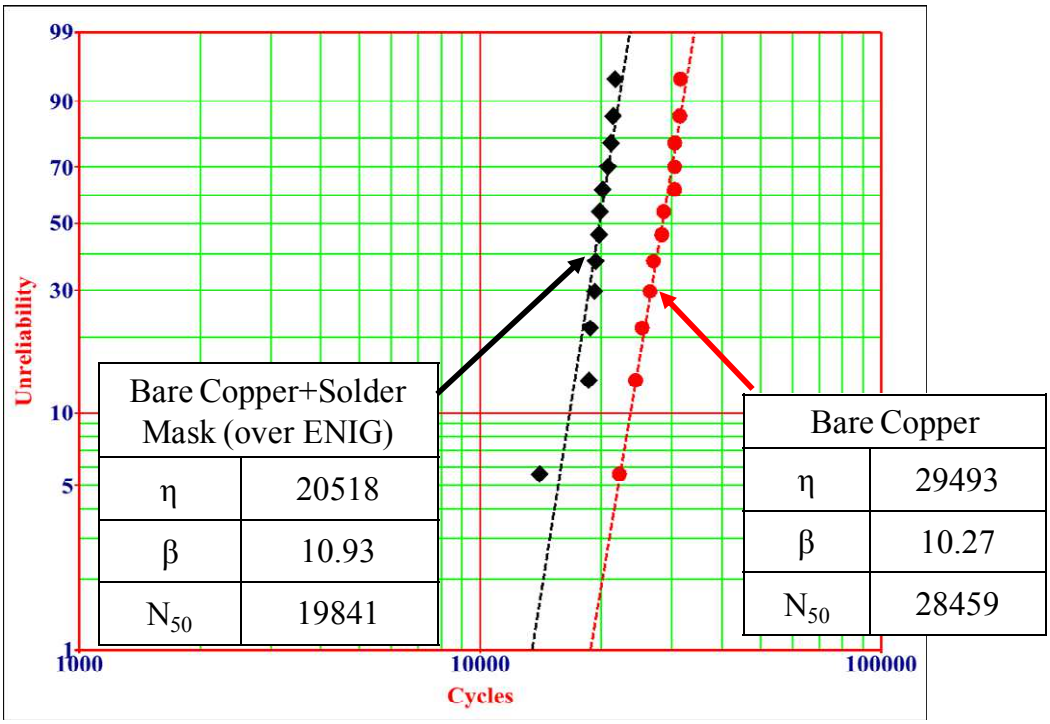

Figure 48: Comparison of solder masked boards and bare copper boards for board strain level: 5000 µstrain, Pad shape: rectangle, Pad width 125 mil and Trace width 80 mil.

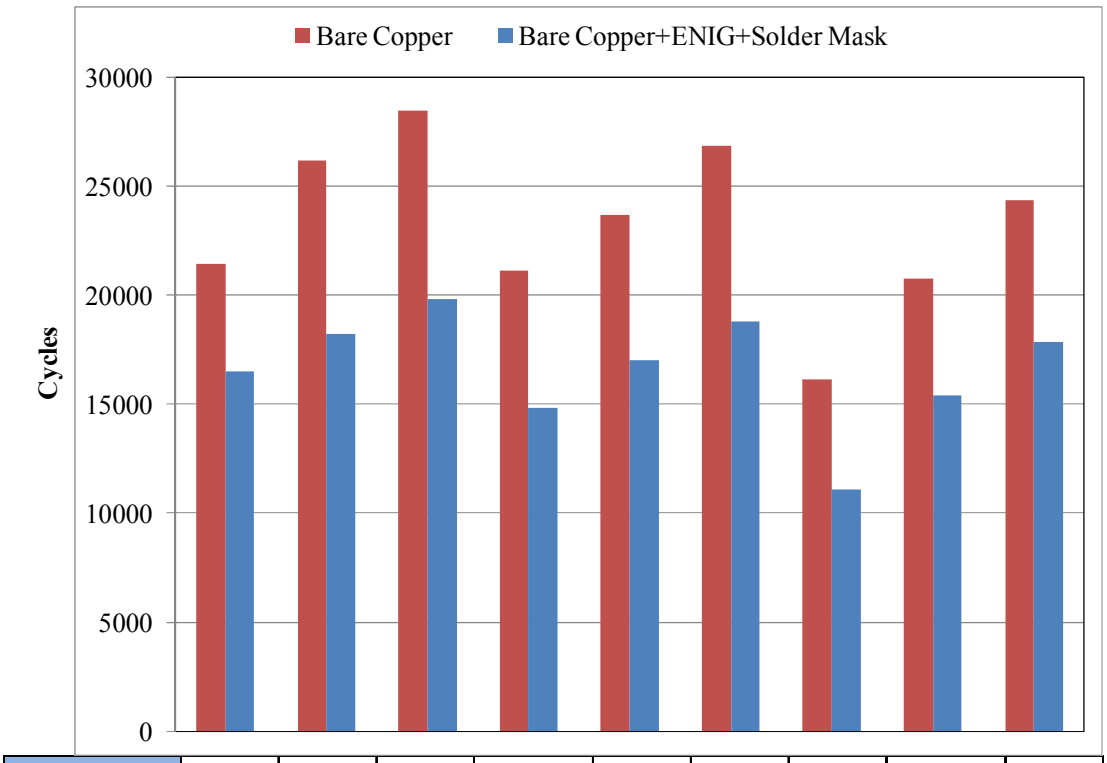

Trace Width (mil)	40	60	80	32	48	65	20	30	40
Pad Shape	Rectangular			Rectangular			Rectangular		
Pad Width (mil)	125			100			62		

Figure 49: Comparison of Cycles to N50 failure for all trace geometries for board strain level: 5000 µstrain (Bare copper vs. Solder masked boards)

Table 13: Failure Statistics for board strain level: 5000 µstrain for solder masked boards

Pad Width (mil)	Pad Shape	Trace Width (mil)	Failure Statistics		
			β	Characteristic Life (η) (cycles)	N50 (cycles)
125	Rectangular	40	11.41	16001	16493
		60	9.79	18933	18238
		80	10.93	20518	19841
100	Rectangular	32	12.93	15269	14842
		48	12.71	17504	17007
		65	10.38	19448	18773
62	Rectangular	20	9.41	11543	11102
		30	11.52	15909	15411
		40	9.94	18555	17883

Figure 50: Trace cracking in solder masked boards

Impact of Assembled Components

In order to understand the fatigue behavior of the copper traces on assembled boards some boards (with solder mask over ENIG) were assembled with resistor components. Three different resistors were used in this study that included a 2512, 2010 and a 1206 chip resistor. The copper traces on the boards assembled with resistors exhibited a reduced fatigue life. The presence of a soldered component further increases the stain at the interface of the trace and the solder pad resulting in a decreased cycles to failure observed in the test. Figure 51 shows that impact of the component assembly on the failure distribution of one of the chosen trace geometries in the test. A similar behavior is observed for all trace and pad geometries on the designed test boards (Figure 52). The complete failure statistics for the solder mask (over ENIG surface finish) boards are provided in Table 14. Figure 53 shows the cracking observed in the traces.

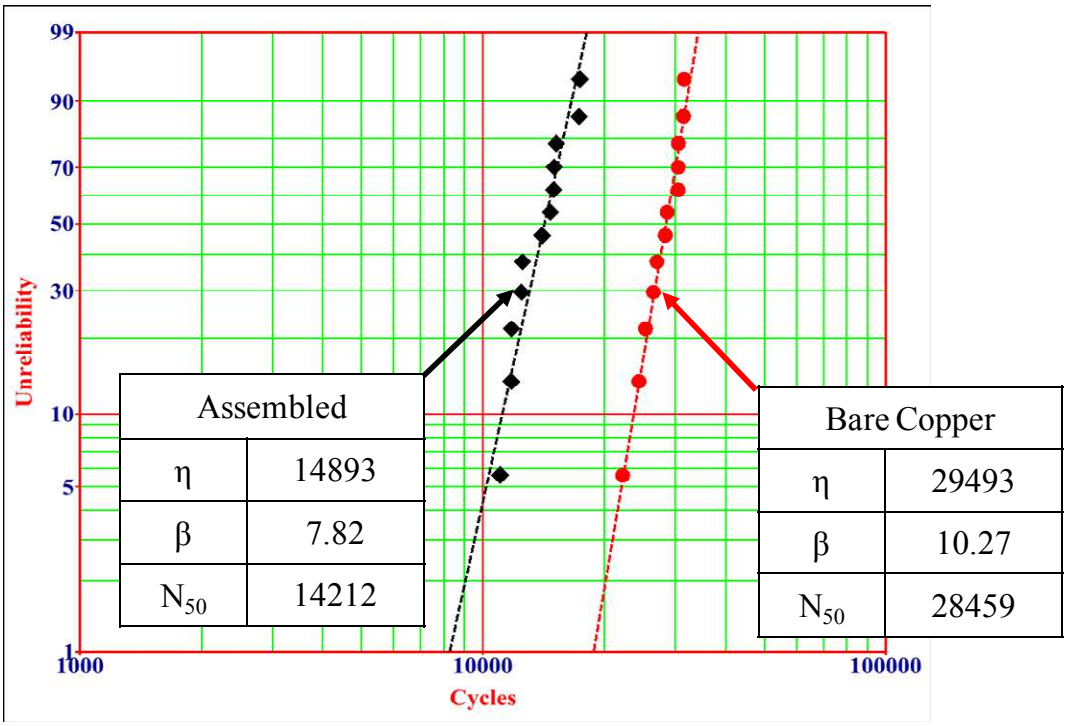

Figure 51: Comparison of solder masked boards and bare copper boards for board strain level: 5000 µstrain, Pad shape: rectangle, Pad width 125 mil and Trace width 80 mil.

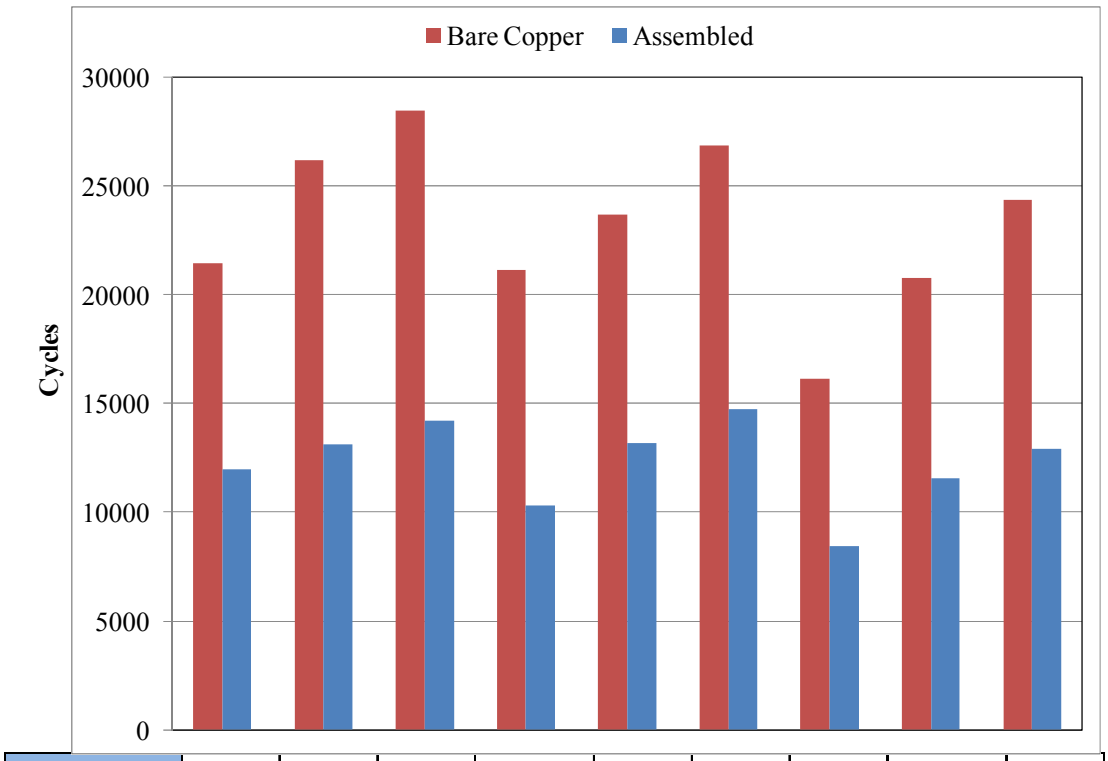

Trace Width (mil)	40	60	80	32	48	65	20	30	40
Pad Shape	Rectangular			Rectangular			Rectangular		
Pad Width (mil)	125			100			62		

Figure 52: Comparison of Cycles to N50 failure for all trace geometries for (board strain level: 5000 µstrain Bare copper vs. assembled boards)

Table 14: Failure Statistics for board strain level: 5000 µstrain for assembled boards

Pad Width (mil)	Pad Shape	Trace Width (mil)	Failure Statistics		
			β	Characteristic Life (η) (cycles)	N50 (cycles)
125	Rectangular	40	8.73	12475	11962
		60	8.02	13743	13130
		80	7.82	14893	14212
100	Rectangular	32	8.55	10788	10335
		48	8.47	13734	13153
		65	7.28	15520	14758
62	Rectangular	20	7.44	8852	8427
		30	7.13	12152	11544
		40	7.92	13550	12937

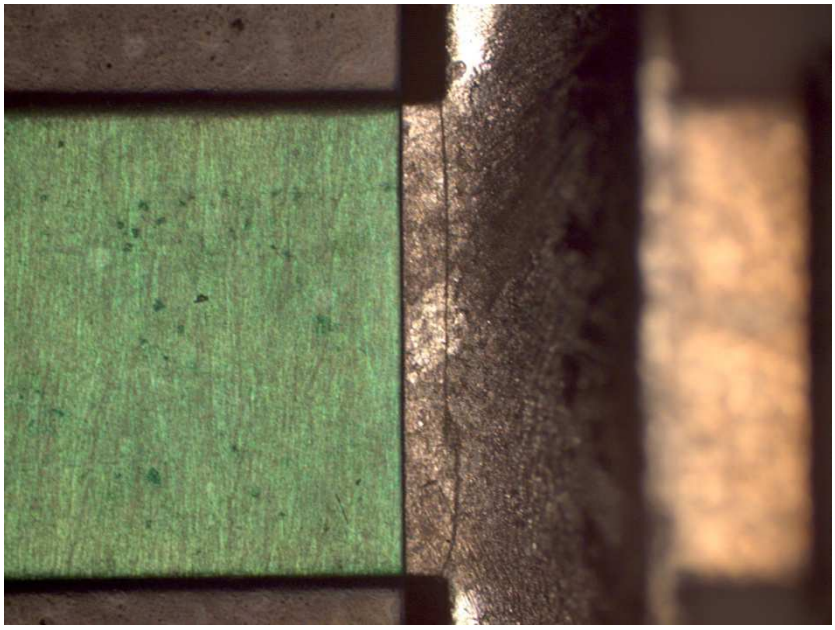

Figure 53: Trace cracking in assembled boards

Chapter 4: Trace Fatigue Life Modeling

A generalized strain-based fatigue model is proposed, to characterize the fatigue durability of the copper traces. A finite element modeling approach is used to evaluate the volume averaged trace strain values at the failure sites observed during the testing discussed in Chapter 3. The results from only the bare copper boards were used for determining the model constants for the trace fatigue life model as the fatigue model is material level model. As such the finite element modeling was conducted only for the bare copper boards. The following sections discuss the finite element modeling approach as well as the determined model constants for the strain based trace fatigue life model.

Finite Element Modeling

A 'global/local' finite element approach using a commercial solver (ABAQUS) was used to simulate the four-point bend experiments conducted in this study. The 'global' model was developed using a coarse mesh and the details regarding the trace and pad geometries were not included in this model for achieving computational efficiency. Further to replicate the actual boundary conditions of the experiment the loading anvils were modeled as rigid bodies in the 'global' finite element model and used for applying the strains observed during the testing (Figure 54).

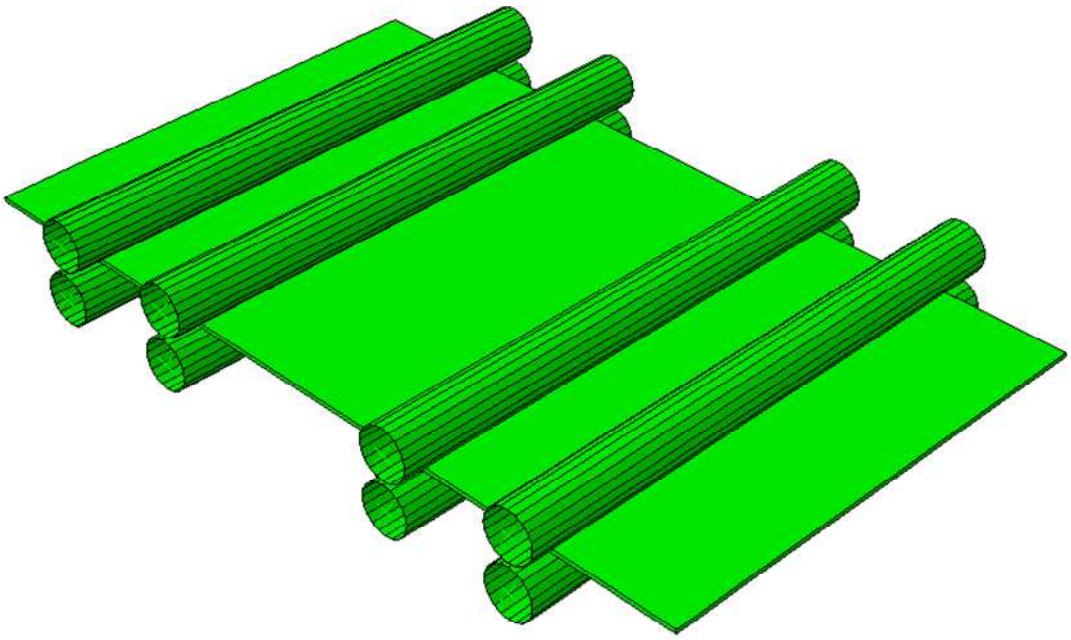

Figure 54: Global finite element model of test

The material model for the board was considered to be linear elastic as the experiments were conducted within the elastic limits of the laminate material. The modulus used for the finite element (in the two planar directions) was obtained from the material characterization of the laminate material conducted in Chapter 2 (Table 5). Typically the cyclic strain ranges do not stabilize until the second or third cycles. To ensure stability in the cyclic stress and strain ranges, the 'global' model was simulated for four cycles (see Figure 55).

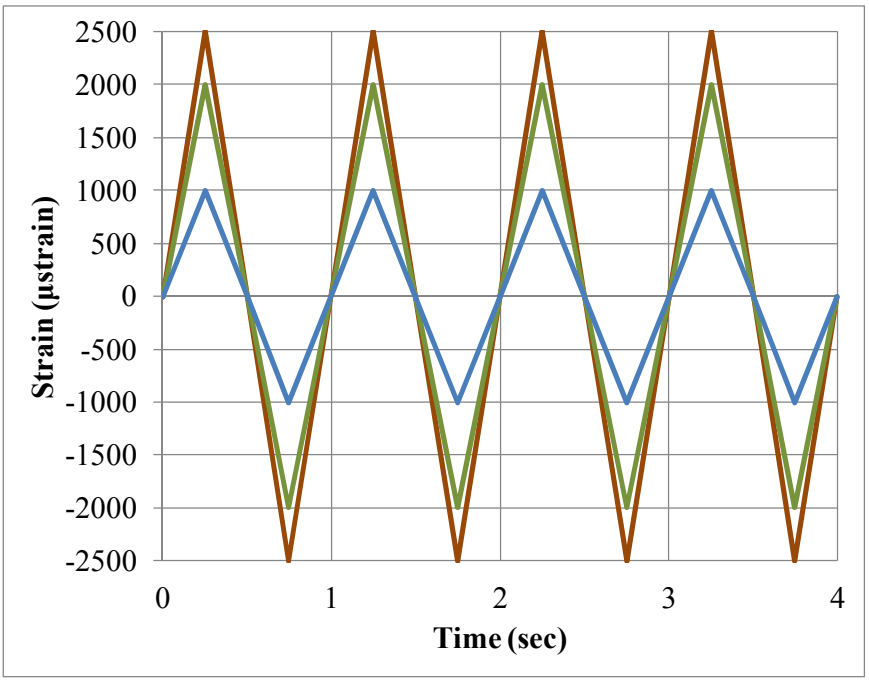

Figure 55: Strain profiles used for simulation

The results from the global modeling (see Figure 56) were used to extract the boundary conditions for a 'local' model. The displacements at the boundaries of the local domain were monitored in the global model and applied to the local model as a boundary condition. The local model included the details of the trace and pad geometries used in the testing.

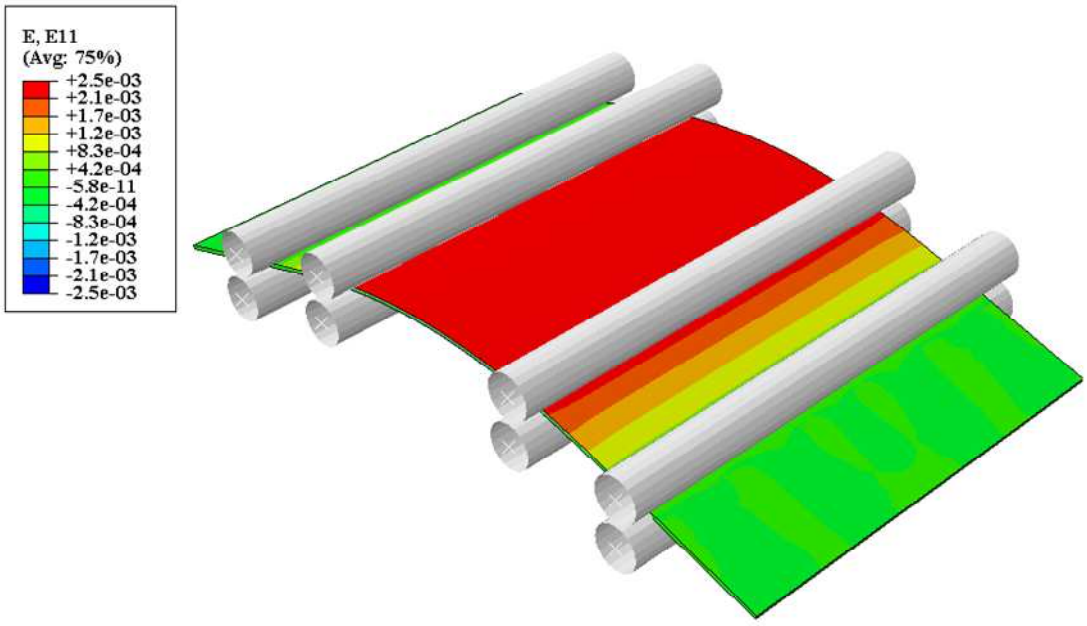

Figure 56: In-plane strain of the global model at maximum displacement

The copper was model as an elastic-plastic material in the 'local' model with the stress-strain response obtained from the characterization study conducted in Chapter 2. 'Local' models were developed for each variation in geometry on the test board (see example in Figure 57).

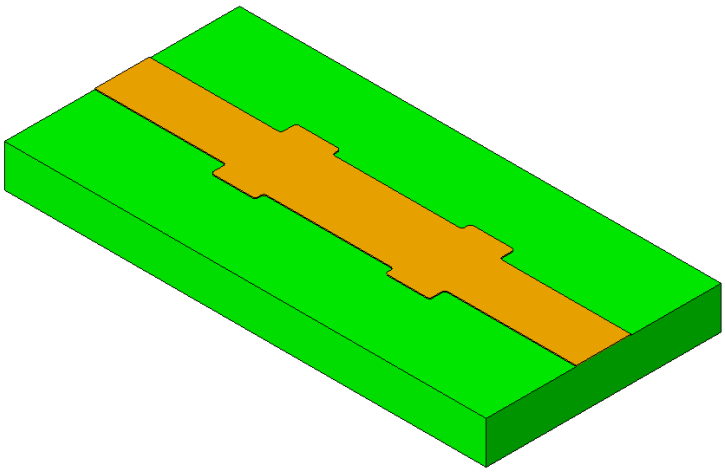

Figure 57: Local model for pad shape: rectangle, pad width 125 mil and trace width 80 mil

First a mesh convergence study was conducted to minimize the error energy for the four point bend experiment. A mesh with much finer densities near the critical cross section of the trace (Figure 58) was then used to solve each of the individual local models

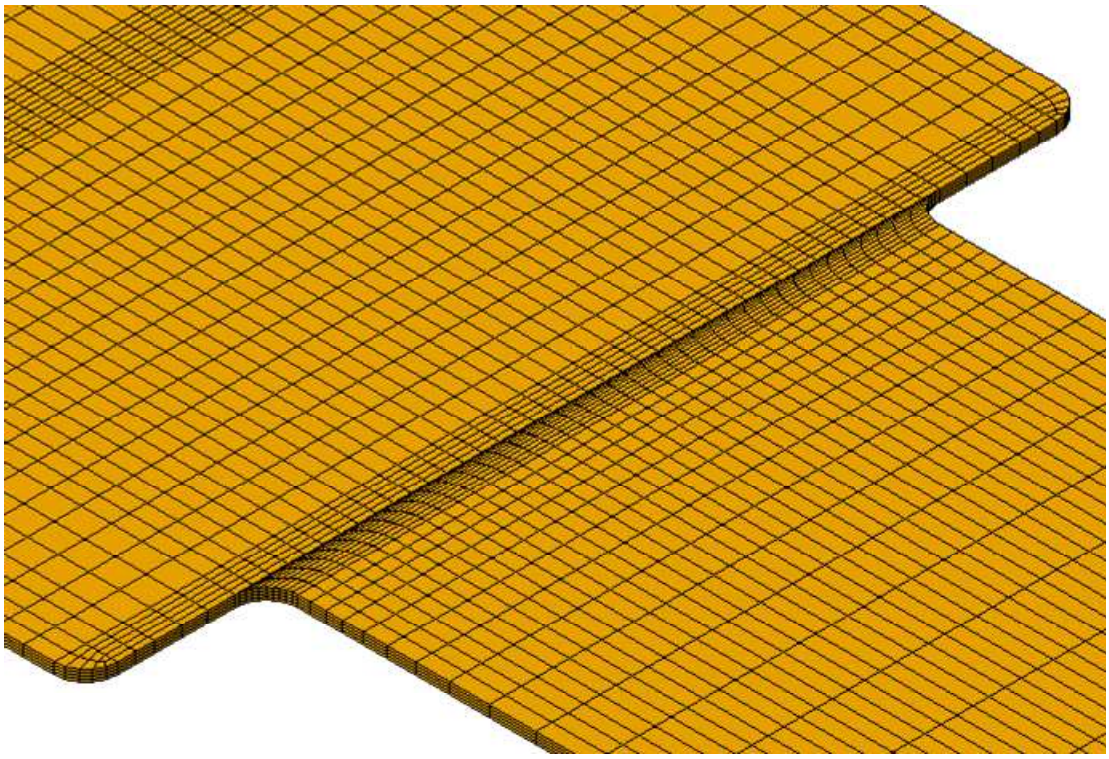

Figure 58: Fine mesh in near trace to pad interface for pad shape: rectangle, pad width 125 mil and trace width 80 mil

The strain and stress in the trace is averaged over the critical cross-section (see Figure 59) that experiences fatigue failure using a 'volume-weighted average' in order to avoid any non-uniformities between the elements. The volume-weighted average is found by first finding the fraction of the total cross-section's volume that belongs to the element. Next, the centroidal value of the results data of interest is multiplied by this volume fraction. This sum of each of these for all the elements of the region being investigated gives the volume weighted average.

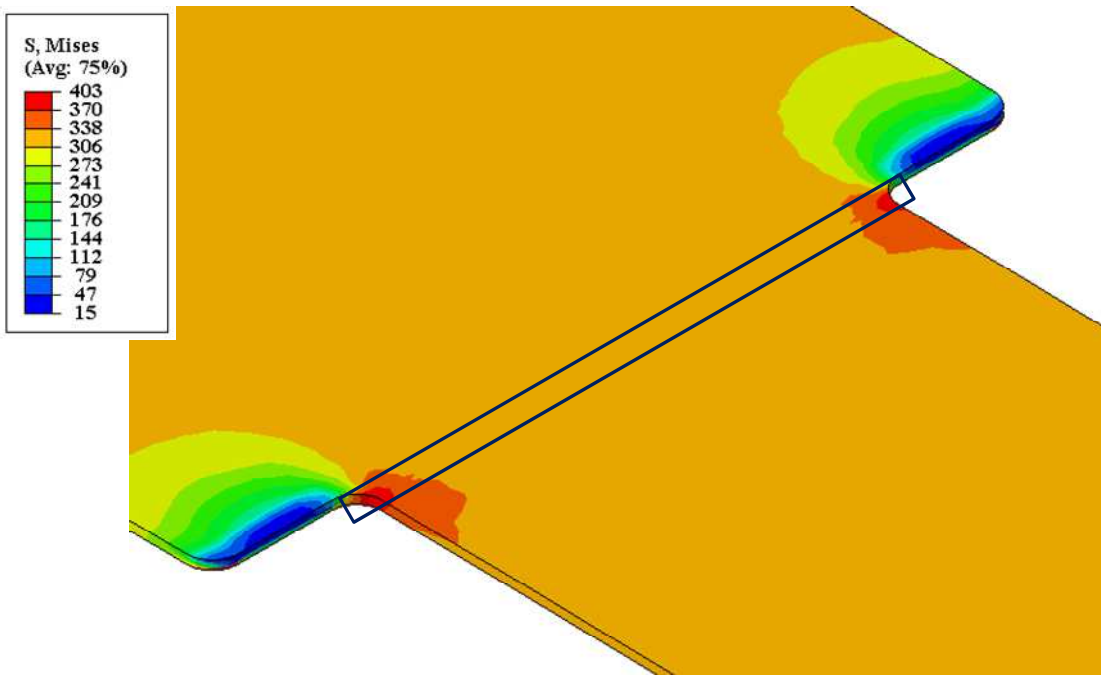

Figure 59: Mises stress contour plot indicating critical cross section of trace for pad shape: rectangle, pad width 125 mil and trace width 80 mil

A stress-strain hysteresis plot was then developed for each of the geometric variations in traces on the test board (see example Figure 60). The volume-weighted average' cyclic strain range in the critical trace region was evaluated from the hysteresis loop obtained from the fourth cycle of loading of the 'local' model. These cyclic strain ranges are reported in Table 15.

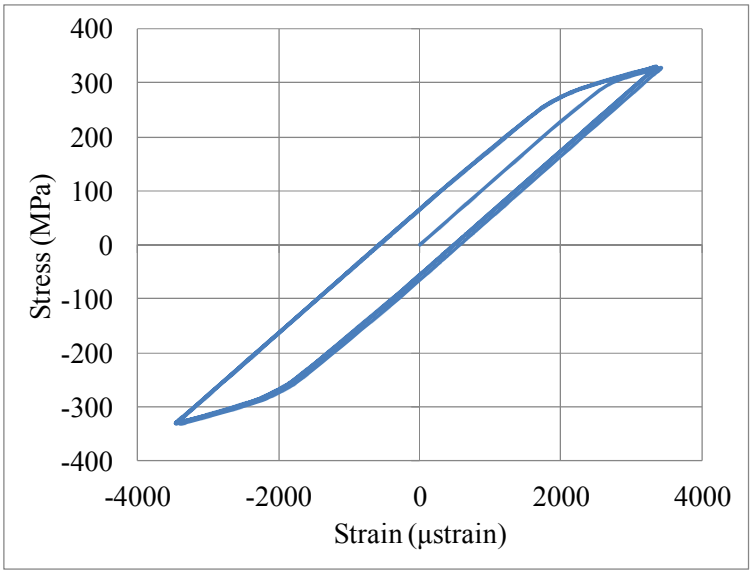

Figure 60: Volume-weighted average cyclic stress-strain hysteresis for pad shape: rectangle, pad width 125 mil and trace width 80 mil

Table 15:Critical trace strain ranges evaluated from stress- strain hysteresis plots

Pad Width (mil)	Pad Shape	Trace Width (mil)	Board Strain Range (µstrain)		
			5000	4000	2000
			Critical Trace Strain Range (µstrain)		
125	Rectangular	40	7402	5922	2961
		60	6996	5597	2799
		80	6813	5450	2725
	Circular	40	7580	6088	3044
100	Rectangular	32	7431	5945	2973
		48	7243	5795	2897
		65	7011	5608	2804
	Circular	32	7610	6088	3044
62	Rectangular	20	8040	6432	3216
		30	7460	5968	2984
		40	7131	5705	2852

`

The cyclic strain range in the copper trace shown in Table 15 was combined with the mean cycles to failure obtained in Chapter 3 (Table 9, Table 10 and Table 11) to determine the constants of total strain based fatigue life model.

Total Strain based Fatigue Life Model

Modeling of fatigue life in structures came about as a by-product of the industrial revolution in the 19th century. It was then that the phenomenon of repeated loading causing failure was first realized when a single load of the same magnitude would not cause failure. Systematic testing to understand 'fatigue' were done in few laboratories most notably by August Wöhler who first introduced the concept of what is now more popularly known as the S-N (stress-life) curve in the 19th century. With the introduction of closed loop fatigue machines in the 1950s and 1960s where the fatigue load could be adjusted every cycle to remain constant immense breakthroughs were made in understanding and modeling fatigue life. It was realized that if the S-N curves were plotted on a double logarithmic scale the curves became almost linear. This equation, (see equation below) more formally known as the Basquin relation, which was first introduced in 1910.

$$\Delta\sigma_a = \sigma_f \left(2N_f\right)^b$$

where '$\Delta\sigma_a$' is the applied stress amplitude, 'σ_f' is the fatigue strength coefficient 'N_f' is the cycles to failure and 'b' is the fatigue strength exponent. The Basquin relationship is often used to determine high cycle fatigue life (HCF).

However, the Basquin relationship does not account for fatigue dominated by plasticity. This regime of fatigue is often referred to as low cycle fatigue (LCF). The Coffin-Manson fatigue model is perhaps the best known and most widely used approach today for modeling LCF. The total number of cycles to failure, 'N_f' , is depicted as being dependent on the plastic strain amplitude, '$\Delta\varepsilon_p$', the fatigue ductility coefficient, 'ε_f' , and the fatigue ductility exponent, 'c'. The relationship among these variables is shown in Equation.

$$\Delta\varepsilon_p = \varepsilon_f(2N_f)^c$$

In order to combine the fatigue modeling of HCF and LCF, people have suggested combining the Coffin-Manson and the Basquin equation. The resulting model is referred to as the total strain-life equation.

$$\frac{\Delta\varepsilon}{2} = \frac{\sigma_f}{E}(2N_f)^b + \varepsilon_f(2N_f)^c$$

where, '$\Delta\varepsilon$' is the applied strain range, 'E' is the elastic modulus 'σ_f' is the fatigue strength coefficient, 'ε_f' is the fatigue ductility coefficient, 'N_f' is the cycles to failure, 'b' is the fatigue strength exponent and 'c' is the fatigue ductility exponent. As can be seen in the Figure 61, the total strain life equation is an improvement over the Coffin-Manson equation and the Basquin equation as it accounts for the both the elastic and plastic regimes of fatigue.

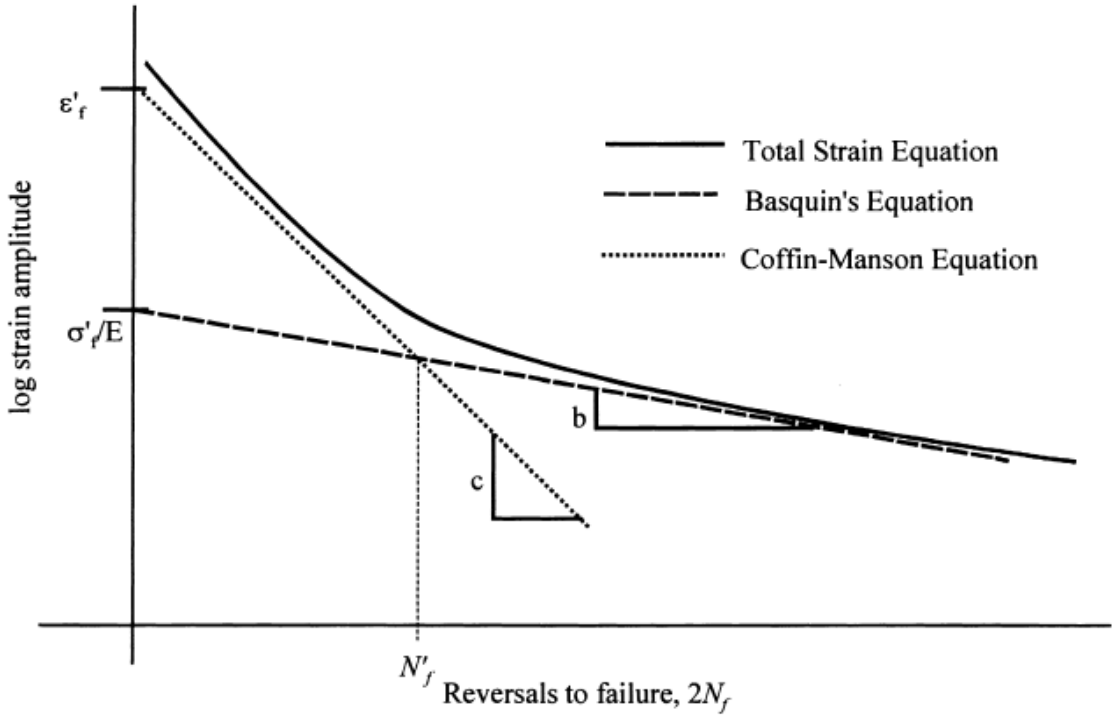

Figure 61: Schematic of the three fatigue life equations.

The mean cycles to failure obtained using experiments conducted in Chapter 3 were plotted against the critical trace strain range obtained from finite element modeling in a log-log plot. A non-liner regression analysis is performed using MATLAB on this data in order to extract the model constants of the total strain life equation. The resulting curve from the non-linear regression is shown in (Figure 62). The model constants for this curve are provided in Table 16.

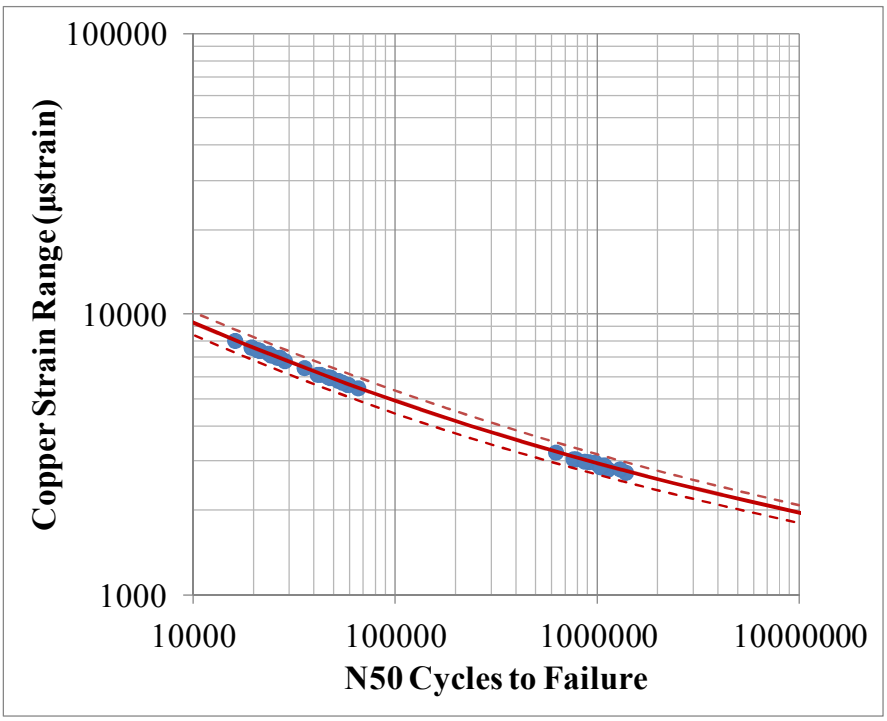

Figure 62: Copper trace fatigue life curve determined in this study.

Table 16: Total strain life model constants determine in this study.

Model Constants	Regressed Values (95% Confidence Bounds)
Fatigue Strength Coefficient (σ_f)	***643.2 MPa*** *(590.8 MPa, 735.2 MPa)*
Fatigue Ductility Coefficient (ε_f)	***21%*** *(19%,25%)*
Fatigue Strength Exponent (b)	***-0.11*** *(-0.10,-0.12)*
Fatigue Ductility Exponent (c)	***-0.43*** *(-0.41,-0.47)*
Elastic Modulus (E)	*114.7 MPa (from stress-strain curve)*

Validating Model Constants

In order to validate the determined models constants the data from the validation testing described in Chapter 3 was used. An estimate of the cycles to failure was

obtained using the derived model and the critical strains obtained from the finite element modeling (for 3000 µstrain board strain range) described in earlier in this chapter. The mean cycles to failure obtained for this load level (shown in Figure 63) was plotted against the estimated cycles to failure (Figure 64). As is seen in the figure the estimated cycles to failure match well with the mean cycles to failure obtained in the experiment.

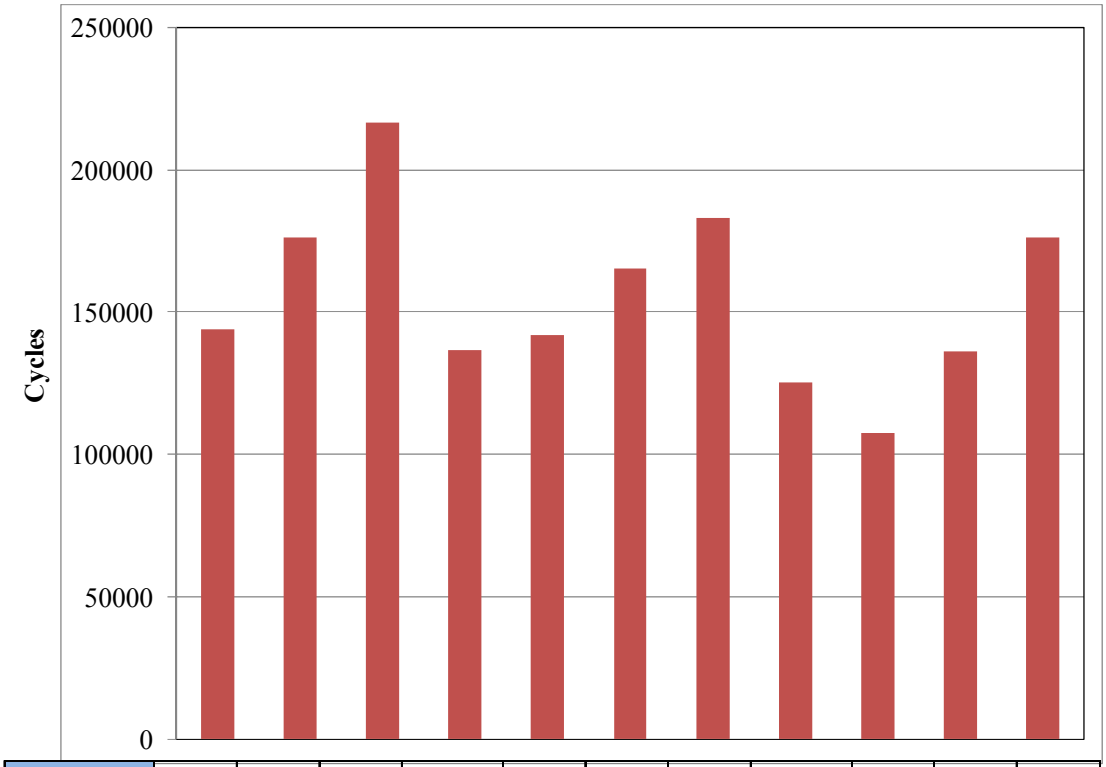

Trace Width (mil)	40	60	80	40	32	48	65	32	20	30	40
Pad Shape	Rectangular			Circular	Rectangular			Circular	Rectangular		
Pad Width (mil)	125				100				62		

Figure 63: Cycles to N50 failure for validation test (3000 µstrain load level).

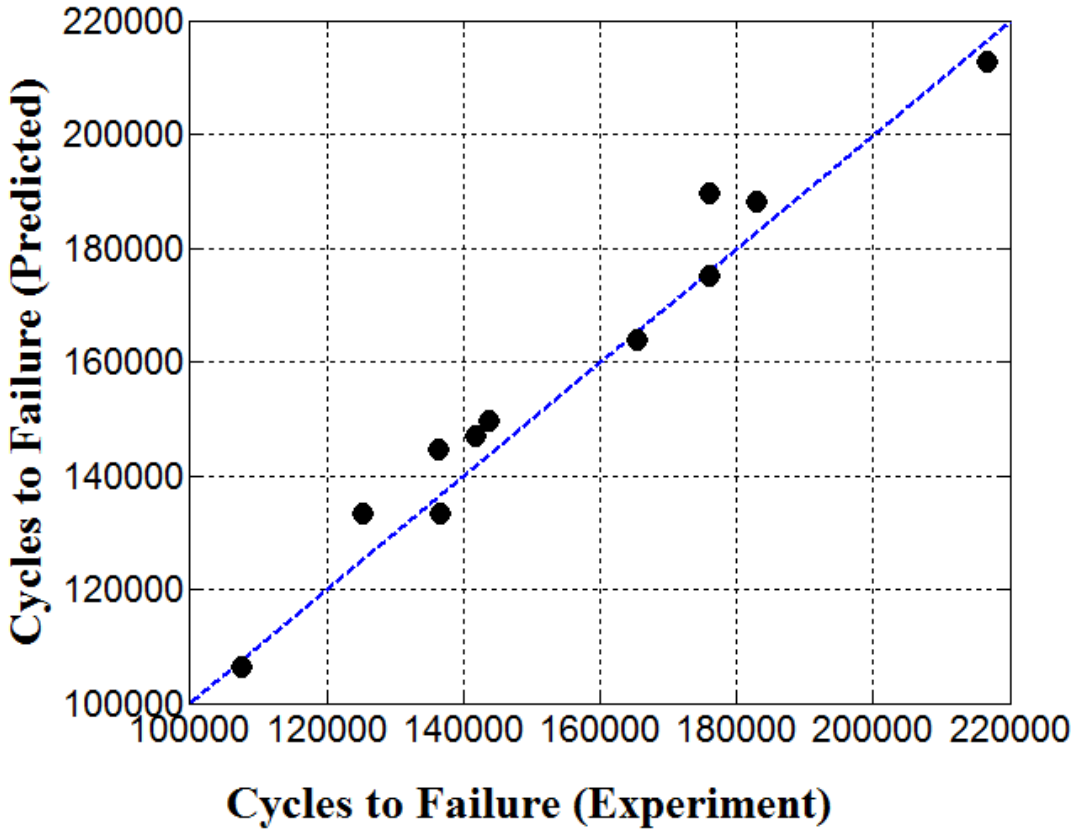

Figure 64: Comparison of experimentally observed cycles to N50 failure and model predicted N50 cycles to failure.

Crack Initiation and Crack Growth

In order to further understand the process of crack initiation and crack growth in the copper traces further experiments were conducted. A bare copper board was initially subject to an inspection process. This inspection included initial resistance measurement for all the traces along with the taking optical microscope images for all the different geometries of traces on the board. The test board was then subjected to a 5000 strain load level. The testing was stopped every 3000 cycles and the inspection procedure described above was repeated. This procedure allowed for monitoring the crack growth in the traces as well as checking for the resistance failure threshold of

20% increase in resistance. As is seen in the Figure 65, after a certain number of cycles the crack in the copper trace starts to nucleate at the trace to solder pad interface. The crack appears on both ends of the trace and propagates until complete failure is obtained when the traces meet near the middle of the trace width.

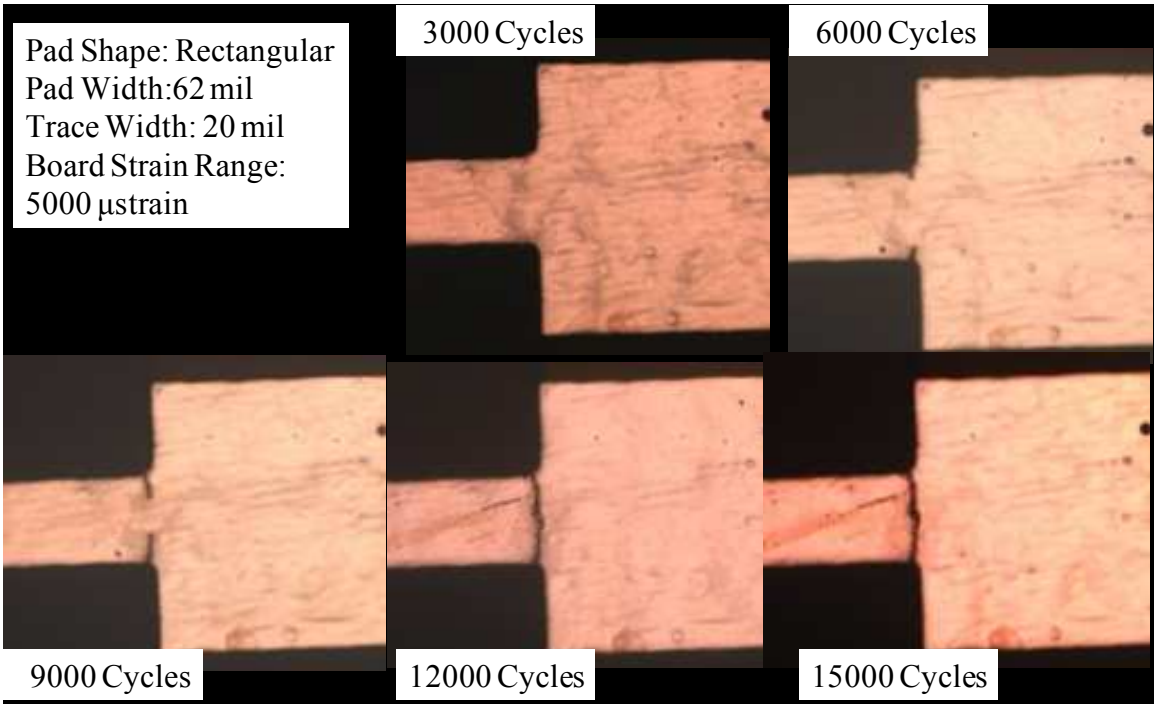

Figure 65: Crack propagation in traces

Similar images were obtained for all the different traces designed on the board. Image analysis was conducted on each of the images to measure the crack lengths at every 3000 cycle interval for all the different trace geometries. The average crack growth was evaluated for each of the differing trace geometries. The Figure 66 shows the comparison crack growth curves for the 62 mil rectangular pads with the three different trace widths (20 mil, 30 mil, 40 mil).

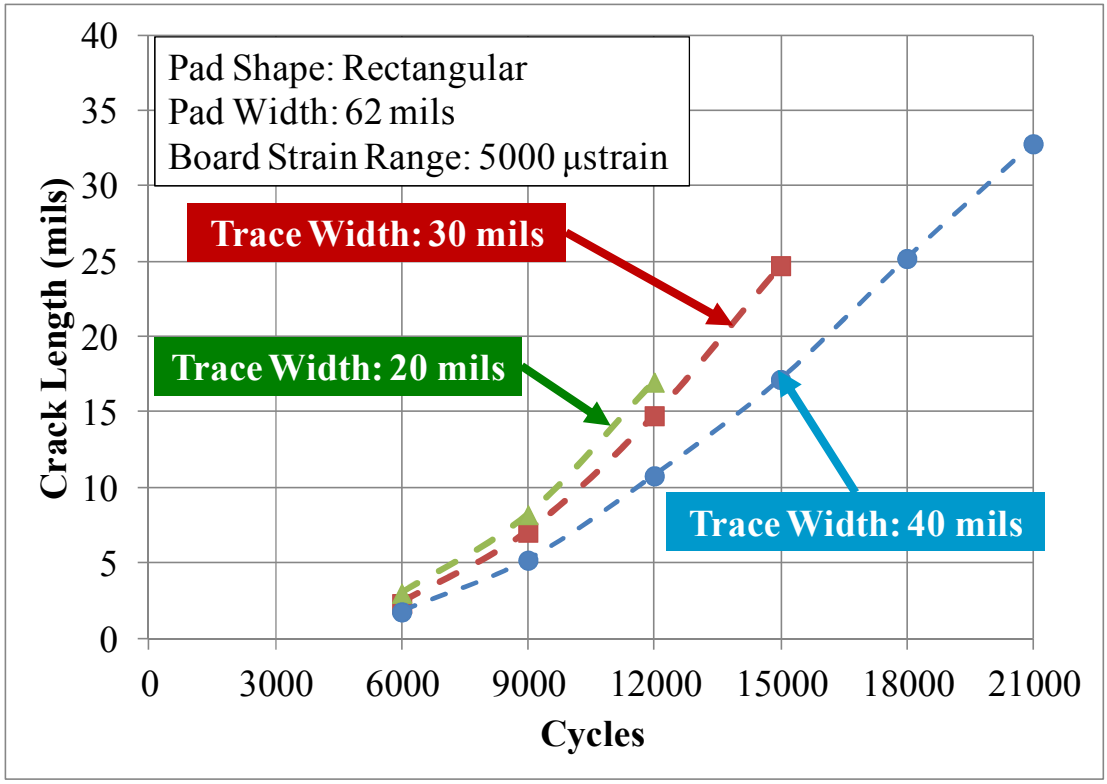

Figure 66: Crack growth curves in traces

The most common form of determining fatigue crack growth data is a log-log plot of advancement of fatigue crack per unit cycle as a function of the amplitude of stress intensity factor. The fatigue crack growth of materials can typically be divided into three regions as is seen in the Figure 67.

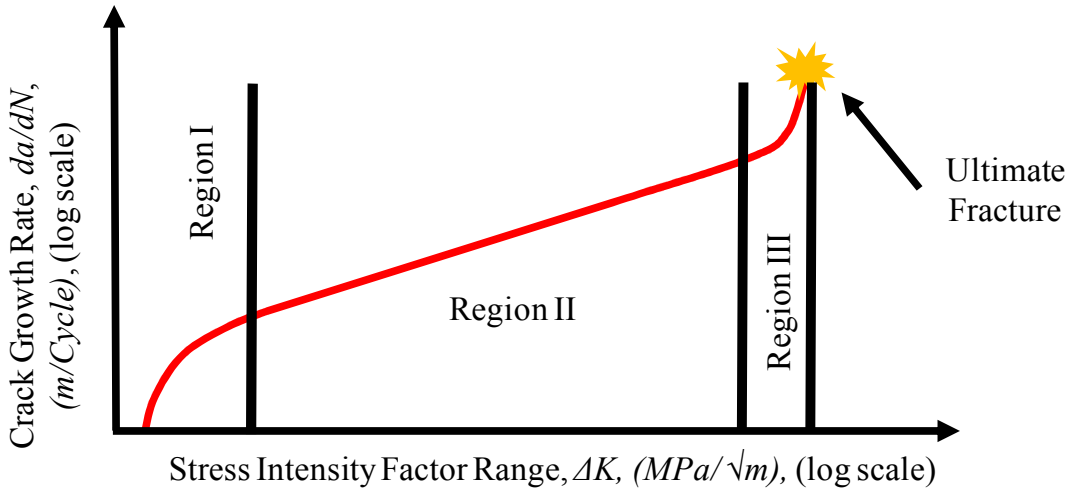

Figure 67: Typical crack propagation curves in materials

The growth (region II) of fatigue cracks are usually modeled using the Paris law for crack propagation [41]. Paris' law gives the advancement of fatigue crack per unit cycle as a function of the amplitude of stress intensity factor (see equation below)

$$\frac{da}{dN} = C(\Delta K)^m$$

where, 'a' is the crack length, 'N' is the number of cycles, 'ΔK' is the amplitude of stress intensity factors, 'C' and 'm' are material constants. Typically crack growth curves shift with the ratio of minimum to maximum stress of cycling, which are often notated as the stress ratio ('*R*'). However, Paris' law does not take into account the impact of 'R' when determining the constants C' and 'm' (see Figure 68).

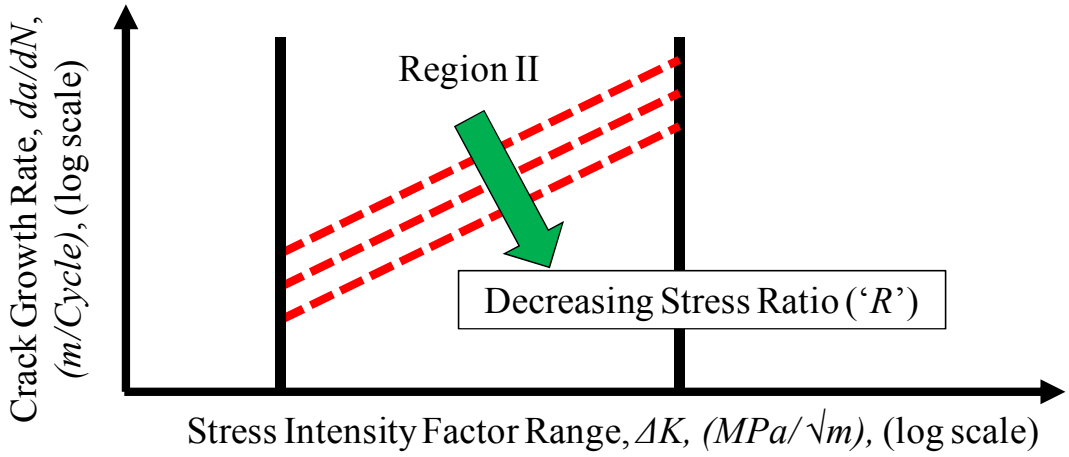

Figure 68: Impact of mean stress on crack propagation

Empirical fatigue-crack-growth equations were developed by Forman, et al., to take into account the stress ratio [42]. The Forman equation (see below) is a modification of the Paris equation to incorporate mean stress and region III fatigue crack growth behavior. As 'ΔK' approaches 'K_c', the denominator approaches zero, thus the crack growth rate, da/dN, gets very large. This describes region III crack growth

$$\frac{da}{dN} = \frac{C(\Delta K)^m}{\left((1-R)K_c - \Delta K\right)}$$

where, 'K_c' is the critical stress-intensity factor at failure, 'ΔK' is the amplitude of stress intensity factors, 'C' and 'm' are material constants.

Another common empirical relationship used to describe mean stress effects with R≥0 is the Walker relationship [43].

$$\frac{da}{dN} = \frac{A(\Delta K)^n}{(1-R)^{n(1-\lambda)}}$$

where, 'A' and 'n' are the Paris coefficient and slope for '$R=0$' and 'λ' is a material constant. The stress ratio, 'R', does not affect the slope, 'n'. The values of 'λ' for various metals range from 0.3 to nearly 1 with a typical value around 0.5. Lower values of 'λ' indicate a stronger influence of 'R' on fatigue crack growth behavior. Since the testing conducted in this study was fully reversed the stress ratios observed in the copper traces were approximately -1. As such for further work, only the Foreman equation was used to determine the material constants for fatigue crack propagation. The value for the critical stress intensity factor for electrodeposited copper foils is taken from previously published literature [44][45].

In classical fracture mechanics, the stress intensity factors have typically been evaluated using analytical and numerical solutions, based on the mode of cracking and crack propagation paths. Typically there are three modes of cracks described in fracture mechanics literature (Figure 69). The cracks observed during this study were as a result of Mode 1 cracks (opening).

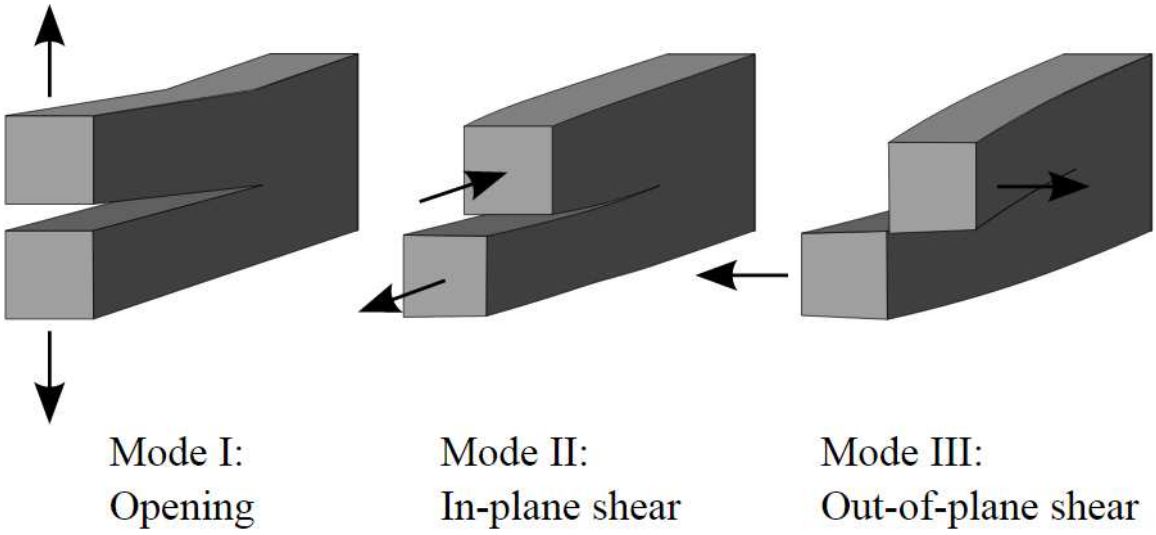

Figure 69: Modes of cracking

Also as discussed previously the cracks observed in the copper traces start propagation from both edges of the width of the trace and propagate towards the center of the trace (Figure 70). Therefore the stress intensity factor was calculated based on the double edge notch specimens [46].

$$\Delta K = \Delta\sigma\sqrt{(\pi a)}F\left(\frac{a}{b}\right)$$

$$F\left(\frac{a}{b}\right) = \frac{1.122 - 0.561\left({}^{a}/_{b}\right) - 0.205\left({}^{a}/_{b}\right)^{2} + 0.471\left({}^{a}/_{b}\right)^{3} - 0.190\left({}^{a}/_{b}\right)^{4}}{\sqrt{1 - {}^{a}/_{b}}}$$

where, 'a' is crack length, 'b' is the half width of the specimen, '$\Delta\sigma$' is the amplitude of stress, and 'ΔK' is the stress intensity factor.

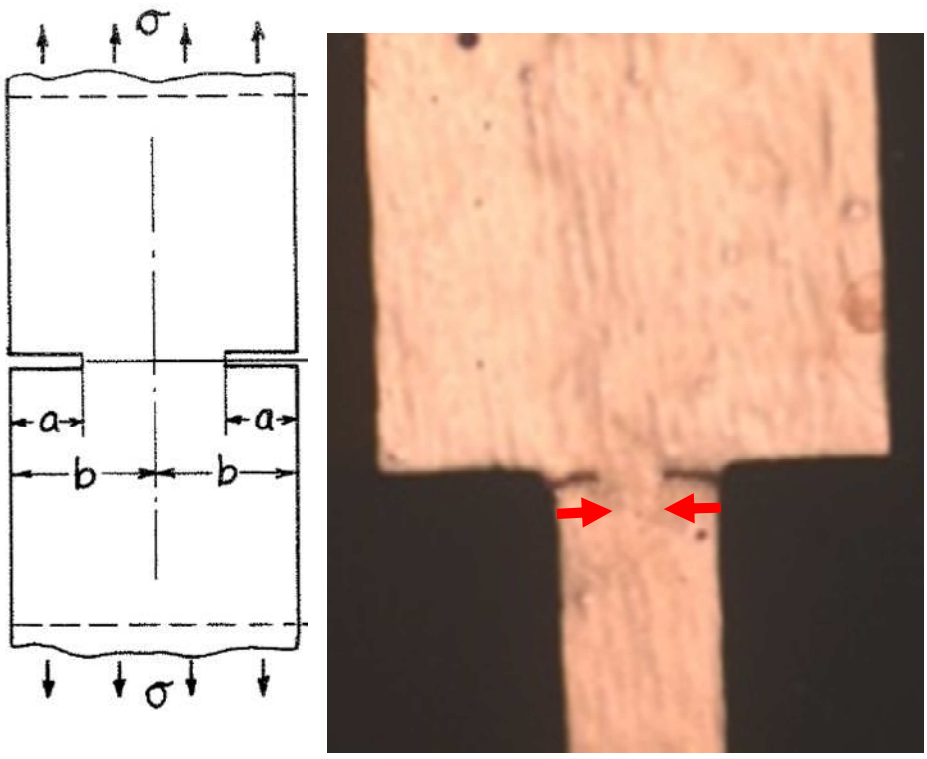

Figure 70: Direction of crack propagation in traces

The stress intensity factor was then evaluated every 3000 cycles based on above equation. The stress values used in the equation were determined based on the finite element modeling discussed earlier in the study. The determined stress intensity factors were plotted against the crack growth data observed in the test (Figure 71). These data points were fitted with a Power law equation to determine the model constants ('*C*' and '*m*') for the Paris law. The averaged model constants for all the crack propagation data are provided in Table 1.

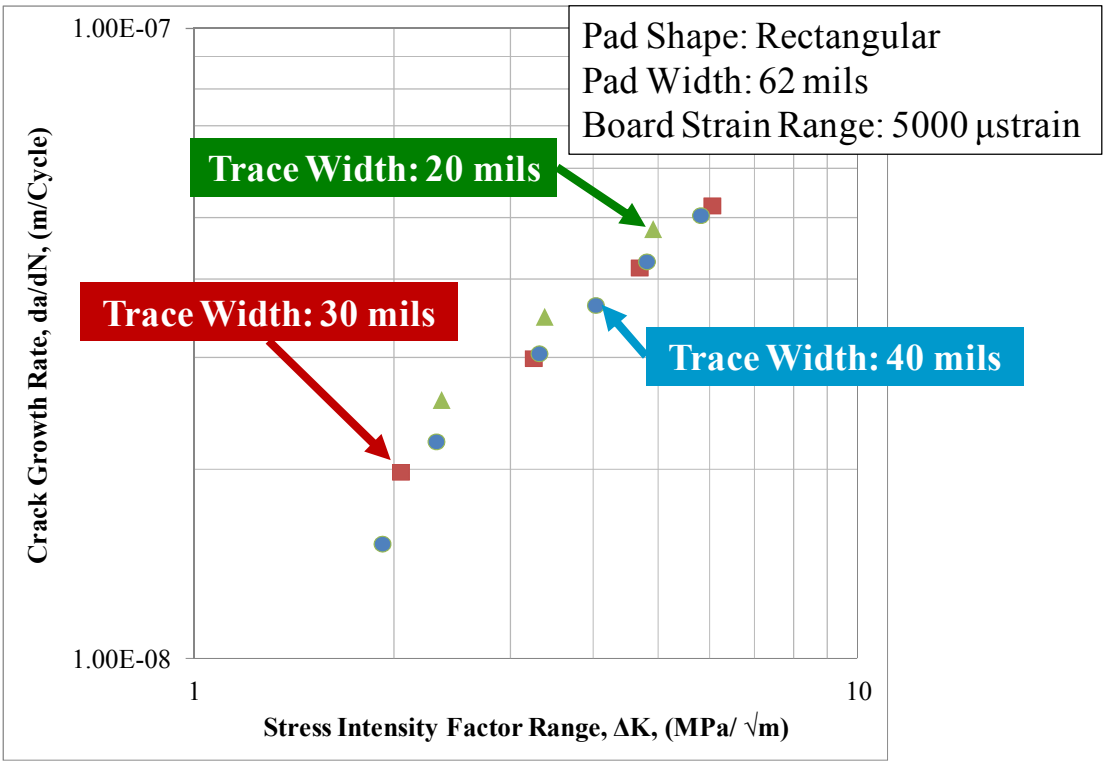

Figure 71: Determination of constant of Paris' law:

Table 17: Example of regressed material constants for fatigue crack growth in traces with pad width 1.575mm and board strain level 5000µstrain.

Determined Crack Propagation Constants	
C	1.02E-8
m	0.92

Chapter 5: Analytical Model for Critical Trace Strain

An analytical model for predicting fatigue life of traces allows us to identify the impact of design changes in the electronics assembly on the fatigue life of traces without building extensive finite element models for each design change. This allows for a quick and easy design optimization of the electronics assembly. In order to develop an analytical model the impact of varying design parameters as well as loading conditions are addressed in the following sections. As the trace fatigue models are essentially strain based models a functional relationship between the estimated trace strain from finite element modeling and each varied parameter will be developed. The list of parameters varied during the test has been listed below

- Load Level
- Trace Design
    - Trace thickness
    - Pad Width
    - Trace Width
    - Pad Length
    - Radius of Curvature at Pad-Trace Interface
    - Trace Orientation

- Assembly variations
    - Impact of surface finish
    - Impact of solder mask
    - Impact of assembled component

The developed analytical model will ideally be a function of all the above stated parameters. The validity of the developed functional form for estimated strain in the trace will be evaluated by comparing with the strain values obtained from the finite element simulations.

The finite element simulations that are used in this study are similar to what has been described in chapter 4, and the constitutive materials used in the finite element modeling are the determined models in chapter 3. Similar to previously described (see chapter 4) finite element modeling a 'global' –'local' model approach is used to determine the trace strain at the solder pad –trace interface. The trace strain range is evaluated using a volume-weighted stress-strain hysteresis evaluated from the finite element modeling. These trace strain values are used for making further comparisons. A flow chart of the process to evaluate trace strain is provided in Figure 72. The use of the analytical model developed in this study would enable designers in design optimization of the electronics assembly.

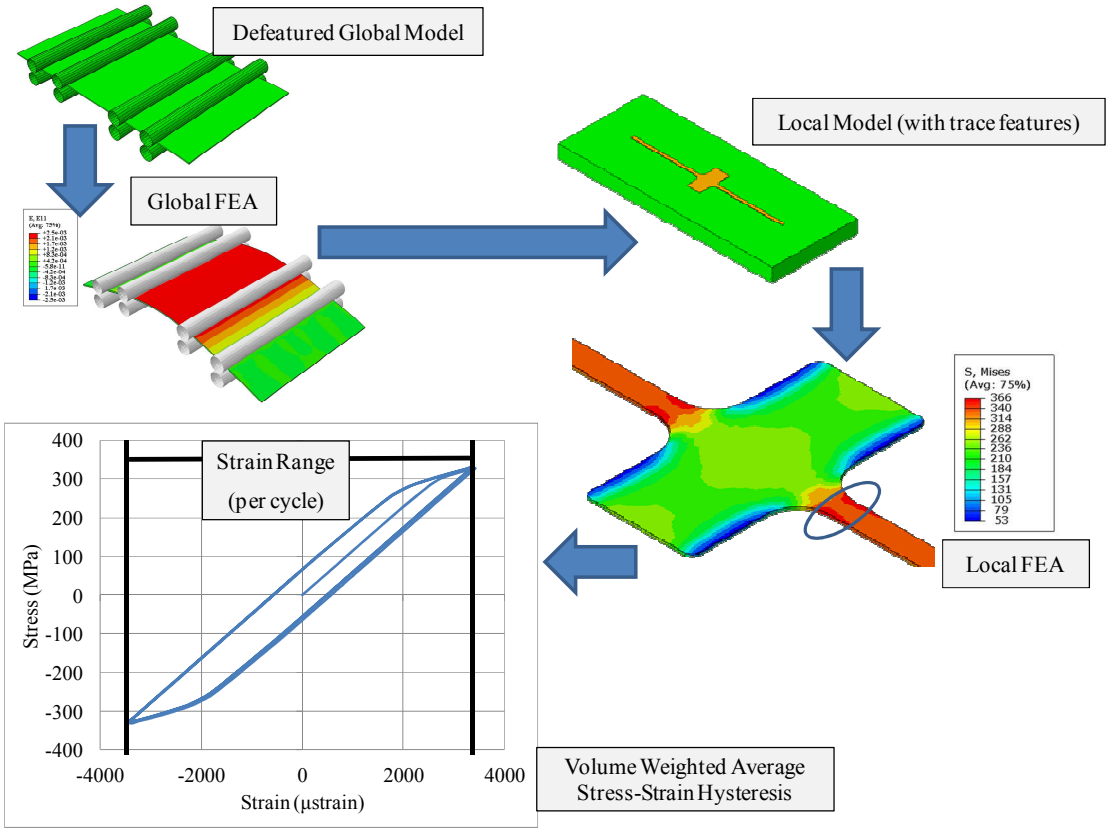

Figure 72: Flow chart for evaluating trace strain

Trace Strain vs. Board Strain

To evaluate the impact of load level, three different load levels were chosen. These included the fully reverse four point bend testing at a board strain range of 2000, 4000 and 5000 µstrain (see Figure 73). Figure 74 provides the evaluated trace strain ranges for three different pad geometries. As is seen in the figure, the trace strain varies linearly with the board strain level (within the tested range).

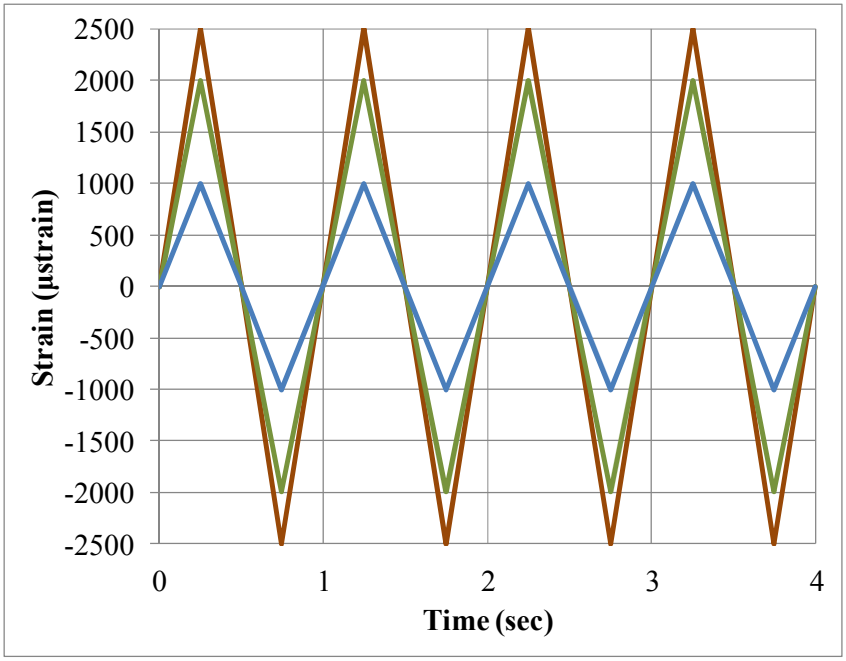

Figure 73: Board strain ranges for analytical model

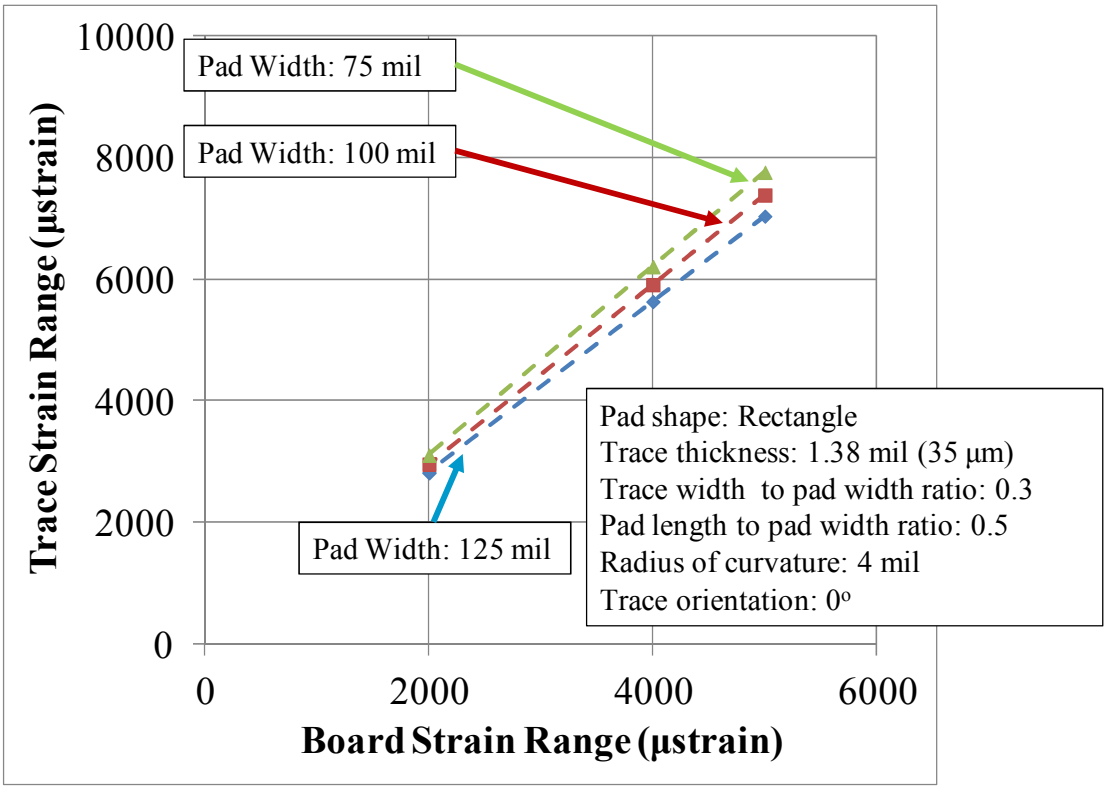

Figure 74: Board strain range vs. trace strain range

Trace Strain vs. Trace Thickness

In order to evaluate the impact of trace thickness on the trace strain under flexural loading, three commonly used thicknesses of traces were used. These included 0.5 oz (18 µm), 1 oz (35 µm) and 2 oz (70 µm). Finite element simulations were conducted at a single board strain level of 4000 µstrain (as the trace strain behaves linearly with board strain). As is seen in Figure 75, there is negligible change in the trace strain with variations in copper thicknesses considered in this study.

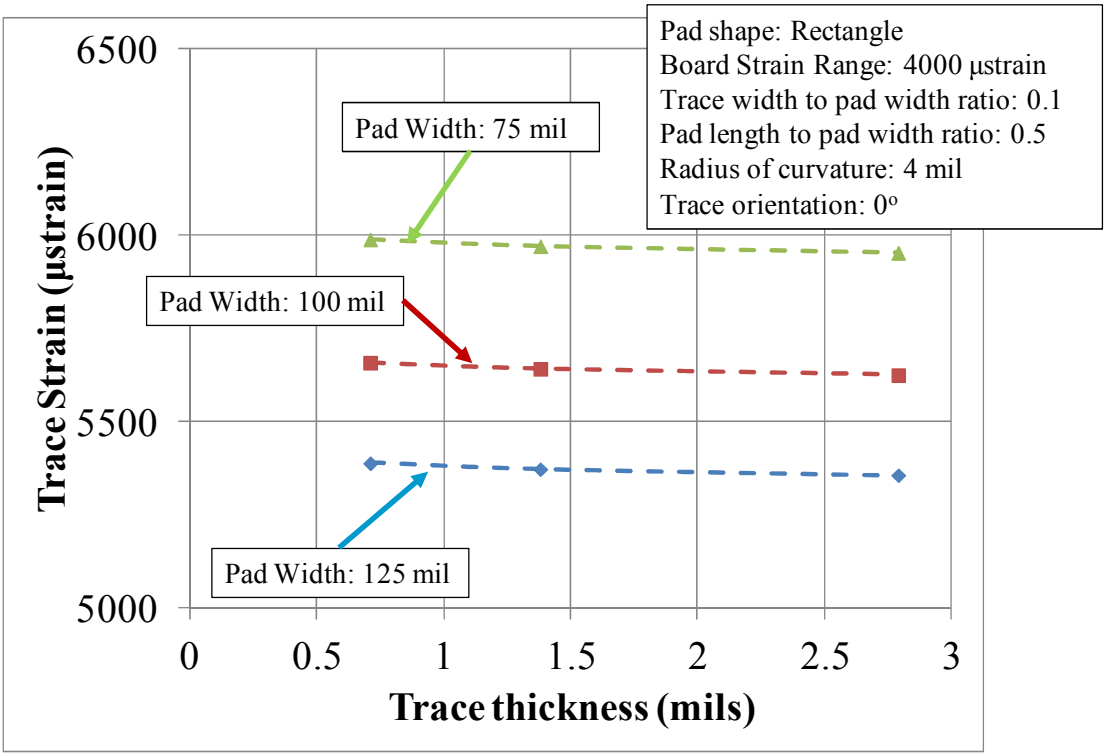

Figure 75: Trace thickness vs. trace strain range

Trace Strain vs. Pad Width

In order to evaluate the impact of pad width on the trace strain under flexural loading, three pad widths were chosen. These included a 75 mil pad, 100 mil pad and a 125

mil pad. Finite element simulations were conducted at a single board strain level of 4000 µstrain (as the trace strain behaves linearly with board strain).As is seen in Figure 76, strain in the traces decreases as the pad width increases.

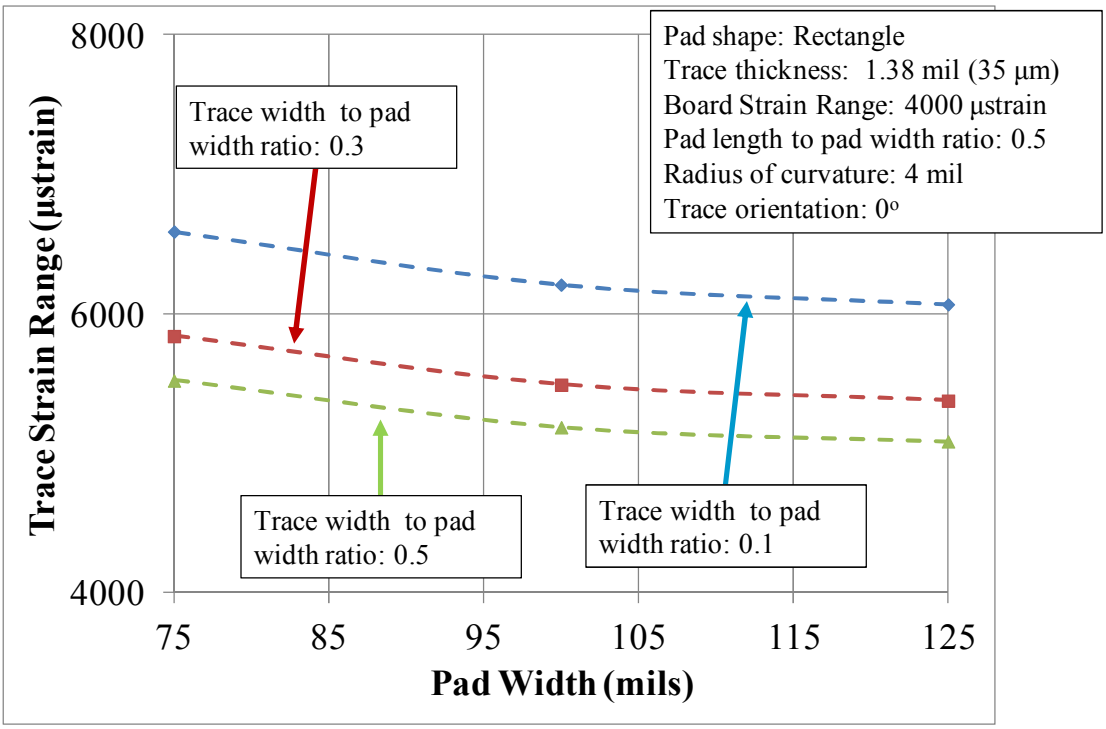

Figure 76: Pad width vs. trace strain range

Trace Strain vs. Trace Width

In order to evaluate the impact of trace width on the trace strain under flexural loading, three trace widths were chosen for each pad width in the design. These included a trace with trace to pad width ratios of 0.1, 0.3 and 0.5. Finite element simulations were conducted at a single board strain level of 4000 µstrain (as the trace strain behaves linearly with board strain). As is seen in Figure 77, strain in the traces decreases as the width of the trace increases.

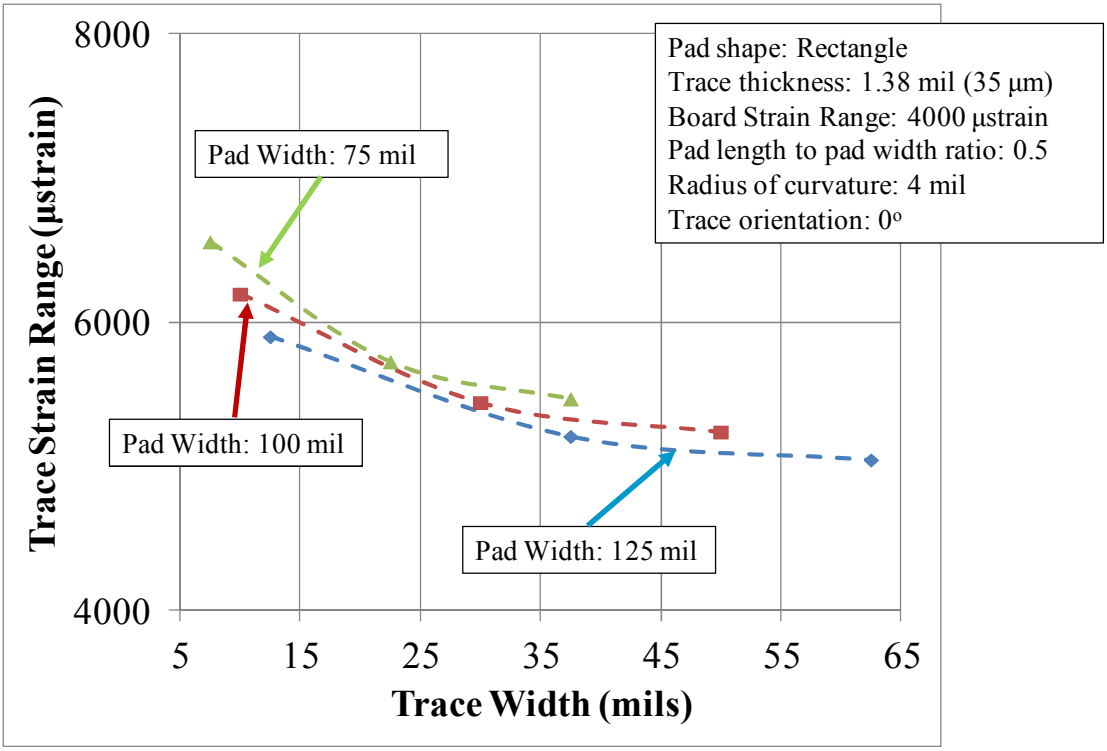

Figure 77: Trace width vs. trace strain range

Trace Strain vs. Pad Length

It was observed in the experiments conducted that the rectangular pads had a longer fatigue life than the circular pads. However, the pads chosen in the study had shorter pad lengths (see Figure 78) than the pad widths. In order to understand the impact of the pad length on the trace strain, three pad lengths were chosen for each pad width. These included pad length with pad length to width ratio of including 0.25, 0. 5 and 1. Finite element simulations were conducted at a single board strain level of 4000 µstrain (as the trace strain behaves linearly with board strain). As is seen in the Figure 79, an increase in pad length resulted in an increase in the strain level of the rectangular pads. The decreased pad length in the experiments therefore resulted in a

decreased strain level in the traces (see Figure 80) which resulted in the improved fatigue life observed by the rectangular pads in the experiments in Chapter 3.

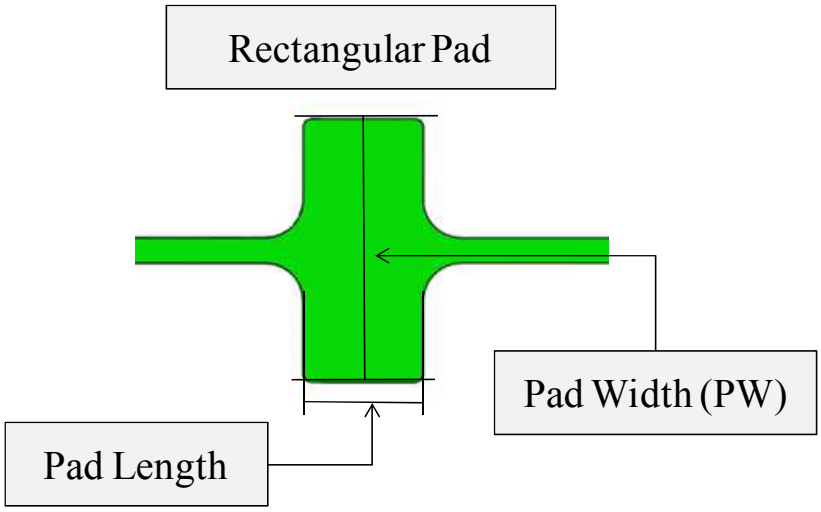

Figure 78: Pad width and pad length in a rectangular pad.

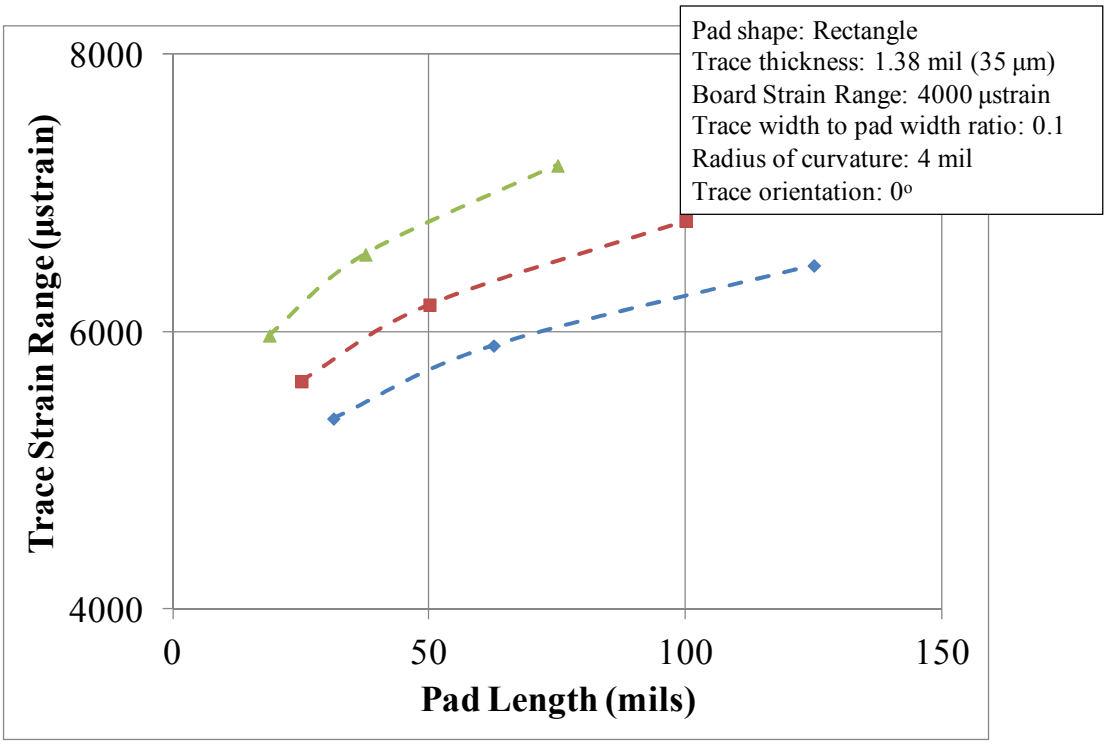

Figure 79: Pad length vs. trace strain range.

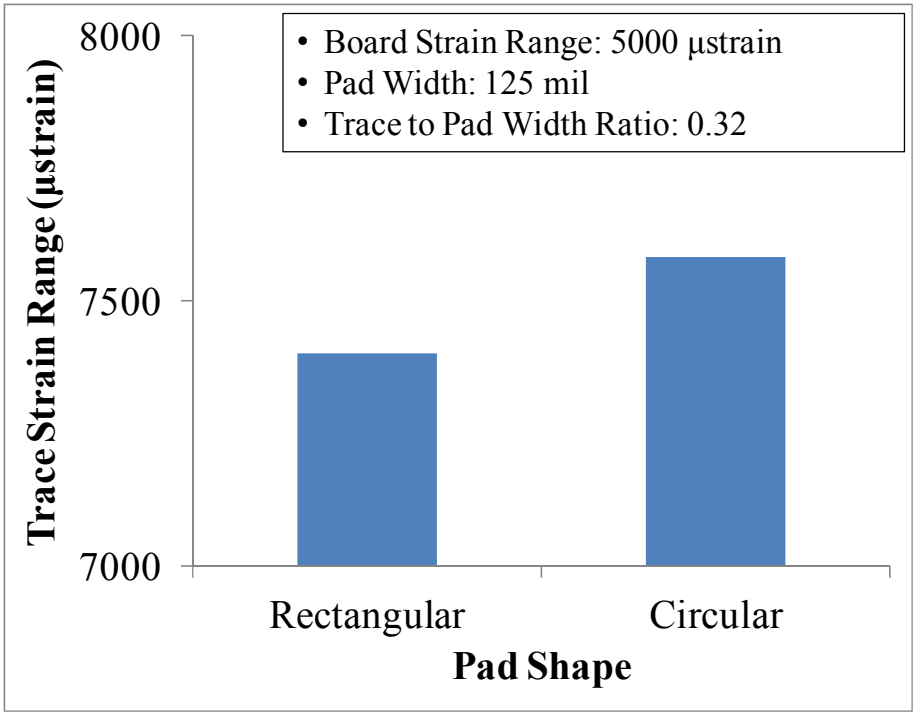

Figure 80: Trace strain ranges for varying pad shapes in the experiment.

Trace Strain vs. Radius of Curvature

To reduce the stress concentration at the trace to pad interface, there is usually a radius of curvature provided at the interface. This radius of curvature however is not a standard across board design and manufacturing. To understand the influence of the radius of curvature on the trace strain experienced at the trace to pad interface simulations were conducted with varying radius of curvatures (including 3 mil, 4 mil and 5 mil). Finite element simulations were conducted at a single board strain level of 4000 µstrain (as the trace strain behaves linearly with board strain). As is seen in the Figure 81, an increase in the radius of curvature resulted in a reduced trace strain. However, this reduction was more significant at lower trace to pad width ratios indicating competing effect of the stress risers.

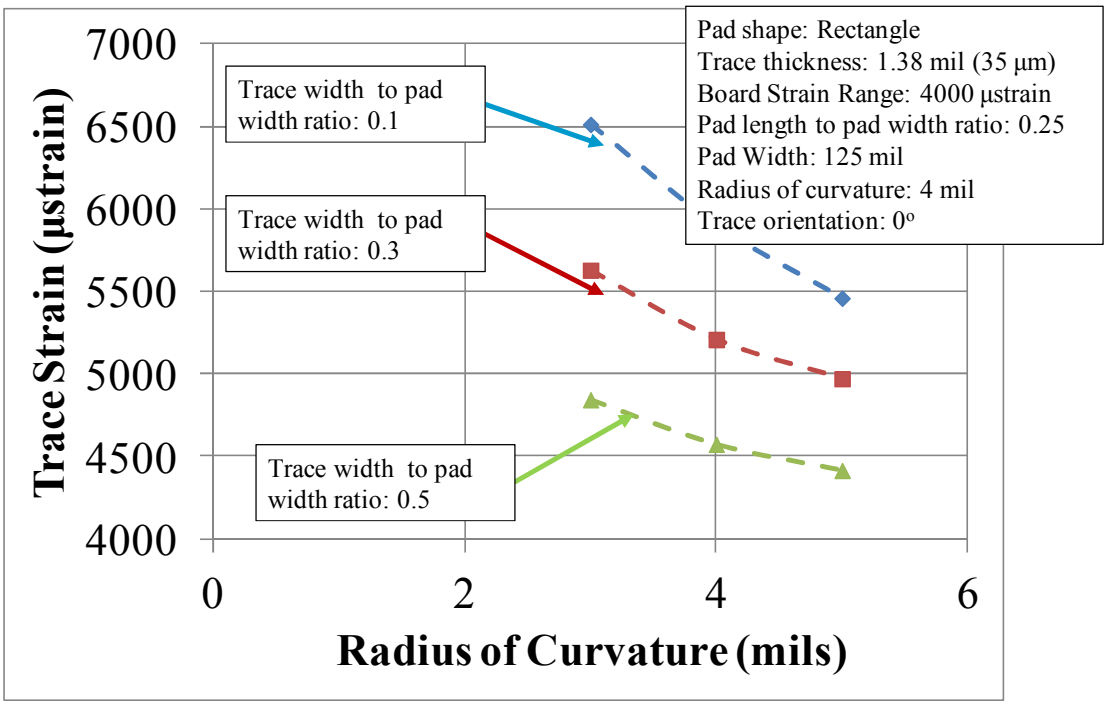

Figure 81: Trace strain ranges vs. radius of curvature at trace to pad interface.

Trace Strain vs. Trace Orientation

It has been established in earlier studies that the orientation of the trace (see Figure 82) plays a significant role in the trace strain under flexural loads [2][3][37]. In order to quantify the influence of trace orientation three trace angles were chosen (0º, 45º and 90º). As is seen in the Figure 83, as the trace strain reduces with the increasing trace angle and reaches a minimum.

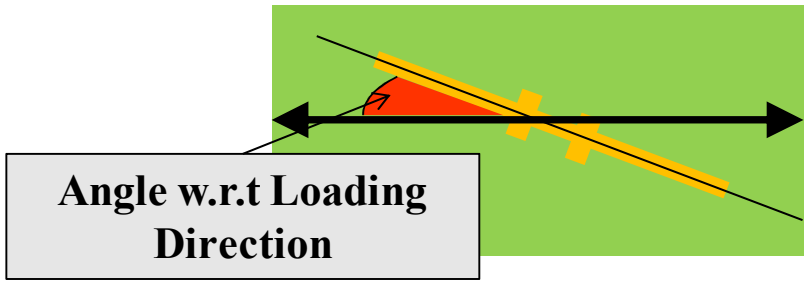

Figure 82: Trace angle with respect to loading direction.

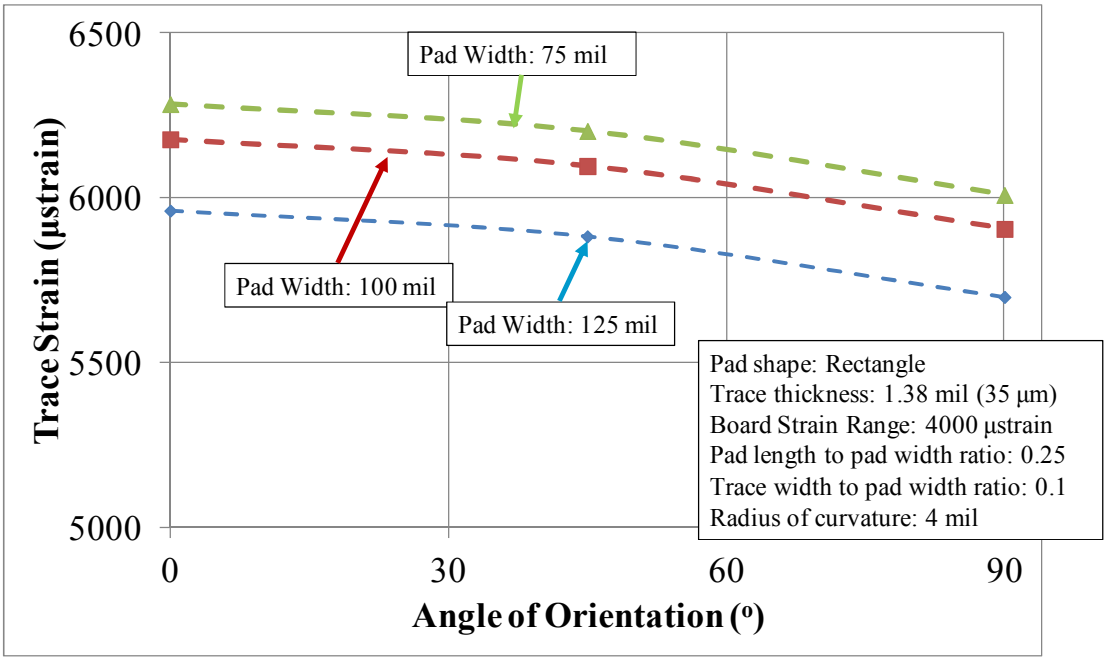

Figure 83: Trace strain ranges vs. trace angle.

Trace Strain vs. Pad shape

The shape of the pad has been shown to have an influence on the trace strain at the trace to pad interface. In order to investigate the impact of pad shape two different pad widths were chosen to namely a circular pad and a tear drop pad (see Figure 84).

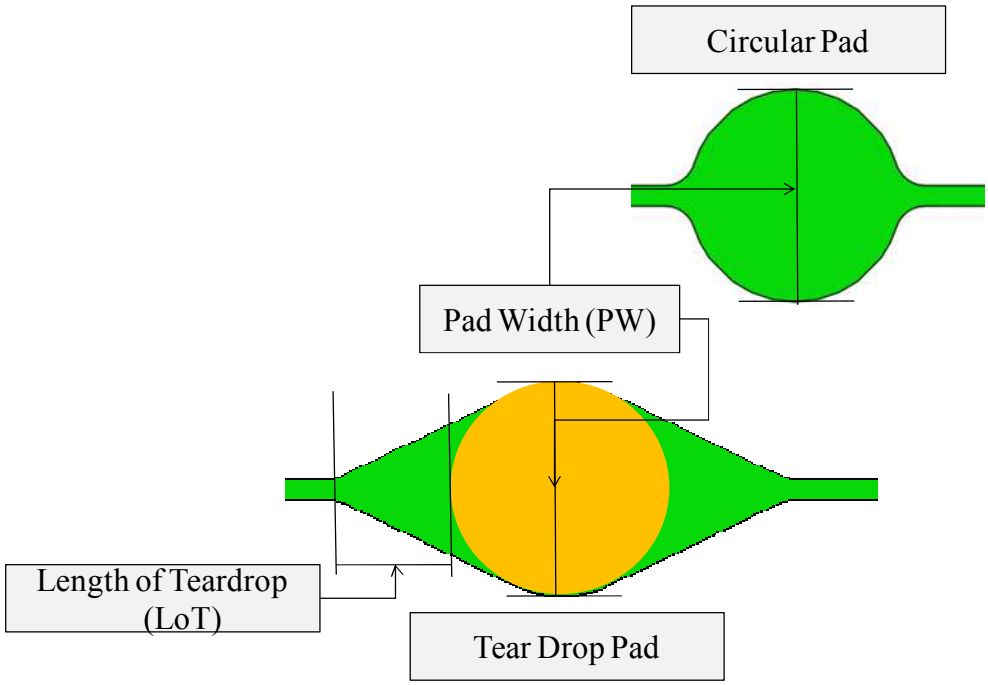

Figure 84: Pad width and length of tear drop in circular and tear drop pads.

Circular Pad

Three different pad widths were chosen to understand the influence of pad shape on the trace strain. The trace strain obtained in circular pads was compared with the strains of a square pad. Finite element simulations were conducted at a single board strain level of 4000 μstrain (as the trace strain behaves linearly with board strain).As, is seen in the figure the circular pads exhibited a lower strain than the square. The trace strain in the circular pad is approximately strain in the square pads multiplied by a factor of .91 across all the pad widths chosen in this study.

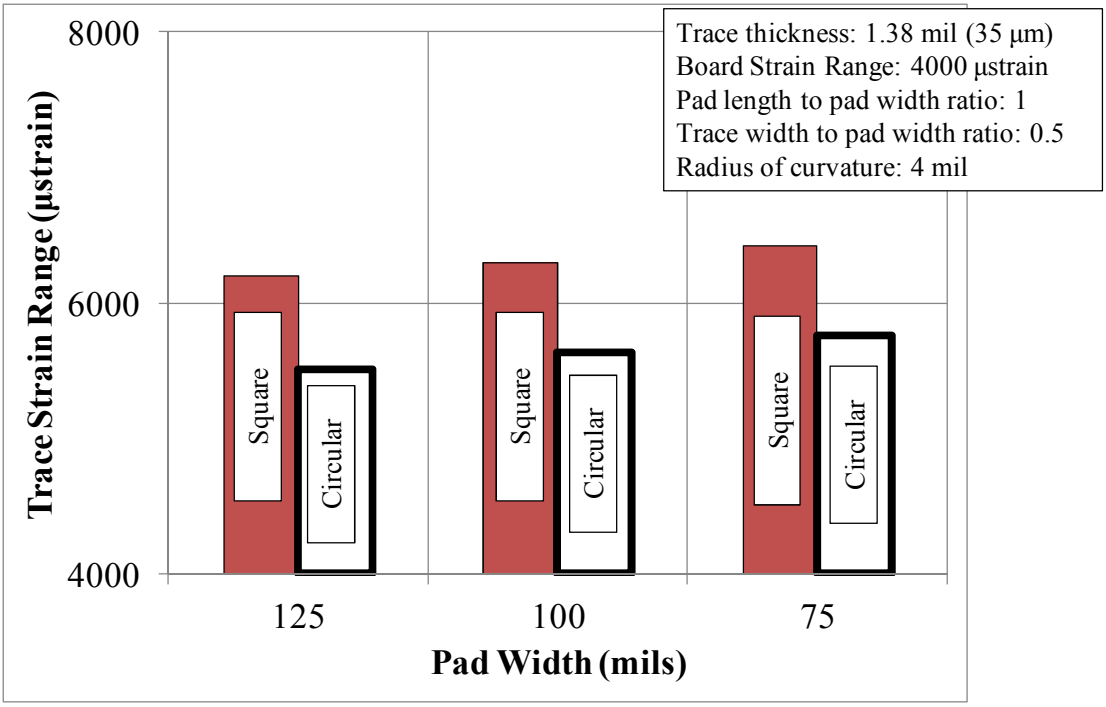

Figure 85: Trace strain ranges – square pad vs. circular pad.

Tear Drop Pad

The trace strain in the tear drop pads are compared with the traces in the circular pads. Increasing the length of the tear drop (see Figure 84) has been suggested in literature as a way to improve the fatigue life of the traces as it reduces the strain at the trace solder pad interface [3]. Three different lengths of tear drop were used in this study to understand the influence of the tear drop shape (including LoT/Pad width ratios of 0, 0.5 and 1). Finite element simulations were conducted at a single board strain level of 4000 µstrain (as the trace strain behaves linearly with board strain). As is seen in the figure increasing the length of tear drop reduces the strain in the traces. However, this behavior stabilizes once the length of the tear drop equals the width of the pad.

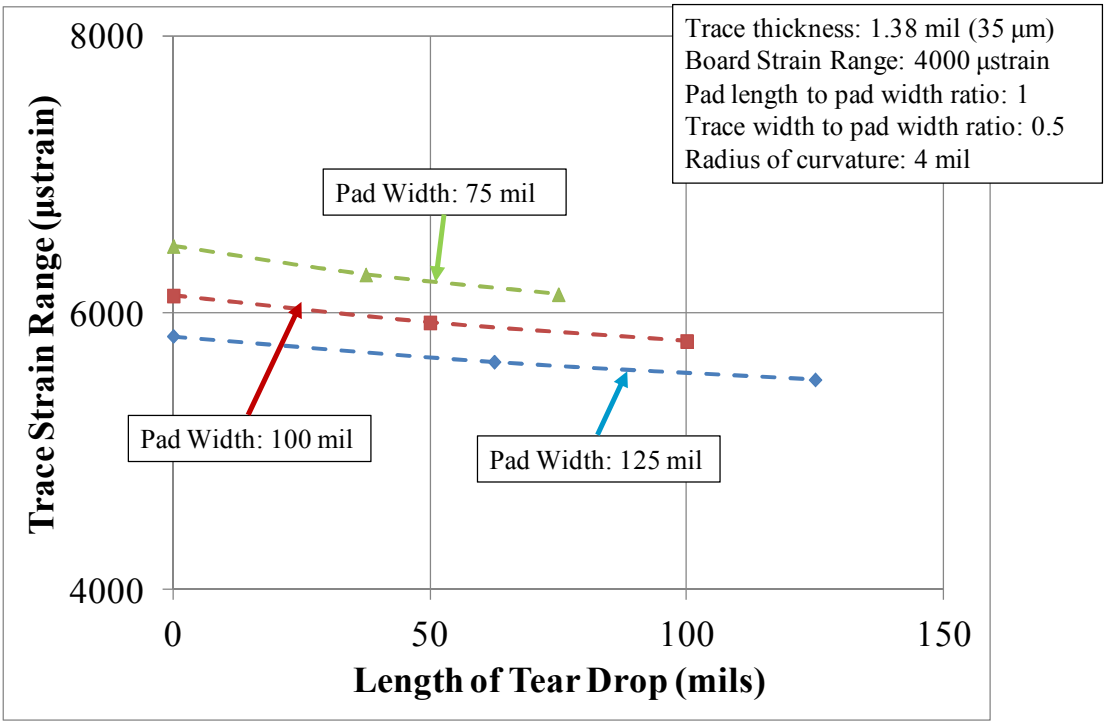

Figure 86: Trace strain ranges (Tear drop pad).

Analytical Model

Based on the relationships observed in the previous sections an analytical model of copper trace strain is developed. As the trace strain is linearly related to the board strain the model of trace strain (εt) is modified to the following formulation

$$\varepsilon_t = \varepsilon_b * K_\varepsilon * k$$

where, 'ε_b' is the board strain level, , '$K\varepsilon$' is a strain concentration factor based on trace and pad geometry and 'k' is a calibration factor accounting for the assembly on the board. The strain concentration factor 'K_ε' will be defined as follows

$$K_\varepsilon = f(P,\ W,\ L,\ R,\ T,\ \theta,\ S)$$

where, '*P*' is a function that accounts for the ratio of pad to board width, '*L*' is a function that accounts for the ratio of pad length to pad width, '*W*' is a function that accounts for the trace to pad width ratio, '*T*' is a function that accounts for the thickness of the trace '*R*' is a function that accounts for the impact of radius of curvature at the trace to solder pad interface, 'θ' is a function that accounts for the angle of trace w.r.t loading direction and '*S*' is a function that accounts for the shape parameter accounting for the shape of the solder pad (rectangular, circular or tear drop). For each parameter, a least square regression was carried out between the parameter and the strain obtained from FEA (keeping all other parameters constant) to determine the functional relationships. Based on these relationships of the strain concentration factor 'K_ε' is regressed to the following form (Figure 87).

$$\boldsymbol{K_\varepsilon = f(P, W, L, R, T, \theta, S)}$$

'P'-f(Pad Width) $\left(\frac{Pad\ Width}{Board\ Width}\right)^{-0.07}$	*'T'-f*(Trace Thickness) 1 copper thickness - 0.5 oz to 2 oz
'W'-f(Trace Width) $\left(\frac{Trace\ Width}{Pad\ Width}\right)^{-0.11}$	*'θ'-f*(Trace Orientation) $e^{\left(0.09\left(\frac{1+\lvert\cos\ \theta\rvert}{2}\right)\right)}$
'L'-f(Pad Length) $\left(\frac{Pad\ Length}{Pad\ Width}\right)^{0.13}$	
'R'-f(Radius of Curvature) $\tanh\left(\frac{m(Pad\ Width - Trace\ Width)}{2(Radius\ of\ Curvature)}\right)$ *'m'*-(0.1 to 0.4)	*'S'-f*(Pad Shape) Rectangle - 1 Circle - 0.9 Teardrop - $0.9\left(\frac{Pad\ Width}{Pad\ Width + Length\ of\ Teardrop}\right)^{0.08}$

Figure 87: Strain Concentration Factor

The calibration factor 'k' can be determined by using the experimental results obtained in chapter 3 and chapter 4, to account for the surface finish, the solder mask as well as the presence of a component (in this case the chip resistor). Thus the 'k' can be further split into the following form

$$k=k_{SF}*k_{SM}*k_{Comp}$$

where, 'k_{SF}' is the calibration factor that accounts for the surface finish, 'k_{SM}' is the calibration factor that accounts for the solder mask and 'k_{Comp}' is the calibration factor that accounts for the presence of an assembled component. These calibration factors are individually determined by comparing the expected strain values (Figure 88) in the copper traces to cause the failure and the trace strains observed in the bare copper finite element simulations. These calibration factors are determined for all the variations in the test vehicle and the average values of these calibration factors are provided in Table 18.

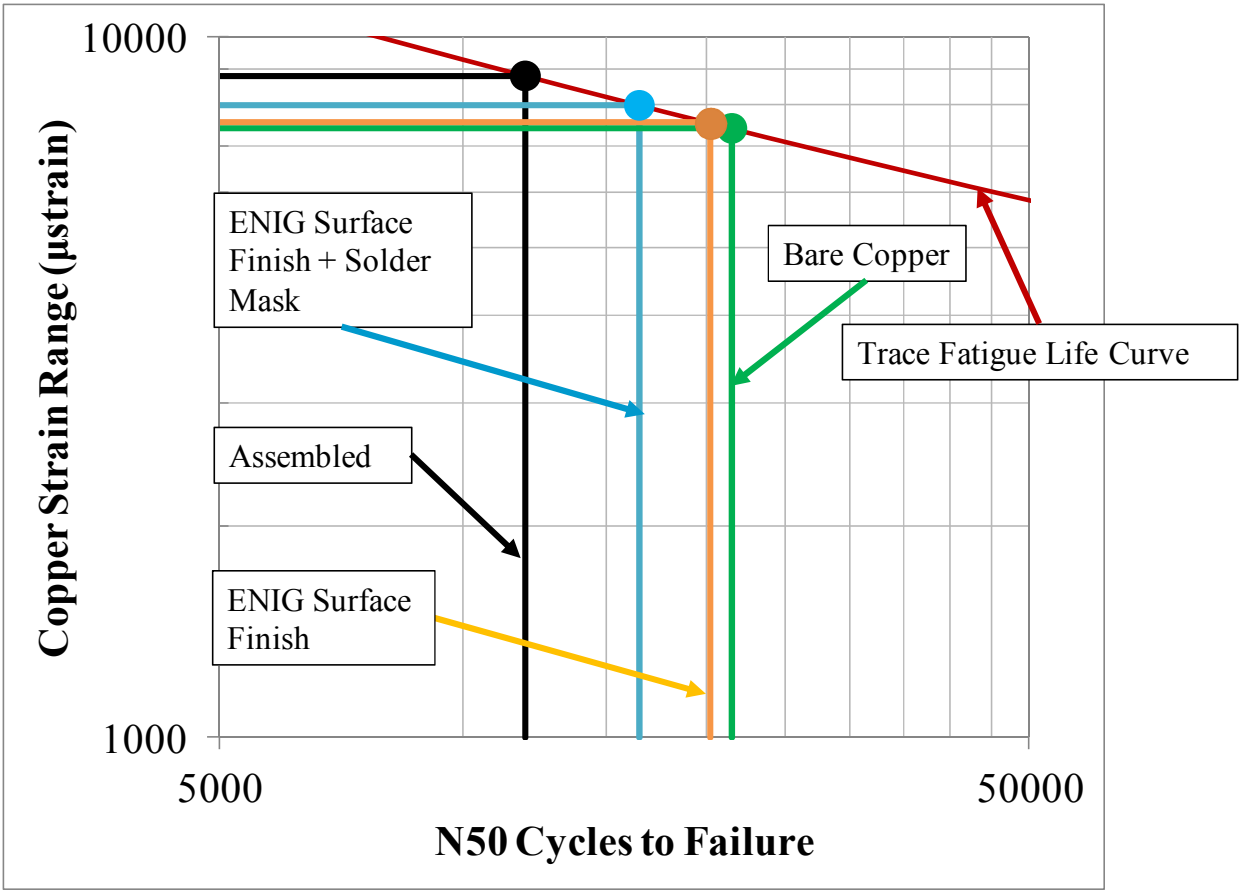

Figure 88: Determining trace strain based on fatigue life curve and experimental cycles to failure for board strain level: 5000 µstrain, Pad shape: rectangle, Pad width 125 mil and trace width 80 mil.

Table 18: Estimated assembly level calibration factors

k_{SF}	1.02
k_{SM}	1.08
k_{Comp}	1.09

Model Validation

In order to validate the developed analytical model, the trace strains were analytically estimated for the traces on the test vehicles used in the experiments described in chapter 3. These boards were tested at 4 different load levels including board strain ranges 2000 µstrain, 3000 µstrain, 4000 µstrain and 5000 µstrain. The analytically estimated strains for the PCBs with the bare copper traces were then compared with the finite element estimated strain for all the different design variations and the load levels. As is seen in the Figure 89, the strain estimated analytically (using the developed model) matches well with the finite element predicted strain in the traces.

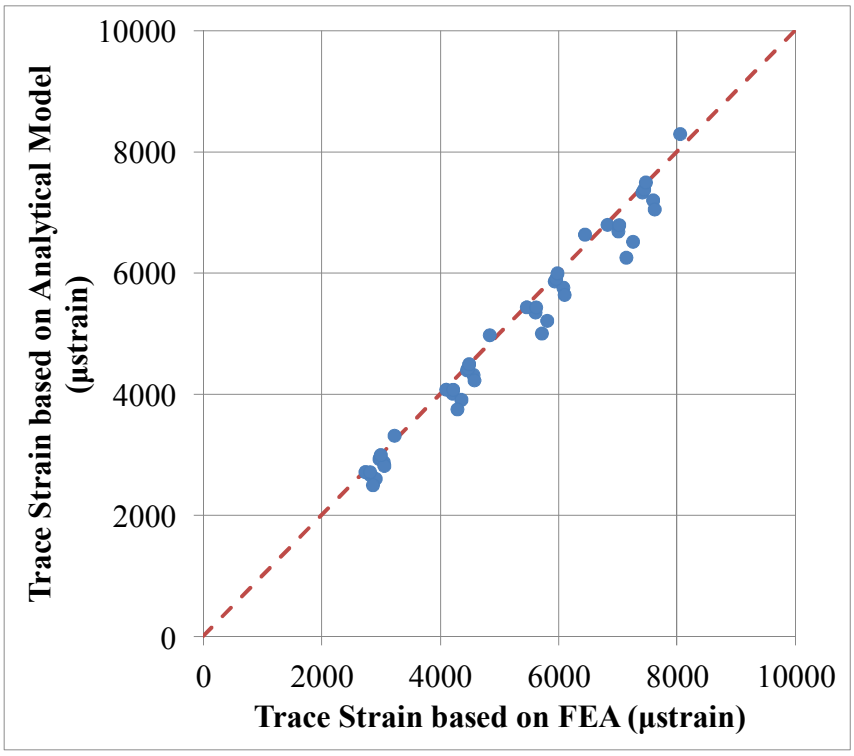

Figure 89: Estimated Trace Strain vs. FEA Strain

Chapter 6: Dissertation Contributions

This dissertation presented insights into the crack propagation behavior of traces on printed circuit boards and provided a methodology for assessing the fatigue life expectancy of copper traces on printed circuit board assemblies subject to mechanical bending. The dissertation contributions are listed below.

1. Determined the copper trace fatigue life model constants based on experimentally measured material properties, and validated the updated model constants against experimental results.
2. Established the Paris law constants for crack propagation in copper traces.
3. Developed an analytical model for evaluating trace strain based on trace design and loading conditions.
    - Quantified the impact of design parameters on trace strain
        1. Pad width
        2. Trace to pad width ratio
        3. Pad width to pad length ratio
        4. Radius of curvature at trace to pad interface
        5. Pad shape
        6. Angle of trace with respect to the loading direction
    - Quantified the impact of assembly level variations on trace strain
        1. Impact of surface finish
        2. Impact of solder mask
        3. Impact of assembled component

Chapter 7: Limitations and Future Work

This dissertation has provided insights into the fatigue behavior of copper traces on rigid electronic assemblies as well established an analytical model for estimating the traces strain that causes the trace to fail. Research can be conducted to further understand the crack initiation behavior in copper traces. Testing can be conducted to monitor the crack growth at multiple load levels and combined with the crack growth that was observed in this study to determine a model for fatigue crack initiation in the copper traces.

In this dissertation the crack initiation behavior was assumed to be the same for a bare copper traces as well as traces which had a surface finish or an assembled component. However, localized changes in ductility as well as the presence of a surface finish can locally alter the mechanical properties such as ductility, strength as well change the threshold stress intensities required for crack initiation in the traces. Further studies need to be conducted in order to investigate the impact of these changes to the initiation of cracks in the copper traces

The fatigue model constants as well as the analytical model derived in this dissertation were based on testing being conducted at a frequency of 1 Hz with zero mean stress. Though copper is widely regarded as strain rate insensitive, the strain rate sensitivity of the laminate material may impact the strain in the copper traces. As such the derived fatigue model constants as well as the analytical model needs to be validated under different rates of loading (for example in vibration or drop loading).

Also the mean stress of loading is known to impact the fatigue behavior of materials. As such further testing needs to be conducted in order to account for the impact of means stress level.

The analytical models was derived in this dissertation was based on foil thickness ranging from 0.5 oz to 2 oz thick copper. However, in some high power electronic applications thicker copper foils may be used. The validity of the analytical model for estimating strain should be evaluated for foil thickness > 2 oz. Further the calibration factors to account for presence of surface finish was based on an ENIG surface finish. As there could be a number of different surface finishes that may be used in the electronic assemblies (Immersion Silver, Immersion Tin, etc), further testing may be needed to determine the calibration factor to be used for different surface finishes in the analytical model for trace strain. Similarly the calibration factor for the presence of component determined in this dissertation was based on the presence of chip resistor. In the presence of other type of packages (such as QFNs, BGAs, LGAs, etc), this calibration factor could be very different. Further testing should also be conducted to determine the calibration factors for the different types of packages that could be present in an electronic assembly.

Bibliography

[1] D. Farley, Y. Zhou, F. Askari, M. Al-Bassyiouni, A. Dasgupta, J.F.J. Caers, J.W.C. DeVries, "Copper trace fatigue models for mechanical cycling, vibration and shock/drop of high-density PWAs", Microelectronics Reliability, 2010, Vol. 50, pp 937-947.

[2] Lall P., Angral A., Suhling J., "Board Trace Fatigue Models and Design Guidelines for Electronics under Shock-Impact", In proceedings of ITHERM, 2010, pp 978-984.

[3] A. Syed, T. Y. Tee, H. S. Ng, R. Anderson, C. P. Khoo, B. Rogers, "Advanced analysis on board trace reliability of WLCSP under drop impact", Microelectronics Reliability, 2010, Vol. 50, pp 928-936.

[4] T .T. Mattila, J.K. Kivilahti, "Failure mechanisms of lead-free chip scale package interconnections under fast mechanical loading", Journal of Electronic Materials, 2005, Vol. 34, pp 969-976.

[5] S. Shetty, V. Lehtinen, A. Dasgupta, V.Halkola, T. Reinikainen, "Fatigue of Chip Scale Package Interconnects Due to Cyclic Bending", Journal of Electronic Packaging, 2001, Vol. 123, Issue 3, pp 302-308,

[6] D. Y.R. Chong, F. X. Che, J. H. L. Pang, K. Ng, J. Y. N. Tan, P. T. H. Low, "Drop impact reliability testing for lead-free and lead-based soldered IC packages", Microelectronics Reliability, 2006, Vol. 46, pp 1160-1171.

[7] K. Jonnalagadda, M. Patel and A. Skipor "Mechanical Bend Fatigue Reliability of Lead-free PBGA Assemblies", In proceedings of the Inter Society Conference on Thermal Phenomena, 2002, pp 915-918.

[8] F. Qi and J. Liu, “Research on Failure Modes of BGA Assemblies with Lead-Free Solder on Different PCB Materials”, In proceedings of the International Conference on Electronic Packaging Technology, 2003, pp 396-400.

[9] Z. Jing, L. Hai, J. Lee, “Board Level Cyclic Bending Test for MCP Package”, In proceedings of the Electronics Packaging Technology Conference, 2007, pp 459-462.

[10] P. Marjamäki, T. T. Mattila, J. K. Kivilahti, “A Comparative Study of the Failure Mechanisms Encountered in Drop and Large Amplitude Vibration Tests”, In proceedings of the Electronic Components and Technology Conference, 2006, pp 95-101.

[11] . Varghese and A. Dasgupta “An experimental approach to characterize rate-dependent failure envelopes and failure site transitions in surface mount assemblies”, Microelectronics Reliability, 2007, Vol. 47, pp 1095–1102.

[12] T. T. Mattila, P. Marjamäki, L. Nguyen, J. K. Kivilahti, “Reliability of Chip Scale Packages under Mechanical Shock Loading”, In proceedings of the Electronic Components and Technology Conference, 2006, pp 584-589.

[13] Vikram Srinivas, Sandeep Menon, Michael Osterman and Michael G. Pecht, “Modeling the Rate-Dependent Durability of Reduced-Ag SAC Interconnects for Area Array Packages Under Torsion Loads,” Journal of Electronic Materials, Vol. 42, No. 8, 2013-

[14] Y. Yuan and B. J. Carpenter, “Trace Crack In Molded Thin Substrate Package, Root Causes And FEM Modeling”, In proceedings of the

International Conference on Electronic Packaging Technology, 2003, pp 449-454.

[15] A. Abdul-Baqi, P. J. G. Schreurs, M. G. D. Geers, "Fatigue damage modeling in solder interconnects using a cohesive zone approach", International Journal of Solids and Structures, 2005, Vol. 42, pp 927–942.

[16] W. W. Lee, L. T. Nguyen, G. S. Selvaduray, "Solder joint fatigue models: review and applicability to chip scale packages", Microelectronics Reliability, 2000, Vol. 40, pp 231-244

[17] W. Engelmaier, "A New Ductility and Flexural Fatigue Test Method for Copper Foil and Flexible Printed Wiring," Proc. of the 21st Annual IPC Meeting, IPC-TP-204, Evanston, 1978.

[18] D. Avery, "Copper Foil for Flexible Circuits," Circuit World, Vol. 14, Issue 2, pp 16-20, 1988.

[19] W. Engelmaier A. Wagner, "Fatigue Behavior and Ductility Determination for Rolled Annealed Copper Foil and Flex Circuits on Kapton," Circuit World, Vol. 14, Issue 2, pp. 30 - 38, 1988.

[20] W. Engelmaier, "Results of the IPC copper foil ductility round-robin study," IPC Publication, no. 947, pp. 66-95, 1987.

[21] H. D. Merchant, M. G. Minor, Y. L. Liu, "Mechanical fatigue of thin copper foil", Journal of Electronic Materials, 1999, Vol. 28, No. 9, pp 998-1007.

[22] R. R. Keller, J. M Phelps, D. T. Read, "Tensile and Fracture Behavior of free standing copper films," Material Science and Engineering, A124, pp 42-52, 1996.

[23] S. Hong and R. Weil, “Low cycle fatigue of thin copper foils”, Thin Solid Films, 1996, Vol. 283, pp 175-181.

[24] Y. Hwangbo and J. H. Song, “Fatigue life and plastic deformation behavior of electrodeposited copper thin films”, Materials Science and Engineering: A, 2010, Vol. 527, Issue 9, pp 2222-2232.

[25] Y. Hwangbo and J. H. Song, “Plastic deformation behavior analysis of an electrodeposited copper thin film under fatigue loading,” International Journal of Fatigue, 2011, Vol. 33, pp 1175-1181.

[26] Hommel, M., Kraft, O. and Arzt, E. (1999). A new method to study cyclic deformation of thin films in tension and compression, Journal of Materials Research 14, 2373–2376.

[27] A. Hardboletz, B. Weiss and G. Khatibi, “Fatigue and fracture properties of thin metallic foils,” International Journal of Fracture, Vol. 107, pp 307-327, 2001

[28] B. Weiss, V. Gröger, G. Khatibia, A. Kotasa, P. Zimprich, R. Stickler, B. Zagar, “Characterization of mechanical and thermal properties of thin Cu foils and wires,” Sensors and Actuators A 99 (2002) 172–182.

[29] H.D. Merchant, G.Khatibi and B. Weiss, “Elastic and elastoplastic response of thin copper foil,” Journal of Material Science, Vol, 39, pp 4157 – 4170, 2004.

[30] G. Simons, Ch. Weippert, J. Dual, J. Villain, “Size effects in tensile testing of thin cold rolled and annealed Cu foils,” Materials Science and Engineering A 416 (2006) 290–299.

[31] Do-Young Lee and Ji-Ho Song, “Fatigue life and plastic deformation behavior of electrodeposited copper thin film under variable amplitude loading,” International Journal of Fatigue 38 (2012) 1–6.

[32] S. Han, K, Seo, W. Kim H. Lee, H. Lee, J Shin and J Lee, “Fatigue behavior of thin Cu foils for flexible printed circuit board,” Solid State Phenomena Vols. 124-126 (2007) pp 1369-1372

[33] C. Y. Chou, C. J. Huang, M. Sano, K. N. Chiang, “Metal Trace Impact Life Prediction Model for Stress-Buffer-Enhanced Package”, In proceedings of the Microelectronics and Packaging Conference, 2009, pp 1-6.

[34] D. Farley, A. Dasgupta, Y. Zhou, l.FJ. Caers, and l.W.C. De Vries, “Fatigue Model based on Average Cross-Section Strain of Cu Trace Cyclic Bending,” 2011 12th. Int. Conf on Thermal. Mechanical and Multiphysics Simulation and Experiments in Microelectronics and Microsystems. EuroSimE 2011

[35] D. Farley, Y. Zhou, A. Dasgupta, J.W.C. DeVries, “An adaptive Cu trace fatigue model based on average cross-section strain,” Microelectronics Reliability 52 (2012) 2763–2772.

[36] H. Kim, K. Hsieh, “Measurement and prediction of embedded copper foil fatigue crack growth in multifunctional composite structure,” Composites: Part A 43 (2012) 492–506

[37] F. Kraemer, S. Rzepka, S. Wiese, and J Lienig, “The Effect of Copper Trace Routing on the Drop Test Reliability of BGA Modules,” 2010 Electronic Components and Technology Conference.

[38] A. Fox, “Mechanical Properties at Elevated Temperature of CuBath ® Electroplated Copper for Multilayer Boards,” Journal of Testing and Evaluation, Vol. 4, Issue 1, pp 74-84, 1976.

[39] D.T. Read, “Tension-tension fatigue of copper thin films,” International Journal of Fatigue, Vol. 20, No. 3, pp 203-209, 1998.

[40] S.H. Hong, K.S. Kim, Y.-M. Kim, J.-H. Hahn, C.-S. Lee, J.-H. Park, “Characterization of elastic moduli of Cu thin films using nanoindentation technique,” Composites Science and Technology, Vol 65, pp1401–1408, 2005

[41] Paris, Paul C.: The Fracture Mechanics Approach to Fatigue. Fatigue –An Interdisciplinary Approach. John J. Burke, Norman L. Reed, and Volker Weiss, Syracuse Univ. Press, 1964.

[42] Forman, R. G.; Kearney, V. E.; and Engle, R. M. : Numerical Analysis of Crack Propagation in Cyclically Loaded Structures. ASME Annual Winter Meeting, Nov. 1966

[43] Walker, K., "The Effect of Stress Ratio During Crack Propagation and Fatigue for 2024-T3 and 7075-T6 Aluminum," Effects of Environment and Complex Load History on Fatigue Life, ASTM STP 462, Am. Soc. for Testing and Materials, West Conshohocken, PA, 1970, pp. 1-14.

[44] Jiddu Bezares, Shuyin Jiao, Yue Liu, Daniel Bufford, Lei Lu, Xinghang Zhang , Yashashree Kulkarni, Robert J. Asaro, “Indentation of nano-twinned fcc metals: Implications for nano-twin stability.” Acta Materialia 60 (2012) 4623–4635.

[45] Yong X. Gan, Chih-Shing Wei, Marca Lam, Xiaoding Wei, Dongyun Lee, Jeffrey W. Kysar, Xi Chen, "Deformation and fracture behavior of electrodeposited alumina nano-particle/copper composite films." J Mater Science (2007) 42:5256–5263

[46] Tada H, Paris P C and Irwin G: 'The stress analysis of cracks handbook', Third Edition, ASME, New York, 2000.

[47] R. Branco, F.V. Antunes, J.A. Martins Ferreira, J.M. Silva, "Determination of Paris law constants with a reverse engineering technique," Engineering Failure Analysis, 2008.